Newly Developed Silicon Nitride Based Nanocomposites with Multiple Functionality

1999

Takafumi Kusunose

Department of Materials Chemistry
Faculty of Engineering
Osaka University

Newly Developed Silicon Nitride Based Nanocomposites with Multiple Functionality

1999

Takafumi Kusunose

Department of Materials Chemistry
Faculty of Engineering
Osaka University

Newly Developed Silicon Nitride Based Nanocomposites with Multiple Functionality

Contents

Chapter 1

Introduction

1. 1 Structural Ceramics

Ceramics are attracting considerable interests, because of their excellent properties such as high strength, high insulation resistance, low density and chemical inertness. Especially, alumina (Al_2O_3), zirconia (ZrO_2), silicon nitride (Si_3N_4) and silicon carbide (SiC) have been expected as high temperature structural ceramics in the 21st century.

Recently, many news on " space trip" come from television, magazine, and so on. In order to realize this dream, atmospheric re-entry vehicles require materials for re-usable heat-resistant structures and thermal protection systems. Metallic materials have been pushed closed to their limit due to undesirable properties at high temperatures. As the most promising candidate for such materials, therefore ceramics are nominated, because ceramics with the excellent thermo-mechanical properties have been supposed to play an important role in the materials used in severe environments such as high temperatures and oxidizing atmosphere. In the future, it is predicted that a nose cap and a wing leading edge of these vehicles as shown in Fig.1-1 will be manufactured by ceramic matrix composites. However, the thermal shock resistance, machinability and fracture toughness of the present ceramics are not sufficient for their practical uses to various machine parts compared to metals. Thus, several investigations have been undertaken for Si_3N_4 based composites to drastically improve the thermal shock fracture resistance and fracture toughness to overcome these disadvantageous properties.

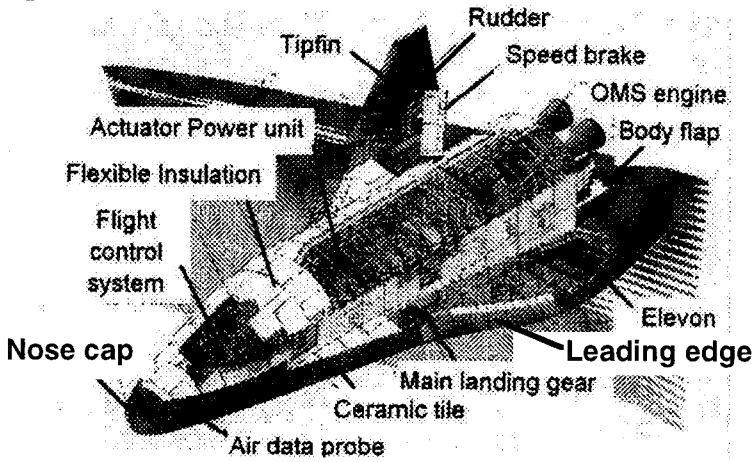

Fig.1-1 Configuration of atmospheric reentry vehicle.

1. 2 Background of Si_3N_4 Ceramics

1. 2. 1 Basic Properties of Si_3N_4 Ceramics

Si_3N_4 is a light, strong covalent bonding material with a good combination of mechanical, thermal and thermo-mechanical properties. Si_3N_4 consists of Si and N atoms which are found in abundant quantities in the earth's crust. Si_3N_4 is classified into two types of crystal structures, α and β phases. The former transforms to the latter at about 1400--1600°C, and the latter decomposes at about 1900°C. The both α and β phases have a hexagonal structure. The c-axis of α- Si_3N_4 is about twice that of β-Si_3N_4. The basic unit of these crystal structures is SiN_4 tetrahedron, as shown in Fig.1-2. An ideal stacking sequence of α-Si_3N_4 crystal structure is A, B, C and D layers along c-axis, as shown in Fig. 1-3 (a) and (b). While β–Si_3N_4 has ABAB---packing structure[1], as shown in Fig.1-3(a). Table 1-1 shows some physical and chemical properties of Si_3N_4 ceramics.

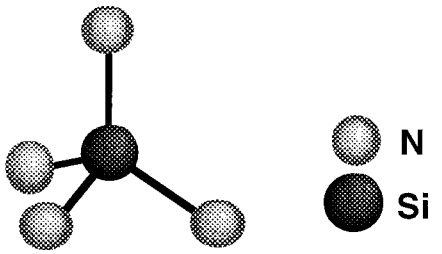

Fig.1-2 A tetrahedral basic unit of Si_3N_4 crystal.

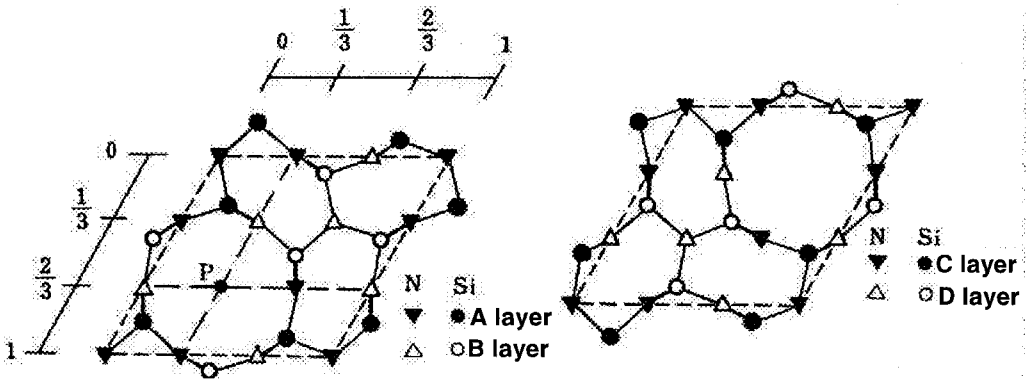

Fig.1-3 Ideal Si-N layers in α and β-Si_3N_4 : (a) AB layers, (b) CD layers.
the α and β -structure have ABCD and ABAB packings.

Table 1-1 Some physical physical and chemical properties of Si_3N_4 ceramics

Crystal structure[2]	hexagonal
Decomposition temperature[2]	1900°C
Bulk density	3.2 g/cm^3
Thermal conductivity (20°C)[2]	10-50 $Wm^{-1}K^{-1}$
Coefficient of thermal expansion (20-1000°C)	2.7-4.0 × 10^{-6} K^{-1}
Electric resistivity	10^{13}-10^{14} Ωcm

1. 2. 2 Sintering of Si_3N_4

Si_3N_4 Powder

The quality of the Si_3N_4 powder is a critical factor for the properties of the final component, and it is strongly dependent on the production technique and subsequent processing steps[3]. Four methods are known: nitridation method of silicon[4,5], carbothermal reduction[6], chemical vapor deposition (CVD)[7], and silicon diimide decomposition[8]. The synthesizing reactions are listed in Table 1-2. The desirable properties of the raw powder are fine particle and its narrow distribution, high purity, and high α-phase content. The particle shape and size, agglomeration and surface oxide phase also influence sinterability and mechanical properties of sintered ceramics. In this work, the starting Si3N4 powder is a α-Si3N4 powder, which is produced by silicon imide decomposition method. This method can provide a fine particle size, narrow size distribution, high purity, and high a-phase content powder.

Table 1-2 Typical synthesis methods of Si_3N_4 powders

Synthesis method	Chemical reaction
Nitridation method of silicon	$3Si + 2N_2 \rightarrow Si_3N_4$
Carbothermal reduction	$3SiO_2 + 6C + 2N_2 \rightarrow Si_3N_4 + 6CO$
Chemical vapor deposition	$3SiCl_4(g) + 4NH_3(g) \rightarrow Si_3N_4(s) + 12HCl(g)$
Silicon diimide decomposition	$3Si(NH)_2(s) \rightarrow Si_3N_4(s) + 2NH_3(g)$

Sintering of Si_3N_4 Ceramics

Very high temperature are usually required for sintering of Si_3N_4 because of its strong covalent bonding and steric structure, and consequently low self-diffusion and dislocation activities. In most cases, the fabrication of fully dense Si_3N_4 bodies is necessary to be processed by liquid-phase sintering, which enhances the mass transport of Si_3N_4. Al_2O_3-Y_2O_3[9], Y_2O_3[10] and MgO[11] are representative sintering additive for densification of Si_3N_4 ceramics.

Fig.1-4 shows schematic illustration of the sintering process of Si_3N_4. Generally, the liquid phase is formed at temperatures of around 1400 to 1600°C, which depends on the liquid phase composition. The α-Si_3N_4 dissolves in liquid phase and elongated β–Si_3N_4 grains precipitate from the liquid phase. After α-β transformation is complete, the elongated grains further grow during the sintering. The mechanical properties of sintered bodies are believed to be strongly dependent on the microstructure such as the grain size and aspect ratio of β–Si_3N_4 grains as well as the grain boundary phases[12,13,14,15].

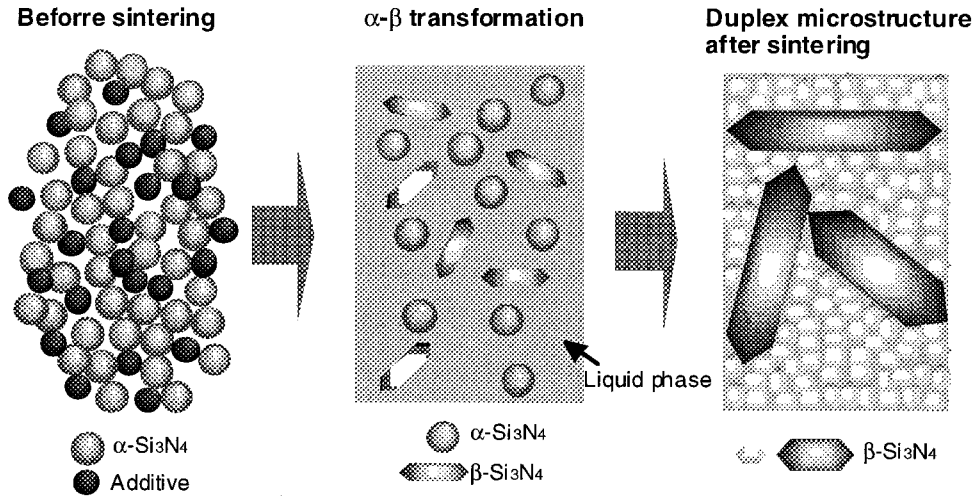

Fig.1-4 Schematic illustration of the sintering process of Si_3N_4.

1. 2. 3 Mechanical Properties of Si_3N_4 Ceramics

Si_3N_4 ceramic material is one of the most promising materials for high temperature structural applications because of their superior mechanical and thermo-mechanical properties. The mechanical properties of Si_3N_4 ceramics are strongly influenced by the microstructure.

Homogeneous microstructure shown in Fig.1-5(a) is usually developed when the β–Si_3N_4 powder is hot-pressed[16].On the other hand, heterogeneous microstructure with the rod -like grains is developed during sintering of α-Si_3N_4, as shown in Fig.1-5(b). It as well-known that the rod-like grains increase the toughness of the material. When α-Si_3N_4 powder is sintered at 1800-2000°C, some large elongated grains with high aspect ratios are developed between smaller equiaxial grains[17].These materials with duplex microstructures are known as " in - situ composites" or " self - reinforced materials" , and have high fracture toughness of 8-11 $MPam^{1/2}$[18,19,20].

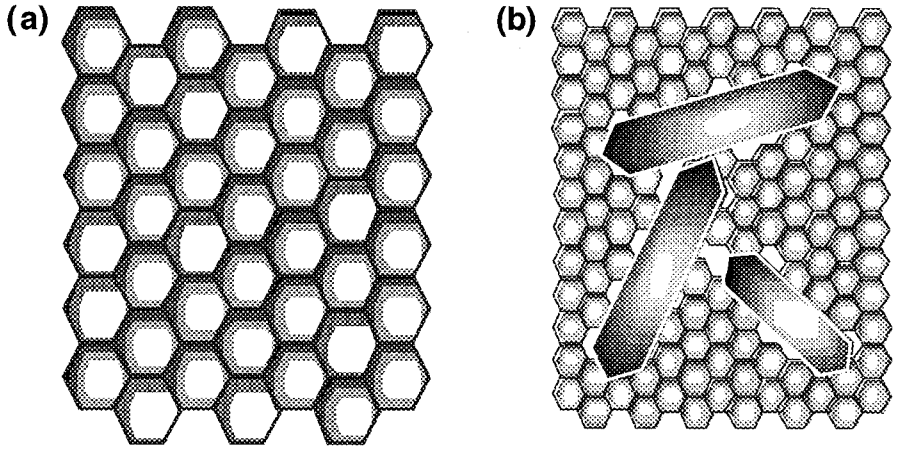

Fig.1-5 Representative microstructures of Si_3N_4 ceramics:
(a) homogeneous and (b) heterogeneous microstructures.

The rod-like grains achieve toughening of Si_3N_4 ceramics by crack bridging and crack deflection, only when cracks propagate along the grain interfaces. The bridging and pull out as toughening mechanism is illustrated in Fig.1-6(a). Generally, this mechanism can be observed in composite materials reinforced by whiskers or fibers. In case of Si_3N_4 ceramics, it is thought that the elongated grains between smaller equiaxial grains play the same role of the whiskers. For this mechanism, the interfacial friction between smaller grains and elongated grains is an important factor, particularly, in the pull out toughening mechanism. The crack deflection is also one of the toughening mechanism as shown in Fig. 1-6(b). The deflection results in toughening due to the reduced driving force on the deflected portion of the crack. A general and simple approach to estimate fracture strength is given by following equation[21]

$$\sigma_f = \frac{1}{Y} \bullet \frac{K_{Ic}}{\sqrt{c}}$$

where σ_f is strength, c is defect size, Y is shape factor of a defect and K_{IC} is fracture toughness.

As seen in this equation, the high strength of Si_3N_4 ceramics are attended by toughening. These excellent properties are one of the reasons why Si_3N_4 is selected as the matrix materials in this work. Table 1-3 shows some mechanical properties of Si_3N_4 ceramics.

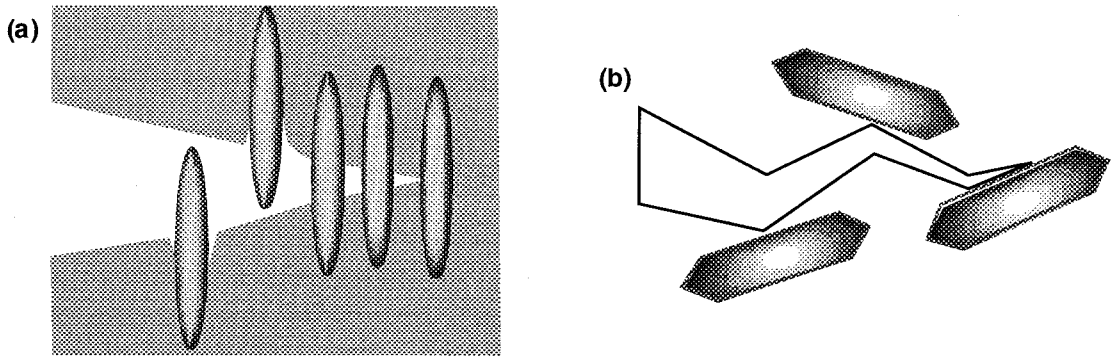

Fig.1-6 Toughening mechanisms of Si_3N_4 ceramics:
(a) crack bridging and (b) crack deflection.

Table 1-3 Mechanical properties of Si_3N_4 ceramics

Young's modulus[22]	240-330 GPa
Vickers hardness[23]	14-20 GPa
Fracture toughness	3-9 $MPam^{1/2}$
Fracture strength	400-1300 MPa

1. 3 Hexagonal BN

1. 3. 1 Crystal Structure of Hexagonal BN

Boron and nitrogen elements are neighbors to carbon in the periodic table, and form 1:1 compounds which are isostructural to the polymorphs of carbon:

h-BN: hexagonal modification with a layered structure similar to graphite, sometimes called " white graphite"

c-BN: high pressure diamond-like modification with cubic zinc blend structure.

w-BN: dense hexagonal modification with wurtzite structure.

Under normal conditions, h-BN is stable, but the other two main forms c-BN and w-BN with a tetrahedral distribution of atoms are stable at high pressures and temperatures as indicated in Fig 1-7. The hexagonal structure of boron nitride is constructed from layers consisting of a flat or nearly flat network of B_3N_3 hexagons with a bond length of 1.446Å and strong covalent bonds between boron and nitrogen atoms within the hexagons[24,25]. Unlike graphite, in boron nitride these hexagons are packed in the third 'c' dimension in such a way that the atoms stack in an orderly array on top of each other with alternating B and N atoms in each layer, as shown in Fig.1-7. Because of this alternation, the interlayer spacing is 1/2c = 0.333 nm and the bonds between layers are weak Van der Waals bond. In addition to structures above mentioned, BN has a semi-crystalline structure called 'turbostratic boron nitride (t-BN).This structure is analogous to turbostratic carbon black, and it can be defined as B_3N_3 hexagon layers stacked roughly parallel to each other with a random rotation and translation above the layer normal which indicates two-dimensional order of atoms. In particular, among several type of BN, h-BN has attracted an increasing interest because of its structure and properties analogue to graphite.

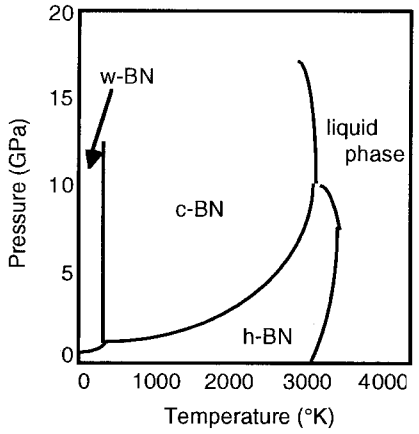

Fig. 1-7 Phase diagram of BN

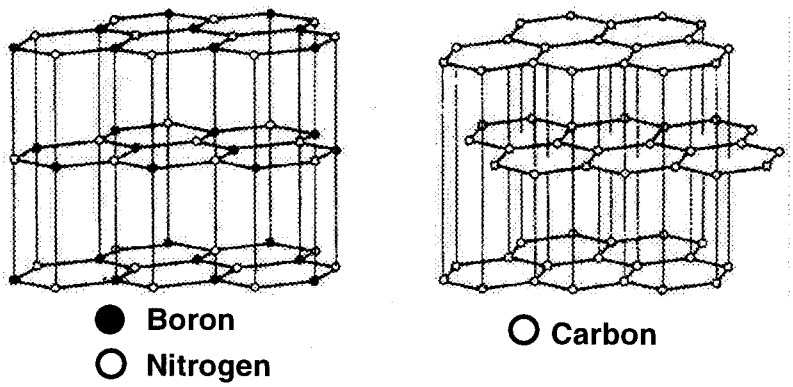

Fig.1-8 Schematic crystal structure of h-BN and graphite.

1. 3. 2 Properties of Hexagonal BN

Hexagonal BN is a widely used ceramic material with excellent properties such as high thermal shock resistance due to its high thermal conductivity, and high electrical resistivity at a wide temperature range. Furthermore, it is chemically inert to molten metals and glasses, organic solvents and acids, and also it keeps its chemical stability at high temperatures[26,27]. In consideration of these properties, the improvement of thermo-mechanical properties of ceramics can be expected by dispersion of h-BN. Some physical properties of h-BN are summarized in Table 1-4.

Table 1-4 Some physical properties of h-BN ceramics

Crystal structure	hexagonal
Decomposition temperature[28]	3300-3400 °C
Bulk density	2.2 g/cm^3
Thermal expansion coefficient[29]	$4.4 \times 10^{-6} K^{-1}$
Electric resistivity	6.3×10^{13} Wcm
Young's modulus	32 GPa
Thermal conductivity	50 $\Omega m^{-1}K^{-1}$
Fracture e strength	60 MPa

1. 4 Ceramic Composites

Ceramic composites can be classified into two types of microcomposite and nanocomposites. The microcomposites have the microstructure, in which micro-sized second phases such as particulate, platelet, whisker and fiber are dispersed at the grain boundaries of the matrix. The main purpose of these composites is to improve the fracture toughness. On the other hand, the nanocomposites can be divided into four types of intragranular, intergranular, intra/intergranular mixed nanocomposite and nano/nano composite as shown in Fig.1-9[30,31,32,33,34,35]. In the intragranular and intergranular nanocomposites, the nano-sized particles are dispersed within the matrix grains and at the grain boundaries, respectively. In the real powder mixing processes, the intra/intergranular mixed nanocomposites are usually obtained. The aims of intragranular dispersions are the dislocation generation and its pinning

during the cooling down process from fabrication temperatures and/or in-situ control of size and shape of matrix grains. The former role of nano dispersoids is important for the oxide ceramics such as Al_2O_3 and MgO which become ductile at high temperatures, while the latter role is significant for the nonoxide ceramics such as Si_3N_4 and SiC with strong covalent bonding even at high temperatures. The intergranular nanodispersoids must play important role in the grain boundaries structure control of oxide and nonoxide ceramics, which gives the improvement of high temperature mechanical properties. In the nano/nano composites, both phases are composed of only nano-sized grains, and the main purpose of this special nanocomposites is to give new functions such as machinability and superplasticity like metals.

Recently, the excellent mechanical and thermo-mechanical properties of the intra/intergranular type of Si_3N_4/SiC nanocomposites have been reported[36,37,38]. The control of these microstructure will be important to improve the properties in this work.

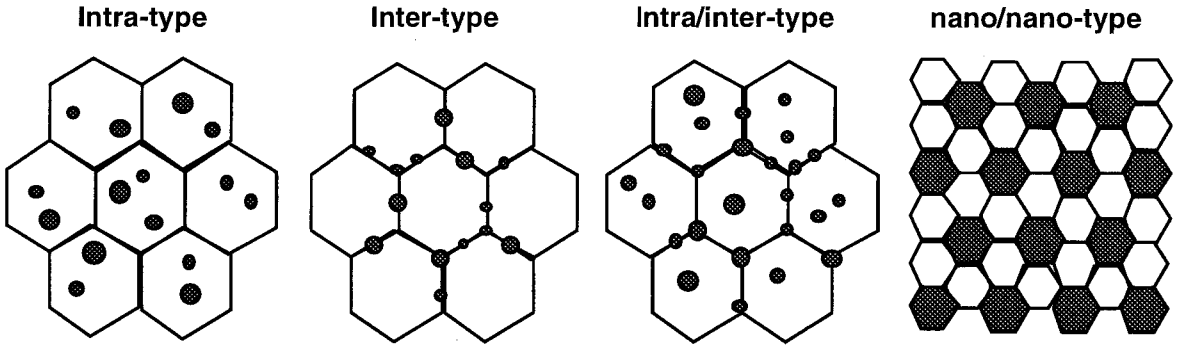

Fig.1-9 Schematic drawings of ceramic based nanocomposites

1. 5 Objectives

In view of the background mentioned above, in the present work, nano-sized h-BN dispersed Si_3N_4 based composites, which are potential to improve thermal shock fracture resistance and machinability as well as high temperature mechanical properties, were investigated. The objective of this work is to find a new process to homogeneously disperse fine h-BN particulates into the Si_3N_4 matrix and to achieve the improvement of mechanical and thermo-mechanical properties and machinability. Additionally, the relationship between the microstructure and the mechanical properties was discussed to clarify the mechanism of the improvement.

The contents of this thesis are as follows.

In this chapter, the properties of Si_3N_4 and BN and the outline of ceramic composites

were reviewed, and the objectives and contents of this work were described.

In the Chapter 2, the Si_3N_4/BN microcomposites were fabricated by using the conventional powder metallurgical fabrication process of commercially available α-Si_3N_4 and h-BN powders. And a new process and structure were also discussed to further improve the mechanical properties of the conventional microcomposite.

In the Chapter 3, the fabrication of the Si_3N_4/BN nanocomposites, in which the nano-sized h-BN particles were homogeneously dispersed within Si_3N_4 grains as well as at the grain boundaries, was attempted by using the chemical process, and their mechanical properties were evaluated.

In the Chapter 4, the thermal shock fracture resistance of Si_3N_4/BN composites were determined. In addition, the coefficient of thermal expansion and Poisson's ratio , which influence to thermal shock fracture resistance, were also measured to elucidate the mechanism of high thermal shock fracture resistance for the nanocomposites.

In the Chapter 5, the high temperature mechanical properties such as high temperature strength, hardness and Young's modulus were studied. The effect of nano-sized h-BN particles, which possesses excellent thermo-mechanical properties, were discussed on the properties of Si_3N_4/BN composites at elevate temperatures.

In the Chapter 6, the machinability of Si_3N_4/BN composites was evaluated. Special emphasis was placed on understanding the effect of micro and nanostructure on the machinability. In order to make clear the deference of deformation mechanism by machining, Hertzian contact test was carried out.

In the Chapter 7, the result of the present work are summarized and some visions in applications of Si_3N_4/BN nanocomposites were described.

References

[1] K. H. Jack, J. Mat. Sci., 11(1976)1135-1158

[2] G. Ziegler, J. Heinrich and G. Wotting, J. Mater. Sci., 22(1987)3041-86

[3] M. L. Torti, Structural Ceramics,29(1998)161

[4] D. R. Messier, P. Wong and A. E. Engram, J. Am. Ceram.,56(1973)171

[5] W. Naruse, M. Nojiri and M. Tada, J. Jpn. Inst. Metals, 35(1971)731

[6] K. Komeya and H. Inoue, J. Mater.Sci.,10(1976)1243

[7] A. Kato, Y. Ono, S. Sawazoe and K. Morida, J. Cerm. Soc. Japan, 80(1972)114

[8] K. S. Mazdniski and C. M. Cooke, J. Ame. Ceram. Soc., 56(1973)628

[9] A. Tsuge and K. Nishida, Am. Ceram. Soc. Bull.,57(1978)424-426

[10] A. Tsuge ,K. Nishida and M. Komatsu, J. Am. Ceram. Soc.,58(1975)323-3266
[11] K. Tsukuma, M. Shimada and M. Koizumi, Am. Ceram. Soc. Bull.,60(1981)910-912
[12] Y. -W. Kim, M. Mitomo and N. Hirosaki., J. Mater. Sci., 30(1995)5178-5184
[13] M. Mitomo and S. Uesono, J. Am. Ceram. Soc.,75(1992)103-108
[14] M. Mitomo, N. Yang, Y. Kishi and Y. Bando, J. Mater. Sci., 23(1988)3413-3419
[15] T. Kawashima, H. Okamoto, H. Yamamoto and K. Kitamura, J. Ceram. Soc.Japan, 99(1991)320-323
[16] F. F. Lange, J. Am. Ceram. Soc., 56(1973)518-522
[17] M. Mitomo and K. Mizuno, Yogyo-Kyoukai-Shi, 94 (1986) 106-111
[18] E. Tani, S. Umebayashi, K. Kishi, K. Kobayashi and M. Nishijima, Am. Ceram. Soc. Bull. 65 (1986)1311-15
[19] C-W. Li and J. Yamanishi, Ceram. Eng. Sci. Proc., 10 (1989) 632-645
[20] T. Kawashim, H. Okamoto, H. Yamamoto and A. Kitamura, J. Ceram. Soc. Japan, 99(1991)320-323
[21] A. A. Griffith, Roy. Soc. Lond. A221(1924)163
[22] A. Giachello, P. C. Martinengo and G. Tommassini, Am. Ceram. Soc. Bull.,59(1980)1212-1215
[23] N. Uchida, M. Koizumi and M. Shimada, J. Am. Ceram. Soc., 68(1985)c-38-40
[24] R. S. Pease, Nature,165 (1950) 722-723
[25] R. S. Pease, Acta Cryst.,5 (1952) 356-361
[26] Ceramic Industry, 138 (1992) 46
[27] K. A. Schwetz, Ullman' s Encyclopedia of Industrial Chemistry, A4 (1985) 295-307
[28] H. Hagiwara, H. Tanzi and S. Tamaki, Ceramic Data Book, (1986)85-93
[29] A. Lipp, K. A. Schwetz and K. Hunold, J. Euro. Ceram. Soc.,5(1989)3-9
[30] K. Niihara, J. Ceram. Soc. Japan, 99 (1991) 974
[31] K. Niihara, K. Suganuma and K. Izaki, J. Mater. Sci.,9 (1990)112
[32] F. Wakai, Y. Kodama, S. Sakaguti, N, Murayama, K. Izaki and K. Niihara, Nature, 344 (1990) 421
[33] A. Nakahira and K. Niihara, J. Ceram. Soc. Japan, 100 (1992) 448
[34] T. Ohji, Y. -K. Jeong, Y. -H. Choa and K. Niihara, J. Am. Soc.,77(1994)3259
[35] T. Sekino and K. Niihara, Nanostructured Materials, 6(1995)663
[36] K. Niihara, T. Hirano, K. Izaki and F. Wakai, Ceram. Trans.,42(1994)207-219
[37] T. Hirano and K. Niihara, Mat. Lett.,22(1995)249-254
[38] T. Hirano and K. Niihara, Nanostructured Materials, 5(1995)808-818

Chapter 2

Conventional Si_3N_4/BN Microcomposites Fabricated by Powder Metallurgical Process

In order to get informations on the microstructure and new fabrication process of Si_3N_4/BN composites with excellent properties, Si_3N_4/BN microcomposites were fabricated by a conventional metallurgical process, in this chapter, and their microstructure - mechanical property relationship was investigated.

2. 1 Introduction

Si_3N_4 ceramics have excellent properties, i. e., high strength, relatively high toughness and high wear resistance. The expansion of application of Si_3N_4 ceramics has been expected especially in the field of engineering ceramics. However, such properties as corrosion resistance to molten metal, thermal shock resistance and machinability are not sufficient for their practical use to various machine parts. In order to improve these disadvantageous properties of monolithic Si_3N_4 ceramics, several attempts have been made to disperse hexagonal BN (h-BN) particles in the Si_3N_4 matrix as a second phase[1, 2, 3]. the h-BN possesses a number of interesting properties such as high thermal conductivity, low coefficient of thermal expansion and chemical inertness. These properties have led to its use in a variety of specialized high-temperature areas including crucibles for molten metals, thermocouple protection tubes, and break rings for horizontal continuous casting of steels.

Recently, a number of scientists and engineers have shown that the thermal shock resistance of ceramic materials such as Al_2O_3, $3Al_2O_3 \cdot 2SiO_2$, Si_3N_4, SiAlON and AlON can be enhanced by the addition of BN[4, 5, 6, 7, 8, 9]. In these studies, however, the composite materials were porous and their fracture strength was extremely low, due to the conventional pressureless sintering[10, 11, 12].

The purposes of this chapter were to fabricate the Si_3N_4/BN composites by using conventional metallurgical process including the hot-press sintering which promote densification and then improvement in the mechanical properties, and to investigate the correlation between the microstructure and the fracture strength to find the information on the microstructure which makes possible to enhance the mechanical properties.

2. 2 Experimental Procedures

2. 2. 1 Fabrication

The experimental procedure is schematically shown in Fig. 2-1. The starting powders for the composites were the commercially available α-Si_3N_4 powder having an average particle size of 0.2 μm (Ube Industries Co. Ltd., Ube, Japan, E-10 grade) and h-BN powder having an average grain size of 9 μm (Denka Co. Ltd., Tokyo, Japan, GP grade). The properties of powders used in this experiment are listed in Table 2-1.

The compositions containing various volume fraction of h-BN powder (0 to 40 vol%) and 2 wt% Al_2O_3 (Taimei Chem. Co. Ltd., Nagoya, Japan, TM-DAR grade) and 6 wt% Y_2O_3 (Nippon Yttrium Co. Ltd.,Tkyo, Japan, RU grade) as the sintering aids were mixed by the conventional wet ball milling method with α-Si_3N_4 powder in ethanol for 24 h using Si_3N_4 balls to ensure the homogeneity of mixed powders. After wet ball-milling, the mixed slurry were dried, and then the mixed powders were dry-ball milled for 6 h to eliminate hard agglomeration. The dried mixtures were placed in a graphite die coated with BN slurry to avoid reaction between the powder and die. The hot press sintering was performed at 1750 °C in nitrogen atmosphere under 30 MPa of applied pressure. Hot-pressing time for the composites containing 0 - 40 vol% of h-BN were changed depending on the BN content from 1h to 4h, to densify and enhance the transformation from α-Si_3N_4 to β-Si_3N_4 entirely. The details of hot pressing program is shown in Fig. 2-2. The heating rate was 15 and 10°C/min from room temperature to 1100°C and from 1100°C to a desired sintering temperature, respectively. The retention time was at 1450°C for 4h to eliminate residual humidity of the dried mixture. The pressure of 30 MPa was applied after holding at 1450°C, and nitrogen gas was introduced at the same time. The obtained hot-pressed sample which was 44 mm in diameter 5 mm in thickness was cut with a diamond saw, ground with a diamond whetstone and polished with 0.5 μm diamond slurry to rectangular bars with 3 x 4 x 37 mm. Surface perpendicular to hot-pressing direction was mainly used for various evaluations of mechanical properties.

2. 2. 2 Characterization

Relative Density

Bulk density was measured by the Archimedes immersion method in toluene at room temperature. The relative density was determined by dividing apparent density by the

theoretical density calculated by assuming the specific gravity of β- Si_3N_4, h-BN, Al_2O_3 and Y_2O_3 to be 3.192, 2.29, 3.987 and 5.031 g/cm^3, respectively.

Young's Modulus

The specimens (3 x 4 x 36 mm) were coated by a carbon painting on one side in order to act as an electrode and then suspended by two thin tungsten wires in correspondence of the nodal points. Flexural vibrations were generated by electrostatic force and resonance frequencies were determined by using an oscilloscope. Young's modulus, E, was calculated by the following equation 2-1,

$$E = 0.9465 \times \frac{M \cdot f^2}{w}\left(\frac{l}{t}\right)^3\left\{1 + 6.59\left(\frac{t}{l}\right)^2\right\} \qquad (2\text{-}1)$$

where M. w, t, l and f are the mass, the width, the thickness, the length of the specimen and the resonance frequency obtained, respectively.

Fracture Strength

The fracture strength was evaluated by a three-point bending test using universal testing machine (Autograph, AG-10TC, Shimadzu Co. Ltd., Kyoto, Japan). The tensile surfaces of specimens were perpendicular to the hot-press direction. Edges were chamfered to eliminate machining flaws that could act as fracture origins. The span length and crosshead speed were 30 mm and 0.5 mm/min, respectively. The fracture strength by the three point bending was calculated with the following equation 2-2:

$$\sigma_f = \frac{3PL}{2bd^2} \qquad (2\text{-}2)$$

where P is the fracture load (N), L is the span, and b and d are the width and thickness of the specimen, respectively.

X-ray Powder Diffraction

The crystalline phases of the hot pressed samples were identified by X-ray powder diffraction analysis (50kV-150mA, RU-200B, Rigaku Co. Ltd., Tokyo, Japan). The X-ray diffraction pattern was taken using Ni filtered CuKα radiation (λ = 1.5418 Å). The scanning rate of 2θ angle was 4° per minute. The identification of phase in sintered specimens was referred to JCPDS (Joint Committee of Powder Diffraction Standards) data.

Microstructure Analysis

For microstructural observation by scanning electron microscopy (SEM, S-5000, Hitachi Co. Ltd., Hitachi, Japan), the specimens were ground with a diamond wheel, and were finally polished by 0.5 μm diamond paste. The polished specimens were chemically etched with NaOH at 350 °C for 3 min. The distribution of h-BN particles and the interfaces of Si_3N_4/BN were identified by transmission electron microscopy (TEM, H-8100, Hitachi Co. Ltd., Hitachi, Japan). Specimens for TEM were thinned to electron transparency by mechanical grinding followed by ion beam milling (model 600, Gatan Inc., U. S. A.).

2. 3 Results and Discussion

2. 3. 1 Microstructure

The crystal phases in the present composite ceramics identified by XRD were β-Si_3N_4 and h-BN in the region of 10-40 vol% BN addition.

Fig. 2-3 shows representative SEM pictures of chemically etched surfaces perpendicular to the hot-press direction for the monolithic Si_3N_4 and the composite containing 15 vol% BN. The Si_3N_4/BN composites fabricated by the conventional metallurgical process under hot-pressing indicated a typical microcomposite structure in which micro-sized h-BN grains dispersed at the grain boundaries. TEM observation indicated that apparent impurity phases were not observed between Si_3N_4 and h-BN as shown in Fig. 2-4. Furthermore, TEM observation revealed that in h-BN grain delaminations of basal plain were caused perpendicular to c axis direction. These delaminations are characteristic for the composites containing h-BN, and can be thought to be generated by thermal expansion mismatch between h-BN and β-Si_3N_4.

2. 3. 2 Density

Fig. 2-5 showed the variation of relative density with BN content for the Si_3N_4/BN composites. The relative density of the composite decrease with an increase in BN content. In all compositions, the composites could not be fully densified by further sintering. The low density observed in the composite may be due to microcrack or spontaneous microcrack generated within h-BN grains by deramination, which caused by thermal expansion mismatch between h-BN and β-Si_3N_4, as shown in Fig. 2-4. Based on the calculation from the observed

relative density and composition, it is deduced that h-BN particles including porosity of 7 % were dispersed into the Si_3N_4 matrix in the Si_3N_4/BN composites.

2. 3. 3 Mechanical Properties

Fig. 2-6 shows the variation in Young's modulus with the BN content for Si_3N_4/BN composites. As expected from the rule of composites, Young's modulus of the composites decreased with an increase in BN content because of the softening of h-BN (Young's modulus of h-BN is about 65 GPa). Also, Fig. 2-6 shows bending strength at room temperature. The bending strength of monolithic Si_3N_4 was about 1350 MPa . By adding 5 vol% BN, the strength remarkably decreased to 880 MPa. Fig. 2-7 shows the polished specimen surface of monolithic Si_3N_4 and Si_3N_4/15vol%BN composites. A number of small and large flaws were observed in the composites which were prepared from the commercially available h-BN powder with average grain size of 9 μm, whereas the monolithic Si_3N_4 did not show such flaws. It is thought that these flaws could be due to the missing or pull-out of h-BN particles or agglomerations of them. Furthermore, SEM observation of fracture origin for Si_3N_4/15vol%BN composite indicated that larger h-BN particles or aggregations of them initiated fracture, as shown in Fig. 2-8. From these result, h-BN particle might act as a processing defect because of its low Young's modulus and delaminations within it. The sudden decrease in bending strength for the composites may be attributed to the larger size of flaw which consists of h-BN particle or its agglomeration. There is a limit to homogeneously disperse fine powder by using the conventional ball milling, when commercially available Si_3N_4 and h-BN powders were used as starting materials. To improve the mechanical properties of Si_3N_4/BN composites, therefore, the development of fine h-BN particles dispersed Si_3N_4 based composite was desired. One of the new approaches for fine second phase dispersion technique is nanocomposite technology, and then in next chapter the processing and mechanical properties of Si_3N_4/BN nanocomposites were described.

2. 4 Conclusions

Si_3N_4/BN composites fabricated by the conventional metallurgical process under hot-pressing indicated a typical microcomposite structure in which micro-sized h-BN grains dispersed at the grain boundaries. The bending strength of the composite suddenly decreased with BN contents. This sudden decrease was due to the large h-BN particles or their agglomerations which act as processing defects. These results suggest that the homogeneous

dispersion of fine h-BN particles is strongly required to improve the mechanical properties of Si_3N_4/BN composites.

Reference

[1] M. Iwasa S. Kakiuch, Yogyo-Kyokai-shi, 93(1985)661-665

[2] K. S. Mazdiyansni and R. Ruh, J. Amer. Ceram Soc.,64(1981)415-419

[3] K. Niihara, L. D. Bentsen and D. P. H. Hasselman, J. Am. Ceram. Soc., 64(1981)c117-118

[4] D.lewis and R. W. Rice, Ceram. Eng. Sci. Proc., 2(1981)712

[5] D. Lewis, R. P. Ingel, W.j. McDonoughs and R. W. Rice, Ceram. Eng. Sci. Proc., 2(1981)719

[6] D. Goeuriot-Launay, G. Brayet and F. Thevenot, J. Mater. Sci. Lett., 5(1986)940

[7] W. Sinclair and H. Simmons, J. Mater. Sci. Lett., 6(1987)627-629

[8] A. Shimpo, H. Ide and M. Ueki, J. Ceram. Soc. Jpn., 100(1992)504-508

[9] G. Peizhi and L. Wenhong, Proceedings of the World Congress on High Technology Ceramics.

[10] T. Funabashi, K. Isomura, A. Harita and R. Uchimura, p. 968-976 (1986), Ceramic materials and Components for Engines. Edited by V. J. Tenney, Amer. Ceram. Soc.,Las Vegas, NV, 1988.

[11] A. Miyamoto, M. Ishikawa, M. Nishi, T. Ishizawa and A. Shironita, Jpn. Tokkyo Koho JP60-2 2,676(85-22, 676), 3 Jun 1985

[12] K. Ixhikawa and K. Katayama, Jpn. Kokai Tokkyo Koho JP63-40, 771(88-40, 771), 22 Feb, 1988

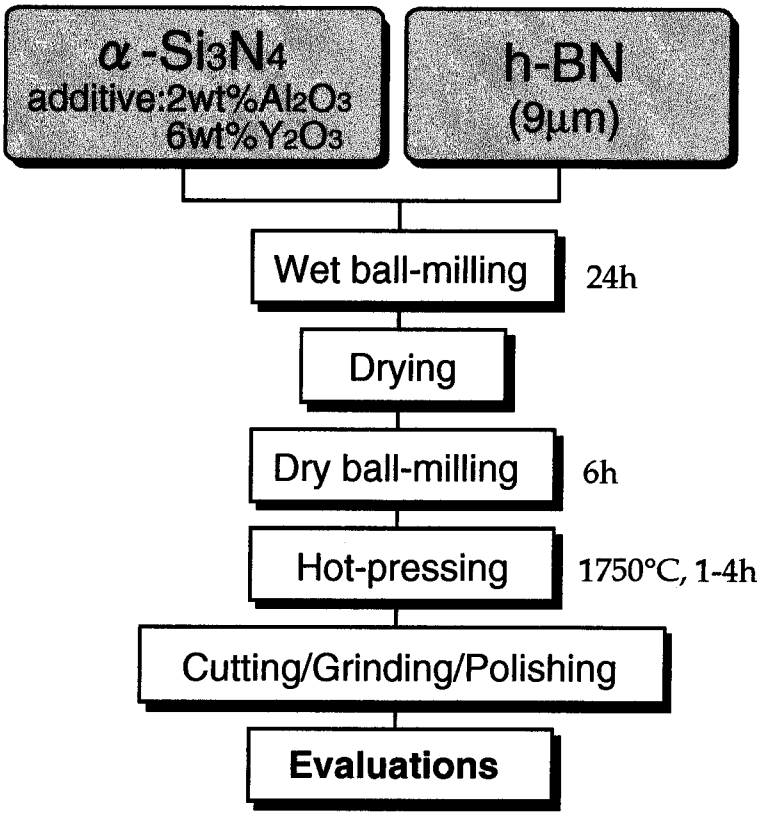

Fig. 2-1. Flow chart of conventional powder metallurgical fabrication process.

Table 2-1. Some properties of starting powders

	Si_3N_4 (E10)	BN (GP)
crystal structure	α-Si_3N_4 > 95%	h-BN
chemical composition (wt%)	N>38.0 O 1.45 C 0.30 Al<0.001 Ca<0.001 Fe<0.001	B_2O_3 0.05 Fe 20 ppm
specific surface area (m^2/g)	10.9	4.9

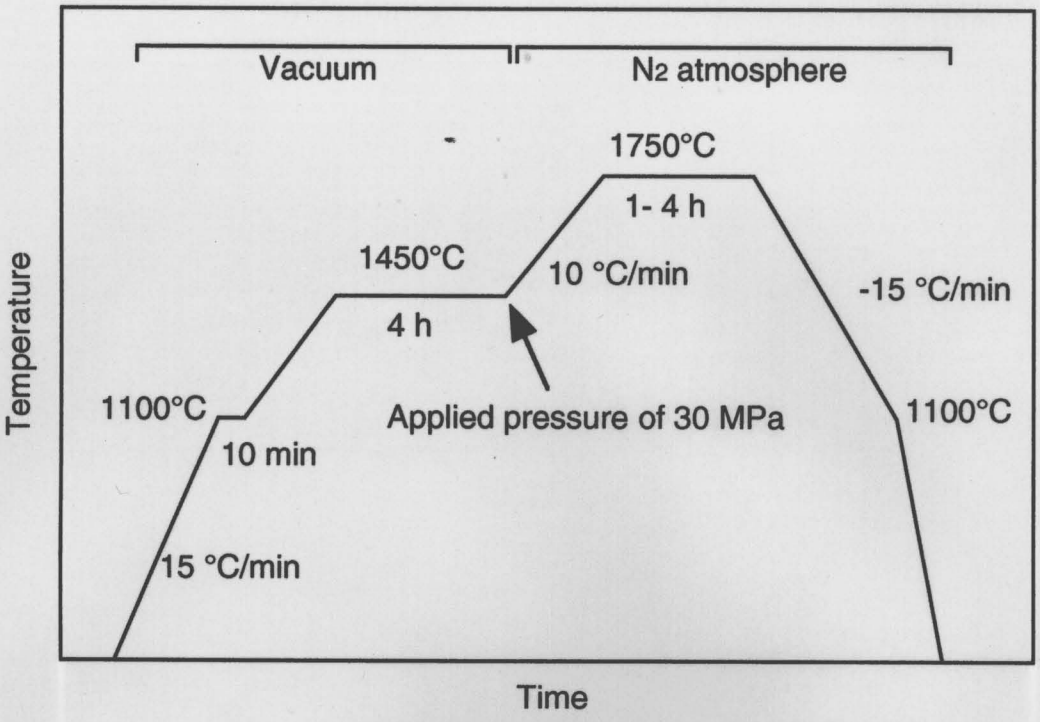

Fig. 2-2. Hot-pressing program

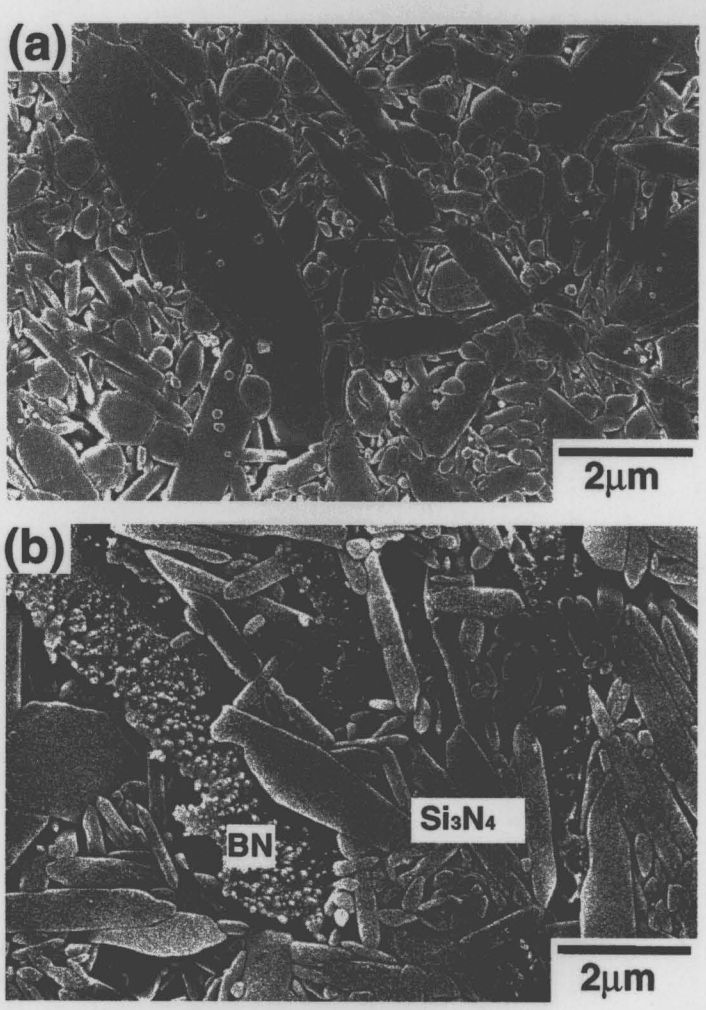

Fig. 2-3 SEM micrographs of polished and etched surface perpendicular to the hot-pressing direction.

(a) Monolithic Si_3N_4

(b) Si_3N_4/15vol%BN microcomposite

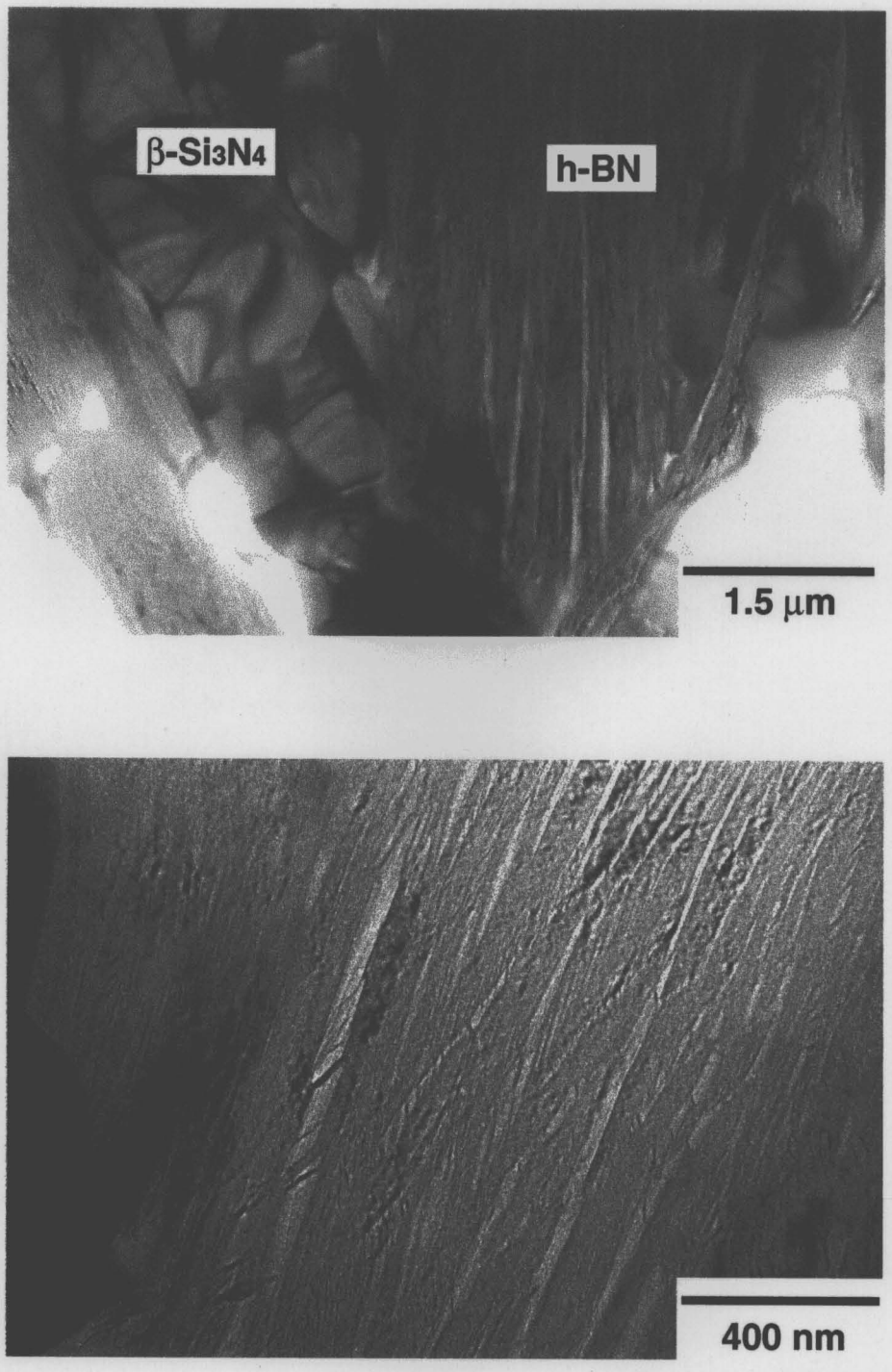

Fig. 2-4 TEM observations of Si_3N_4/15vol%BN microcomposite.

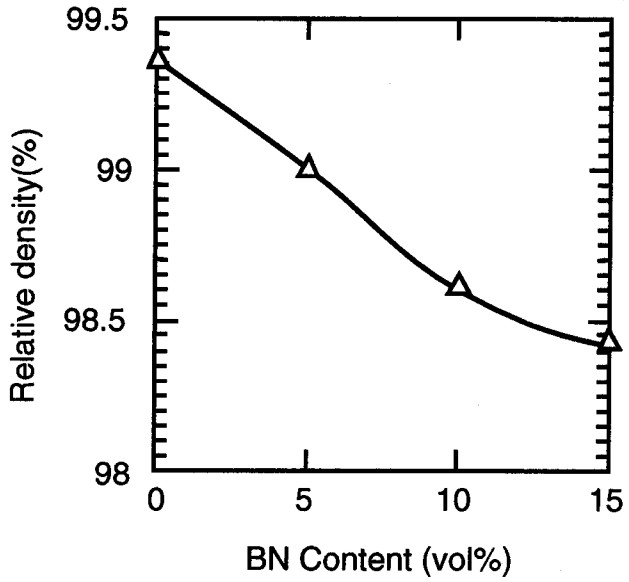

Fig. 2-5 Variation of relative density with BN content for Si_3N_4/BN composite.

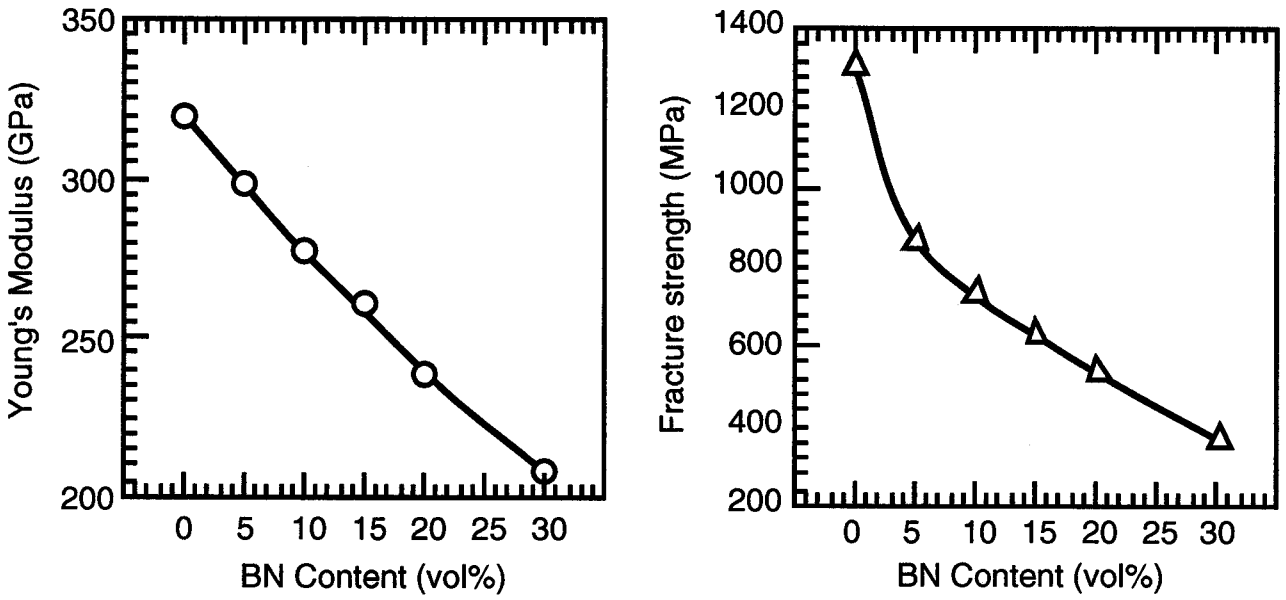

Fig. 2-6 Effects of h-BN content on fracture strength of microcomposites.

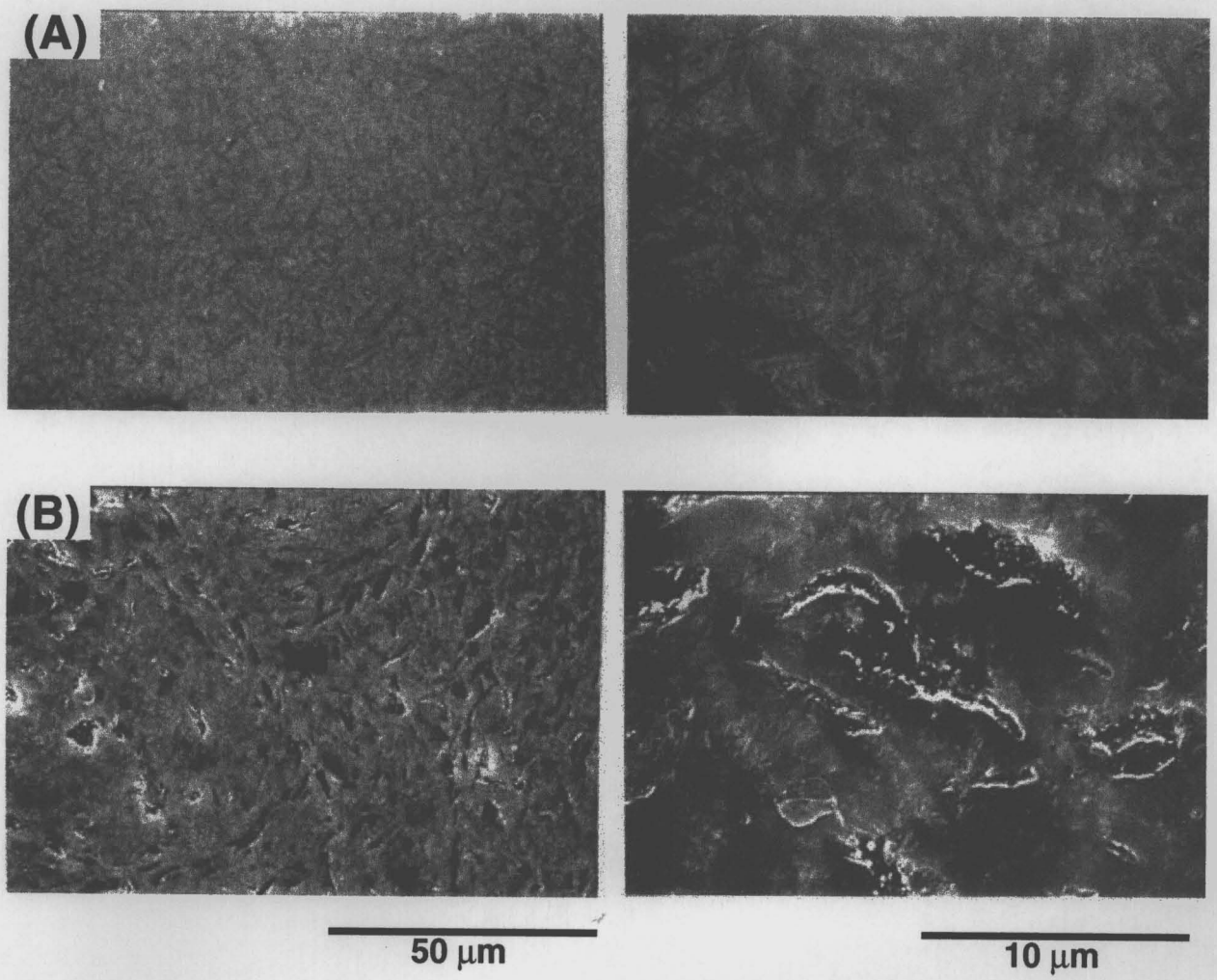

Fig. 2-7 SEM observations of polished surfaces for monolithic Si_3N_4 (A) and Si_3N_4/15vol%BN microcomposite (B).

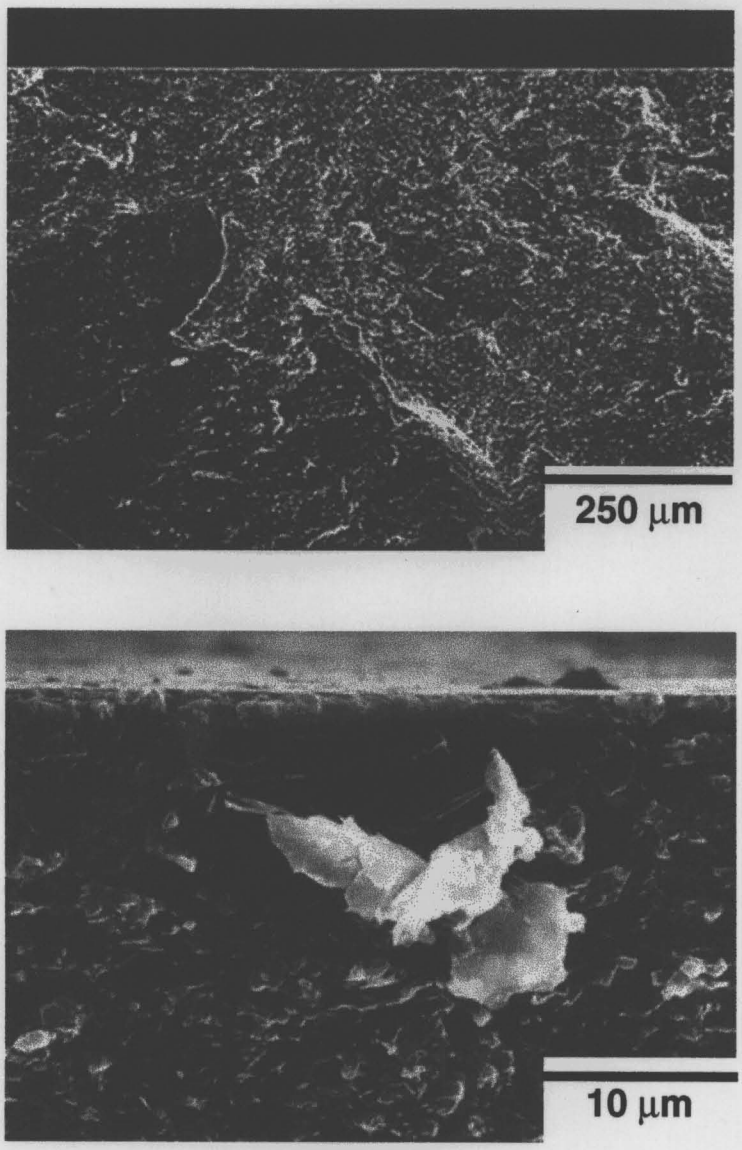

Fig. 2-8 Fracture origin of Si_3N_4/BN microcomposite.

Chapter 3

Si_3N_4/BN nanocomposite Fabricated by Chemical Process

The novel chemical process for fabrication of Si_3N_4/BN nanocomposite was devised to improve the mechanical properties. The Si_3N_4/BN nanocomposites containing 0 to 40 vol% h-BN were successfully fabricated by hot-pressing α-Si_3N_4 powders, on which t-BN with disordered layer structure was partly coated. The t-BN coating on α-Si_3N_4 particles was prepared by heating α-Si_3N_4 particles covered with a mixture of boric acid and urea at 1100°C for 8h in hydrogen gas. TEM observations of this nanocomposite revealed that the nano-sized hexagonal BN (h-BN) particles were homogeneously dispersed within Si_3N_4 grains as well as at grain boundaries.

As expected from the rule of composite, Young's modulus of both micro- and nanocomposites decreased with an increase in h-BN content, while the fracture strength of the nanocomposites prepared in this work was significantly improved, compared to the conventional microcomposites. The strongly improved fracture strength for the Si_3N_4 nanocomposites was chiefly attributed to the reduction of flaw size which was induced from the inhibition of matrix grain growth by the nano-sized BN dispersions.

3.1 Introduction

As possible candidates for structural ceramics in 21th century, Si_3N_4 ceramics have attracted many attentions. Si_3N_4 ceramics are material with high strength, excellent toughness, high wear resistance and good oxidation resistance, and their applications have been extended especially in the field of engineering ceramics. On the other hand, h-BN is well-known as a material with notable properties such as excellent corrosion resistance to molten metal, high thermal shock resistance and machinability. This combination of the relative properties in Si_3N_4 /h-BN system has been attempted by many scientists[1,2]. But the remarkably decrease in fracture strength with an increase in BN content has been observed[3]. This decrease in fracture strength of the conventional Si_3N_4/BN composites is thought to be caused by the aggregation of h-BN particles resulting from the mixing of commercial powders. Therefore, homogeneous dispersions of second phase in the matrix is probably effective for

enhancing the mechanical properties.

Recently, Niihara and his colleagues have investigated nanocomposites in which the nano-sized particles are dispersed within the matrix grains and/or at the grain boundaries[4,5,6,7,8,9,10]. They revealed that the nanocomposites exhibited the improved mechanical properties. In early nanocomposites, hard and strong dispersoids were mainly incorporated into the matrix to improve the mechanical properties. But in later years soft and weak materials like metals have also been used as dispersoids, and the enhancement of the fracture strength was also found even by addition of soft and weak dispersoids[11,12,13]. These results imply that the nano-sized h-BN dispersion could be expected to improve the mechanical properties of Si_3N_4 ceramics, if the homogeneous dispersion of nano-sized BN is realized in the composites. However, it has not been reported that the mechanical properties of Si_3N_4 ceramics were improved by nano-sized soft and weak ceramic dispersoid such as h-BN.

The purpose of this study is to find a new process to homogeneously disperse fine h-BN particles in the Si_3N_4 matrix, and to investigate the microstructure and the mechanical properties, additionally to elucidate the strengthening mechanism of the nanocomposites.

3.2 Approach to Si_3N_4/BN Nanocomposite

It is difficult to homogeneously disperse fine h-BN particles into the matrix Si3N4 powder by using the conventional powder mixing method like a ball-milling method. Besides, the pure and fine h-BN powder is not commercially available. In order to have the microstructure with homogeneous dispersion of h-BN into Si_3N_4 ceramics, the new synthetic method are needed to be developed. Thus, we proposed a novel chemical process to precipitate the h-BN precursor, which is soluble in any solvent and can readily changed to the h-BN, on the α-Si_3N_4 particles. Boric acid is very suitable as a boron source of h-BN as previously described. Fig. 3-1 shows the formation schematics of α-Si_3N_4/BN-precursor composite powders and Si_3N_4/BN nanocomposites. It has been reported that h-BN is synthesized by reducing a mixture of boric acid and nitrogen compound in ammonia gas [14,15,16,17]. In this study, the reduction method to use urea as a nitrogen source was chosen, because urea is harmless and soluble in various solvents, and it produces little impurity during the synthesis of h-BN.

3.3 Experimental Procedures

3. 3. 1 Fabrication

In this method, the boric acid and urea were selected for producing the BN precursor coating films on α-Si_3N_4 powders. The starting powders for the composites were the commercially available α-Si_3N_4 powder having an average particle size of 0.2 μm (Ube Industries Co., Ltd., Ube, Japan, E-10 grade) and boric acid (Wako Pure Chemical Industries Ltd., Tokyo, Japan, Reagent grade) and urea (Wako Pure Chemical Industries Ltd., Tokyo, Japan, Reagent grade) as the BN precursors.

The experimental procedure is presented schematically in Fig. 3-2. The BN content was adjusted to be 5, 10, 15, 20, 30 and 40 vol%. In this new process, α-Si_3N_4 powder, boric acid and urea were mixed by the conventional wet ball milling method with Si_3N_4 balls and ethanol in a plastic bottle for 24h to ensure the homogeneity of mixed powders. Before drying, a small amount of ion exchanged water was added to the slurry to completely dissolve boric acid and urea and to prevent boric acid from evaporating. The dried mixtures were reduced at 1100°C in hydrogen gas, and then heated at 1500°C in nitrogen gas to produce the Si_3N_4-BN composite powder. The composite powders were ball-milled with the sintering aid (2 wt% Al_2O_3 + 6 wt% Y_2O_3) for 72 h. After second step of ball-milling, the slurry were dried, and then the powders were dry-ball milled for 6h to eliminate hard agglomerations. For comparison, the commercially available BN powder with an average grain size of 9 μm was also used to fabricate Si_3N_4/BN microcomposites.

The dried mixtures were placed in a graphite die coated with BN slurry to avoid reaction between the powder and die. Hot pressing was performed at 1750°C in nitrogen atmosphere under 30 MPa of applied pressure. Hot-pressing time for the composite containing 0 to 20, 30 and 40 vol% of h-BN were set to be 1h, 3h and 4h to densify and to entirely transform α-Si_3N_4 into β-Si_3N_4, respectively. The details of hot pressing program is shown in Fig. 2-2. The heating rate was 15 and 10°C/min from room temperature to 1100°C and from 1100°C to sintering temperature, respectively. The retention time at 1450°C was for 4h to eliminate residual humidity of the dried mixture. The pressure of 30 MPa was applied after holding at 1450°C, and nitrogen gas was introduced at the same time.

The obtained hot-pressed sample which was 44 mm in diameter and 5 mm in thickness was cut with a diamond saw, ground with a diamond whetstone and polished with 0.5 μm diamond slurry to rectangular bars with 3 x 4 x 37 mm. Surface perpendicular to hot-pressing direction was used for various evaluations of mechanical properties.

3. 3. 2 Evaluation

Bulk density was measured by the Archimedes immersion technique in toluene. The fracture toughness was estimated by indentation microfracture method with 196 N load[18]. The fracture strength was evaluated by a three-point bending test at room temperature. The tensile surfaces of specimens were perpendicular to the hot-pressing direction. The span length and crosshead speed were 30 mm and 0.5 mm/min, respectively. The crystalline phase of the reduced composite powders and the hot-pressed samples were determined by X-ray diffraction analysis (XRD). The microstructure was observed by scanning electron microscope (SEM) and a transmission electron microscope (TEM). The microchemical analysis was done using an energy dispersive X-ray (EDX) analyzer attached to TEM. These measurement methods are described in detail in the previous chapter.

Image Analysis

The grain size and its distribution were deduced from SEM photographs of chemically etched specimen surfaces by an image analysis technique (NIH image written by Wayne Rasband at U.S. National Institutes of Health and available from the Internet by anonymous ftp from zippy.nimh.nih.gov or on floppy disk from NIST, 5285 Port Royal Rd., Springfield, VA22161, part number PB93-504868).This software make possible to measure simultaneously the area and aspect ratio of each grain, and converts the area into an equivalent circle to obtain its equivalent diameter. At least 2000 grains were measured for each sample.

Orientation

The degree of the preferred orientation of β-Si_3N_4 grains was evaluated by X-ray diffraction of the faces of polycrystalline blocks of the sintered materials which were oriented perpendicular or parallel to the hot -press direction. The ratio of X-ray intensity of (101) and (210) planes (I_{101}/I_{210}) was used as a parameter of preferred orientation[19]. Since X-ray intensity of (00l)plane which is perpendicular to the c-axis is very weak, X-ray intensity of (101) plane, which has relatively strong X-ray intensity and a small angle to the c-plane, was used[20,21]. Dependence of the ratio (I_{101}/I_{210}) on BN content were also determined for the Si_3N_4/BN composites.

In the present work, we proposed a new visible method to evaluate the degree of the preferred orientation of β-Si_3N_4 grains. In this test, the angle of major axis of β-Si_3N_4 grain from

perpendicular to the hot-pressing direction was measured as a parameter of the preferred orientation, as shown in Fig. 3-3. The angle of major axis were deduced from SEM photographs of chemically etched surface parallel and perpendicular to the hot-pressing direction by using image analysis technique. At least 2000 grains were measured for each sample.

3.4 Results and Discussions

3. 4. 1 Fabrication

Determination of Reduction Temperature

In order to determine the reduction temperature, boric acid (1 mole) and urea (2 moles) were mixed and gradually heated in hydrogen gas, because of no literature data except for reduction in ammonia. X-ray diffraction patterns of the h-BN formation by reducing at elevated temperatures were shown in Fig. 3-4. Boric acid and urea were observed for the dried mixture after wet ball-milling, but these peaks disappeared with the appearance of the new considerably broad peak during reduction at 300°C for 7h in hydrogen. This broad peak became very sharp at around 25°(2θ), which corresponds to the turbostratic BN (t-BN), during reduction at 1100°C for 8h. This reduced powder indicated the nearly same peak as commercially available h-BN powder due to progressed hexagonality by heating at 1750°C for 1 h in nitrogen gas, which are necessary conditions to sinter Si_3N_4. By considering these results, it was decided that the powder reduction in this study was carried out at 1100°C for 8h in hydrogen gas to produce Si_3N_4/t-BN composite powders.

Fabrication of Nano-sized BN Dispersed Si_3N_4 Composites

Fig. 3-5 illustrates the transformation of crystalline phases in the fabrication process of the Si_3N_4/BN composite through the chemical route using boric acid and urea as a BN source. As seen in this figure, the starting powder before hydrogen reduction consisted of boric acid and urea, and the precipitated boric acid and urea did not react on α-Si_3N_4 powders during drying process. The reduced product showed almost same peaks as the starting powder except for the disappearance of those of boric acid and urea and the appearance of a broad peak arising from t-BN. This is good agreement with the XRD data for the mixture consisting of only boric acid and urea reduced under the same condition.

Fig. 3-6 shows representative TEM pictures and EDX analysis for the reduced powder

corresponding to (c) in Fig. 3-5. It can be observed that the α-Si_3N_4 powders are surrounded with a low contrast phase. Based on the observation of a disordered layer using higher magnification TEM and identification of boron using EDX, it was found that the reduced powders were α-Si_3N_4 particles partly coated with t-BN. It is well known that t-BN is transformed into h-BN,[22,23,24,25,26] analogous to the structure change of graphite at 2000°C in nitrogen. Actually, the broad peak of t-BN at around 25°(2θ) developed into the peak of (002) reflection of h-BN at 26° (2θ) during hot-pressing the reduced powder at 1750°C for 1h in nitrogen gas. This result agreed with BN produced by reduction of only boric acid and urea at 1750 °C for 1h. The observed sintered body could be identified as a composite consisting of β-Si_3N_4 and h-BN.

Fig. 3-7 shows TEM pictures for the hot-pressed Si_3N_4/BN composite processed through the chemical route developed in this work. Nano-sized BN particles were homogeneously dispersed within Si_3N_4 grains as well as at grain boundaries. Apparent impurity phases were not observed at the interface between the Si_3N_4 matrix and intragranular BN dispersions. As shown in Fig. 3-8, the graphite-like structure was observed for the intragranular BN dispersions. Delaminations parallel to basal plane was also observed due to thermal expansion mismatch between β-Si_3N_4 and h-BN, which is characteristic of h-BN composites. These observation means that the Si_3N_4/BN nanocomposites with homogeneous BN dispersions were successfully fabricated through a chemical process, followed by reduction and hot-pressing.

3. 4. 2 Microstructure

Fig. 3-9 shows the chemically etched microstructures for the Si_3N_4/15vol%BN microcomposite and nanocomposite. The microstructure of the microcomposite confined large BN grains dispersed at grain boundaries of elongated β-Si_3N_4 grains. On the other hand, the nanocomposite showed the finer microstructure with small equiaxed BN particles and rod-like Si_3N_4 matrix grains. The grain size distributions for monolithic Si_3N_4, Si_3N_4/BN microcomposites and nanocomposites are shown in Fig. 3-10. The nanocomposites indicated the narrow grain size distribution at the side of fine grain compared to the monolith and the microcomposites. Nano-sized BN dispersoid inhibited not only the normal grain growth but also the abnormal grain growth, whereas the abnormal grain growth of Si_3N_4 was exhibited in the monolith and the microcomposites. These results were good coincident with the SEM observations in Fig. 3-9. From these observation, it is included that the finer BN particle significantly inhibited grain growth of Si_3N_4 matrix.

TEM observation showed the grain boundary migration in Si_3N_4/BN nanocomposites were restrained by nano-sized BN particles, as shown in Fig. 3-11. This effect will be more pronounced for the increased volume fraction of h-BN particles, due to the pinning effect.

The interaction between second phase particle and grain boundary migration is often explained by a Zener's pinning effect[2 7]. Zener has shown that the maximum restraining force for the grain boundary migration caused by a spherical second phase particles with a radius of r is equal to $\pi r^2\sigma$, where σ is the interface energy. Therefore, the restraining force caused by a second phase particle is proportional to r square. However, the number of the second phase particle per unit volume, n is given by

$$n = \frac{3}{4} \cdot \frac{f}{\pi \cdot r^3} \qquad (3\text{-}1)$$

where f is the volume fraction of second phase particle. Thus the total restraining force for grain boundary migration caused by second phase particles per unit volume becomes

$$n\pi r^2 \sigma = \frac{3}{4} \cdot \frac{\sigma_f}{r} \qquad (3\text{-}2)$$

This equation means that, when the volume fraction of second phase particle is constant, the restraining force for grain boundary migration is inversely proportional to r. In short, the smaller second phase induces the larger total restraining force for grain boundary migration. As considered above, the inhibition of grain growth for Si_3N_4/BN nanocomposite may be attributed to the pinning of grain boundary migration by finer nano-sized BN particle.

From this theory, the microstructure of the Si_3N_4/BN nanocomposites can be understood as follows. When grain boundary reaches a second particle, the boundary energy will decrease by a value proportional to the cross-sectional area of the particle. A breakaway stress will then have to be applied in order to release the boundary from the pinning particle. Clearly, the smaller particles provide less effective pinning than the larger ones. They will be more likely to become inclusions within the grain, because the decrease of the boundary energy is small, and boundaries can easily break away from them. Conversely, larger particles tend to remain at grain boundaries as shown in Fig. 3-11 because they significantly decrease the boundary energy requiring the larger breakaway stresses.

Orientation

Fig. 3-12 shows the SEM micrographs of polished and etched section parallel to the hot-pressing direction for monolithic Si_3N_4, the Si_3N_4/BN microcomposite and nanocomposite. The microstructure perpendicular to the hot-pressing direction for all samples consisted of fine and large rod-like Si_3N_4 grains with random orientation as shown in Fig. 3-9, while the larger elongated grains particularly lay perpendicular to the hot-press direction in the section parallel to the hot-press direction. Furthermore, in the microcomposite large h-BN grains were also orientated preferentially. It is well-known that the c-axis of hexagonal β-Si_3N_4 crystal with the rod-like shape preferentially oriented perpendicular to the hot-pressing direction[28,29,30,31,32,33]. And also, the basal plane of h-BN has a preferred orientation as the same direction because of the morphology of its crystallographic anisotropy[34]. Since the grains of β-Si_3N_4 and h-BN are rod-like and plate-like, respectively, both materials easily orient preferentially during hot-pressing.

Fig. 3-13 shows BN content dependence of the X-ray intensity ratio (I_{101}/I_{210}) for the faces of the Si_3N_4/BN microcomposites and the nanocomposite. The sintered bodies were examined by XRD with respect to the two directions. One was perpendicular to the hot-press direction, and the other was parallel to the hot-press direction. The ratio I_{101}/I_{210} of the section parallel to the hot-pressing direction increased with the increase in BN content. In particular, the degree of the preferred orientation of the microcomposites was significantly higher than that of nanocomposites. These results mean that the c-axis of β-Si_3N_4 orients preferentially perpendicular to the hot-pressing direction by addition of large amount of h-BN particles, and this behavior is accelerated with increasing the size of the h-BN particle.

These analysis of X-ray intensity ratio can give the information on the entire bulk, but the information of each grain can not be obtained. As seen in Fig. 3-12, the larger elongated β-Si_3N_4 grains with high aspect ratio oriented preferentially, however, the relatively equiaxed and small grains lay in random. To further understand the microstructure of Si_3N_4/BN composites, therefore, the information on correlation between individual grain shape and inclination is necessary. Fig. 3-14 and 3-15 show the preferred orientation of the surface perpendicular and parallel to the hot-pressing direction, respectively. The comparison of aspect ratio is suitable for this evaluation, because this parameter can well express the anisotropy of grain growth. In the surface perpendicular to the hot-pressing direction for all materials, the significant difference was not observed between aspect ratio and inclination of elongated β-Si_3N_4 grain as shown in Fig. 3-14. But, it was found, in another direction, that the grains with higher aspect ratio oriented preferentially perpendicular to the hot-press direction, especially in the microcomposite as represented in Fig. 3-15. This tendency would be more

apparent at higher BN content.

These differences of the preferred orientation between the nanocomposites and the microcomposites may be attributed to the size of h-BN as a second phase. In the hot-press sintering, h-BN plates firstly lie perpendicular to the hot-pressing direction, and fine equiaxed α-Si_3N_4 grains grow into rod-like β-Si_3N_4 grains among h-BN plates, as shown in Fig. 3-16. As h-BN content increased, the space between h-BN plates will be narrower. Consequently, the microcomposites containing a larger volume of h-BN indicated higher degree of the preferred orientation than the monolith and the nanocomposites, since β-Si_3N_4 grains elongated along h-BN plates as seen in Fig. 3-17. In contrast, in the nanocomposites, the preferred orientation was suppressed because of fine and relatively equiaxed h-BN grain as a dispersoid. Thus, the observed preferred orientation will influence the mechanical properties. From these results, it is found that the Si_3N_4/BN nanocomposites had fine and homogeneous microstructure due to inhibition of abnormal grain growth and low preferred orientation, compared to the monolith and the microcomposites.

3. 4. 3 Mechanical Properties

Young's Modulus

Fig. 3-18(a) shows the variation of Young's modulus with BN content for the Si_3N_4/BN composites. Young's modulus of both conventional microcomposites and nanocomposites decreased with increasing in the content of h-BN with low Young's modulus of 65 GPa.

It is well-known that Young's modulus of composite corresponds to intermediate between the upper and lower bounds on Young's modulus. Voigt model[3 5] assumes that the strain in each constituent is the same, whence the Young's modulus Eu of the composite becomes

$$E_U = V_2 E_2 + (1 - V_2) E_1 \qquad (3\text{-}3)$$

where V_2 is the volume fraction of the phase with modulus E_2, and E_1 is the modulus of the other phase. Reuss model[3 6] assumes that the stress in each phase is the same, whence the modulus of the composite E_L is

$$\frac{1}{E_L} = \frac{V_2}{E_2} + \frac{1 - V_2}{E_1}. \qquad (3\text{-}4)$$

The designations E_U and E_L indicate the upper and lower bounds on the Young's

modulus.

The measured Young's modulus of Si_3N_4/BN composites are almost consistent with intermediate between the upper (E_U) and lower bounds (E_L) on Young's modulus.

Fracture Strength

Fig. 3-18(b) showed the variation in fracture strength with BN content for the Si_3N_4/BN composites. In comparison with conventionally fabricated microcomposites, the nanocomposites fabricated by the chemical process peculiar to the present work were successful in retaining relatively high strength in spite of decrease of Young's modulus due to the soft h-BN addition (Young's modulus of h-BN and Si_3N_4 are about 65 and 350 GPa, respectively). The fracture strength of the nanocomposites was higher than monolithic Si_3N_4 by adding h-BN up to 5 vol%, and the strength was approximately two times higher than that of the microcomposites even at higher BN content

In common brittle ceramics, fracture strength, σ_f, can be expressed by the following equation[3 7],

$$\sigma_f = \frac{1}{Y}\frac{K_{IC}}{c^{1/2}} \qquad (3\text{-}5)$$

where Y, K_{IC} and c are shape factor of a defect, fracture toughness and defect size, respectively. Based on this linear fracture mechanics concept, the strength of brittle ceramics is controlled by the fracture toughness and the critical flaw size, which is strongly related to processing defects (such as agglomerates of second phases, large pores, and abnormally grown grains). The fracture toughness was not remarkably influenced by the nano-sized BN dispersions.

Fig. 3-19 shows the polished specimen surfaces of Si_3N_4/BN composites. In the microcomposites a number of small and large flaws were observed, whereas the surfaces of the monolith and the nanocomposites was without noticeable flaws. It is thought that these flaws could be due to the missing or pull-out of BN particles or those agglomerates. Furthermore, from SEM observations of fracture surfaces, it was found that the large or agglomerated h-BN particles initiated fracture for the microcomposites. However, as shown Fig. 3-20, in the nanocomposites such large agglomerations due to BN dispersions were not observed, and moreover, the fracture origin was too fine to identify. In addition, the matrix grain size of the nanocomposites was considerably refined by the nano-sized BN dispersions compared to the Si_3N_4 monolith and Si_3N_4/BN microcomposites. This should be attributed to the inhibition of the grain growth of Si_3N_4 caused by grain boundary pinning due to the nano-sized h-BN dispersions. Thus, it is concluded that the observed high strength of

Si_3N_4/BN nanocomposites must be chiefly attributed to the inhibition of grain growth by the nano-sized BN dispersion, and also due to the reduction of flaw size as a processing defect.

3. 5 Conclusions

(1) The Si_3N_4/BN nanocomposites, including the nano-sized BN up to 40 vol%, were fabricated by novel chemical route with hot-pressing the α-Si_3N_4 powders covered partly with t-BN. TEM observations revealed that the nano-sized h-BN particles were homogeneously dispersed within the Si_3N_4 grains as well as at the grain boundaries.

(2) The Si_3N_4/BN nanocomposites had finer and more homogeneous microstructure due to inhibition of abnormal grain growth and low preferred orientation by nano-sized BN dispersion, compared to the monolith and the microcomposites.

(3) Young's modulus of both microcomposites and nanocomposites decreased with increasing h-BN content according to the rule of mixtures, but the strength of the nanocomposites was significantly improved, compared with the conventional microcomposites. The enhancement of the fracture strength was attributed to the inhibition of grain growth and also due to a decrease in flaw size by nano-sized h-BN dispersions.

References

[1]T. Funabashi, K. Isomura, A. Harita and R. Uchimura, p. 968-976 (1986), Ceramic materials and Components for Engines. Edited by V. J. Tenney, Amer. Ceram. Soc.,Las Vegas, NV, 1986

[2] K. S. Mazdiyasni and Robert Ruh, J. Am. Ceram. Soc., 64(1981)415-418

[3] D. Goeuriot-Launay, G. Brayet, F. Thevenot, J. Mater. Sci. Lett., 5(1986) 940-942

[4] K. Niihara, J. Ceram. Soc. Jpn., 100 (1991) 974-982

[5] K. Niihara, K. Suganuma and K. Izaki, J. Mater. Sci., 9(1990)112

[6] A. Nakahira and K. Niihara, J. Ceram. Soc. Jpn.,100(1992)448

[7] T. Ohji, Y. -K. Jeong, Y. -H. Choa and K. Niihara, J. Am. Soc., 77(1994)3259

[8] K. Niihara, T. Hirano, K. Izaki and F. Wakai, Ceram. Trans., 42(1994)207-219

[9] T. Hirano and K. Niihara, Mat. Lett., 22(1995)249-254

[10]T. Hirano and K. Niihara, Nanostructured Materials, 5(1995)808-818

[11] T. Sekino and K. Niihara, Nanostructured Materials, 6(1995)663

[12] T.Sekino, T. Nakajima, S. Ueda and K. Niihara, J. Am. Chem. Soc., 80(1997)1139-1148

[13] T.Sekino and K. Niihara, J. Mater. Sci., (1997) in print.
[14] T. E. O'Connor, J. Am. Chem. Soc., 84 (1962) 415-418
[15] J. Thomas, Jr., N. E. Weston and T. E. O'Connor, J. Am. Chem. Soc., 84(1963)4619-4622
[16] M. Hubaacek, T. Sato and T. Ishii, J. Solid State Chem., 109(1994)384-390
[17] R. T. Paine and C. K. Narula, Chem. Rev., 90 (1990) 73-91
[18] K. Niihara, R. Morena and D. P. H. Hasselman, J. Mater. Lett., 1(1982)13
[19] Y. Nishikawa, T. Nishida and Y. Okamoto, Rep. Asahi Glass Found Ind. Technol., 43(1983)59-63
[20] Y. Goto and A. Tsuge, J. Euro. Ceram. Soc., 6(1990)269-272
[21] Y. Goto, H. Ohta and M. Komatsu, Yogyo-kyokai-shi, 94(1986)167-171
[22] V. Brozek and M. Hubaacek, J. Solid State Chem., 100 (1992)120-129
[23] S. Alkoy, C. Toy, T. Gonul and A. Tekin, J. Euro. Ceram. Soc., 17(1997)1415-1422
[24] T. Hagio, K. Nonaka and T. Sato, J. Mater. Sci. Lett., 16(1997)795-798
[25] W. Sinclar and H. Simmons, J. Mater. Sci. Lett.,6(1987)627-629
[26] T. Hagio, K. Kobayashi and T. Sato, J. Ceram. Soc. Jpn., 102(1994)1051-1054
[27] C. Zener, quated by C.S. Smith: Trans. Metall. Soc. AIME, 175(1948)15
[28] R. Kossowsky, j. Mater. Sci., 8(1973)1603-15
[29] F. Lee and K. J. Bowman, J. Amer. Ceram. Soc., 75(1992)1748-55
[30] F. F. Lange, J. Am. Ceram. Soc., 56(1973)518-22
[31] K. Nuttall and D. P. Thompson, J. Mater. Sci., 9(1974)850-53
[32] J. E. Weston, P. L.Pratt and B. C. H. Steele, J. Mater. Sci., 13(1978)2137-46
[33] J. E. Weston, P. L.Pratt and B. C. H. Steele, J. Mater. Sci., 15(1980)1568-76
[34] W. Kimm and Y.-W. Kim, J. Amer. Ceram. Soc., 81(1998)1669-72
[35] W. Voigt, Lehrbuch der Kristallphysik, (1928)739
[36] A. Reuss, A. Angew. Math Mech., 9(1929)49
[37] A. A. Griffith, Roy. Soc. Lond., A221(1924)163

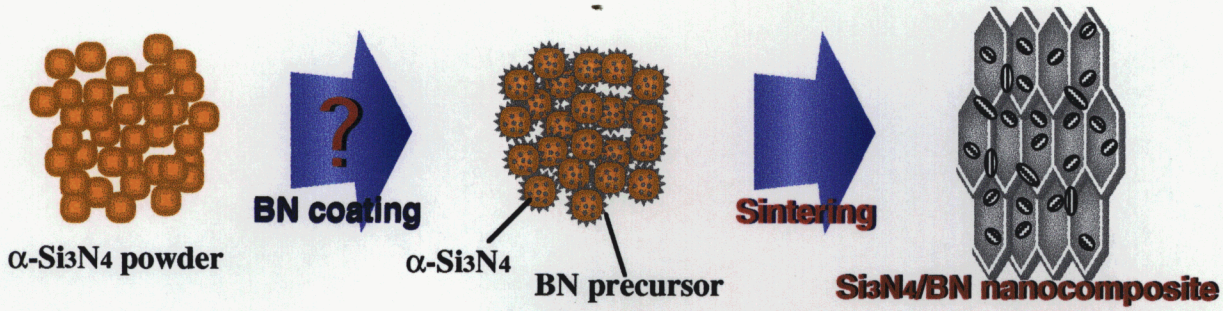

Fig. 3-1 Fabrication Image for Si_3N_4/BN Nanocomposites.

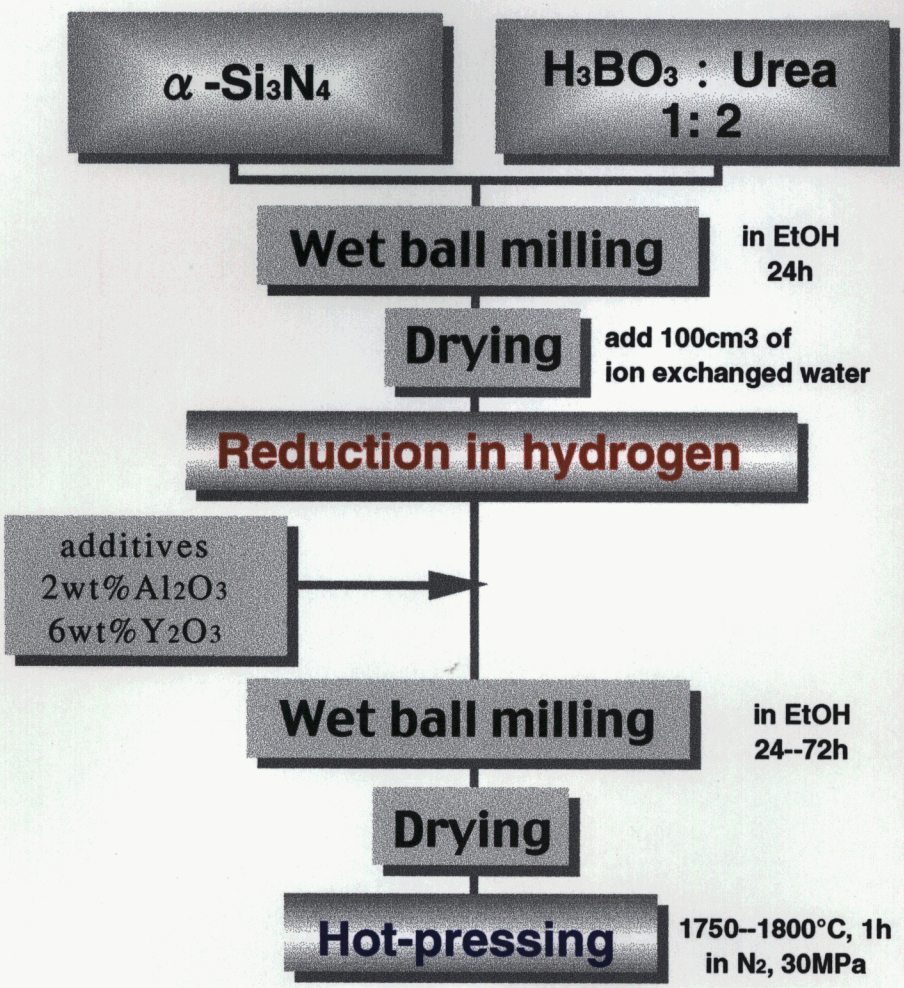

Fig. 3-2 Flow chart for Si_3N_4/BN nanocomposites.

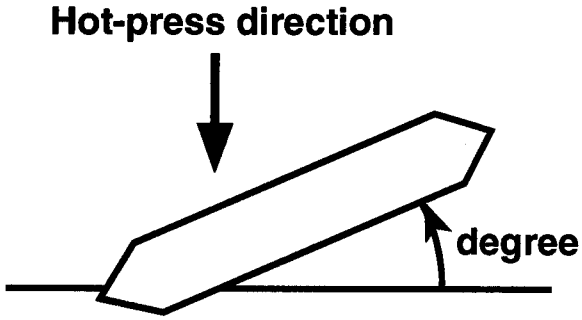

Fig. 3-3 The angle of major axis of β-Si_3N_4 grain from perpendicular to the hot-pressing direction.

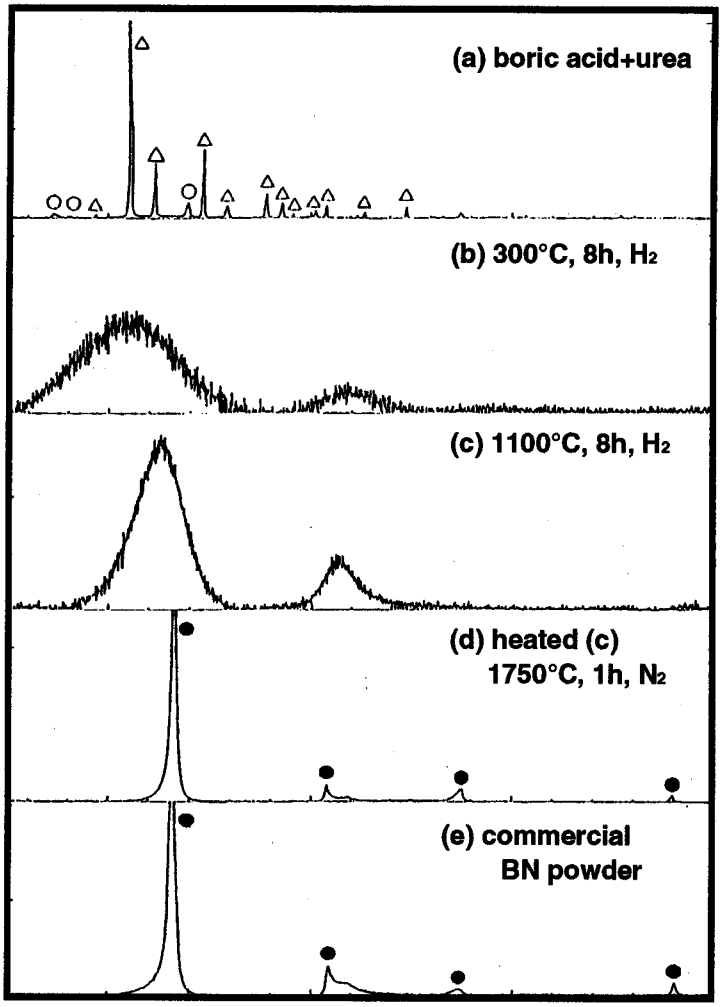

Fig. 3-4 XRD patterns of a mixture of boric acid and urea, showing the formation of h-BN during reduction.
○:boric acid, △:urea, ●:h-BN

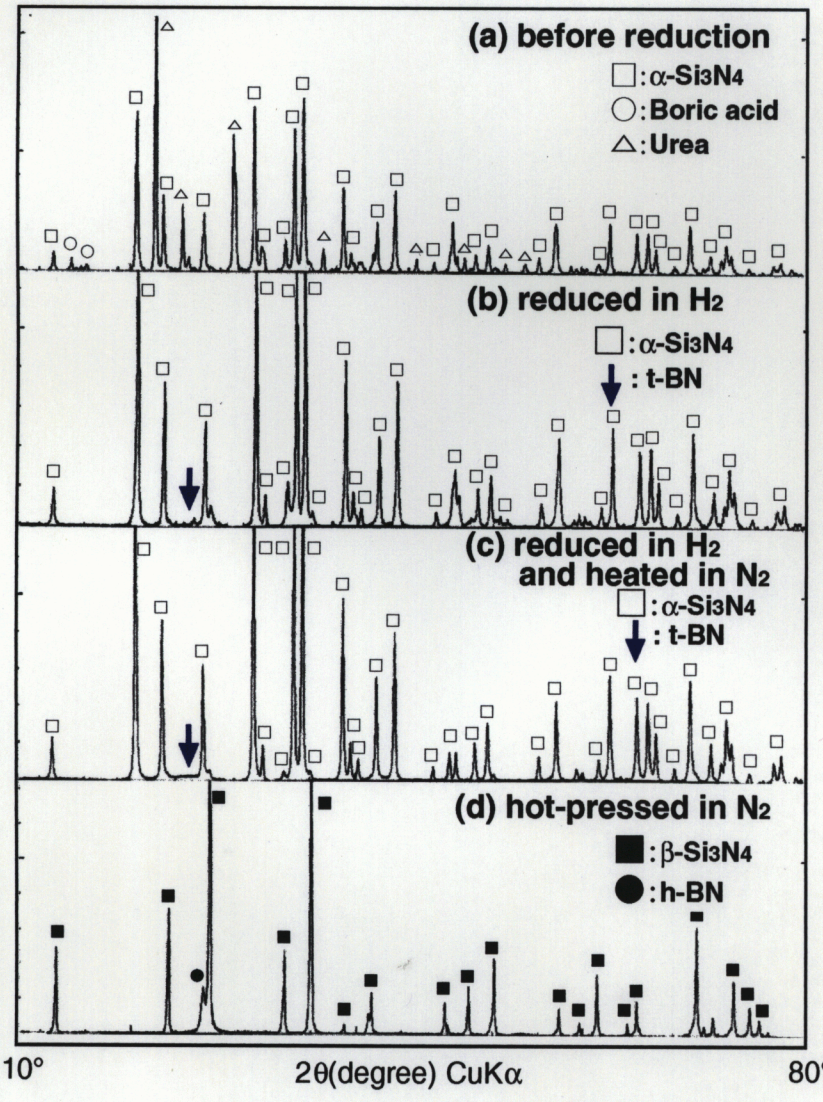

Fig. 3-5 XRD patterns of the Si_3N_4/BN composite synthesized by the chemical route with reduction and hot-pressing.
(a) before reduction.
(b) reduced at 1100 °C for 8 h in H_2
(c) reduced at 1100 °C for 8 h in H_2 and
and heated at 1500 °C for 8 h in N_2.
(d) hot-pressed at 1750 °C for 1 h.
□:α-Si_3N_4 ○:boric acid △:urea ●:BN ■:β-Si_3N_4

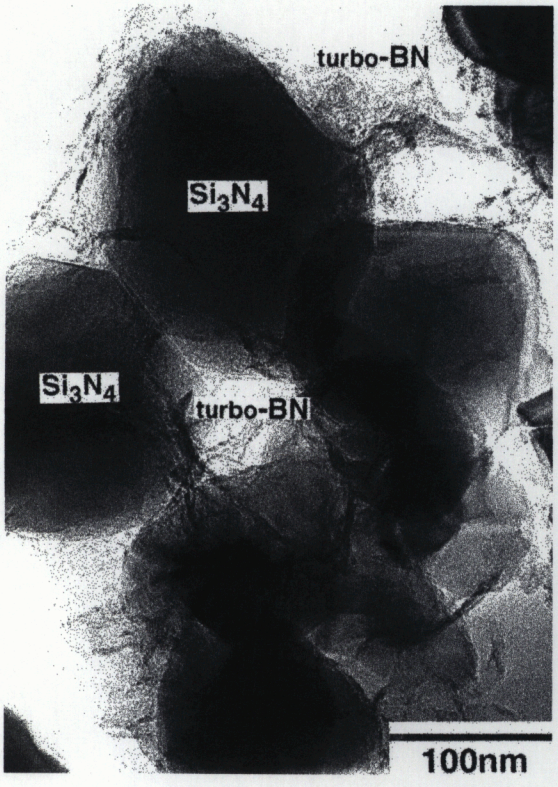

(a) Low magnification.

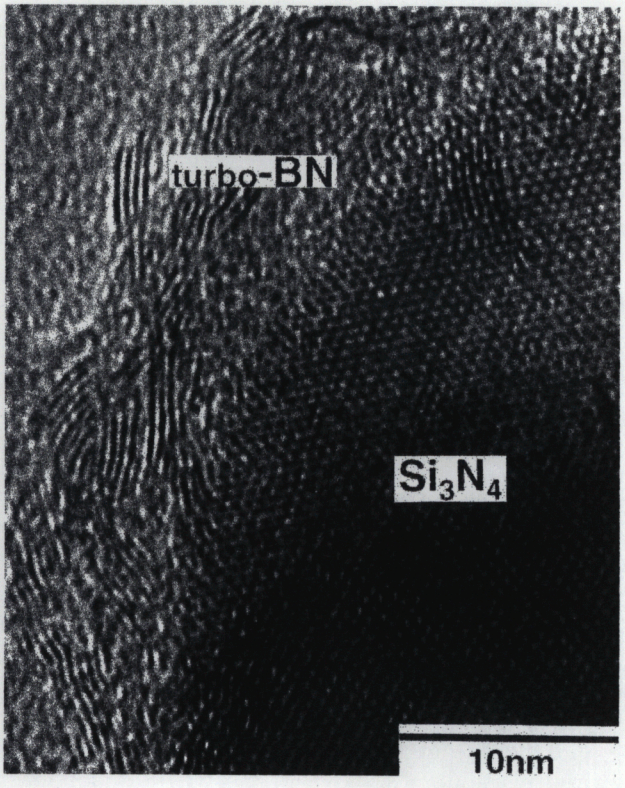

(b) Higher magnification.

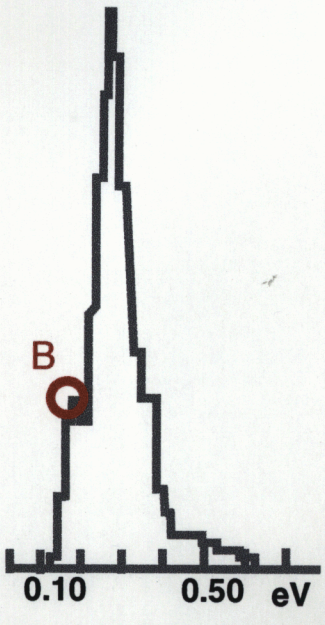

(c) EDX analysis of the turbostratic area.

Fig. 3-6 TEM micrographs and EDX analysis of t-BN formed on the surface of α-Si_3N_4 powder heated at 1100 °C in H_2.

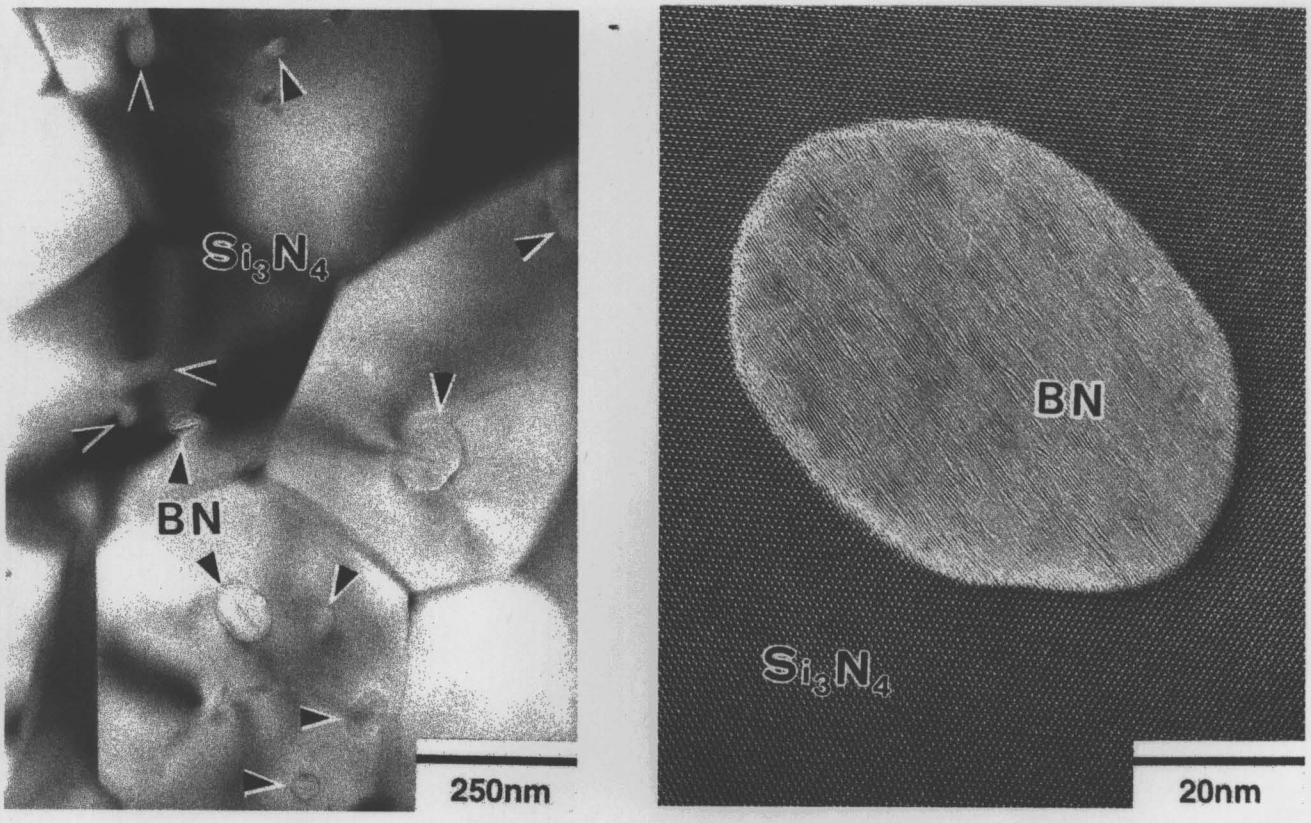

(a) Low magnification. (b) The intragranular BN particle.

Fig. 3-7 TEM micrographs of hot-pressd Si_3N_4/BN nanocomposites

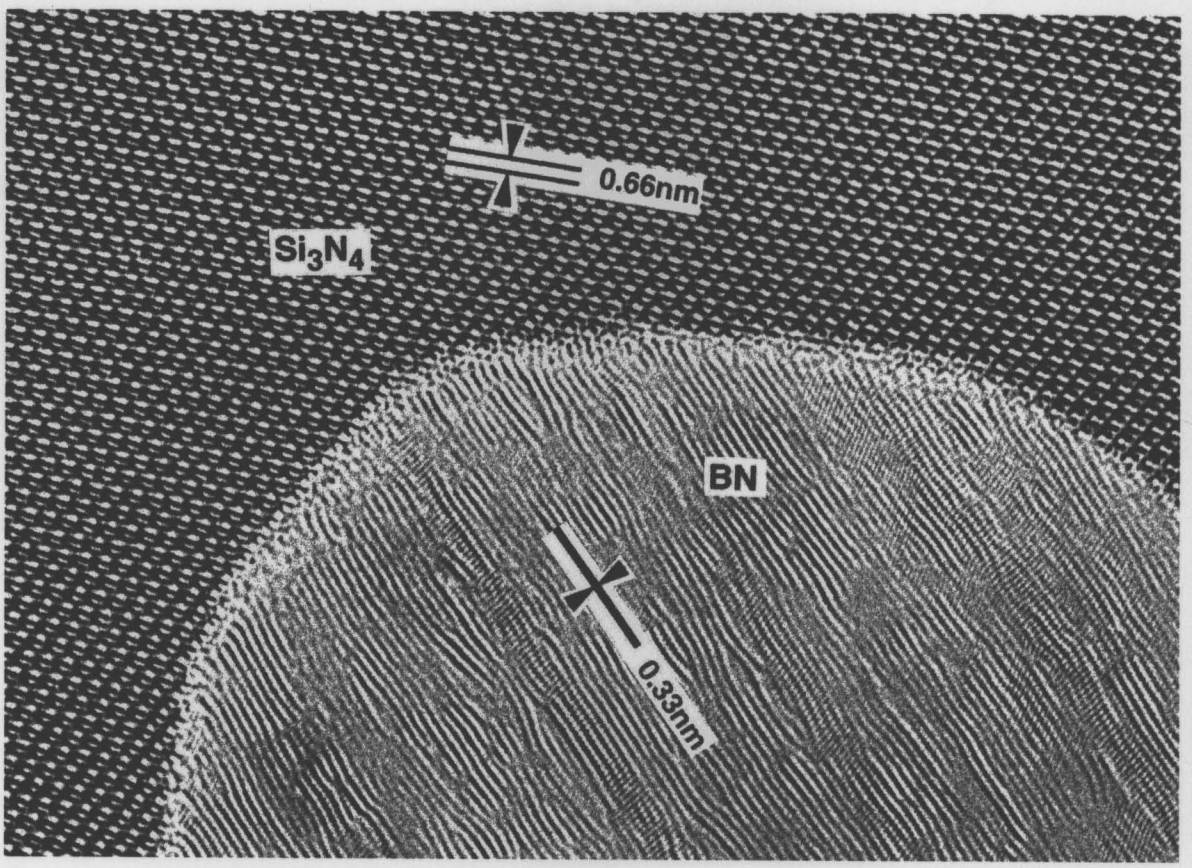

Fig. 3-8 Interface structure between Si_3N_4 matrix and intragranular h-BN particle.

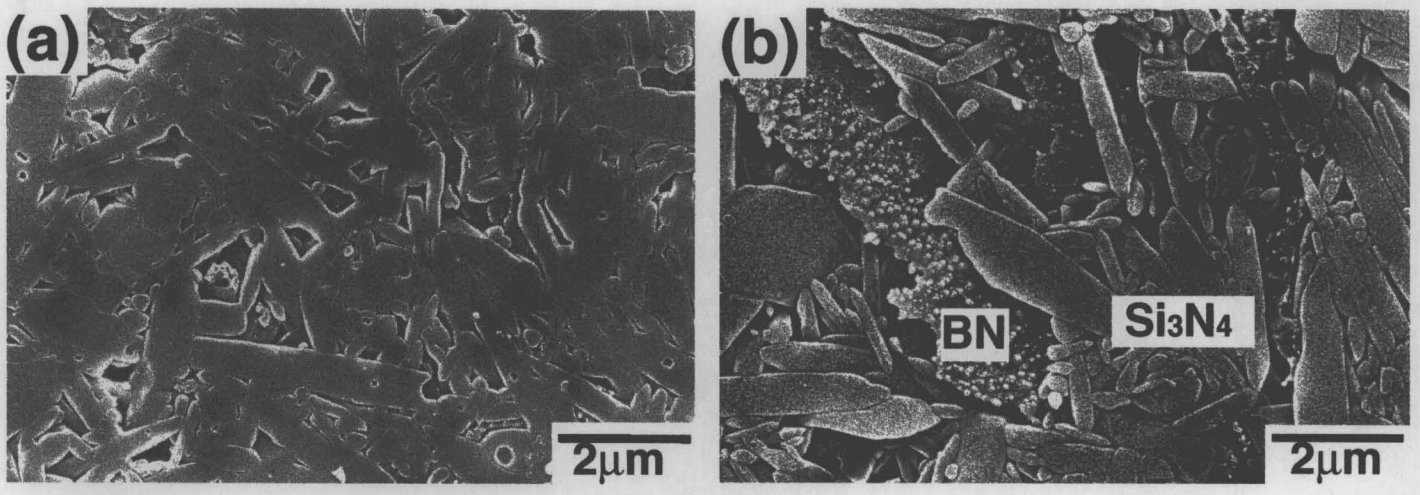

Fig. 3-9 SEM micrographs of polished and etched surfaces for Si_3N_4/15vol%BN nanocomposite (a) and microcomposite (b).

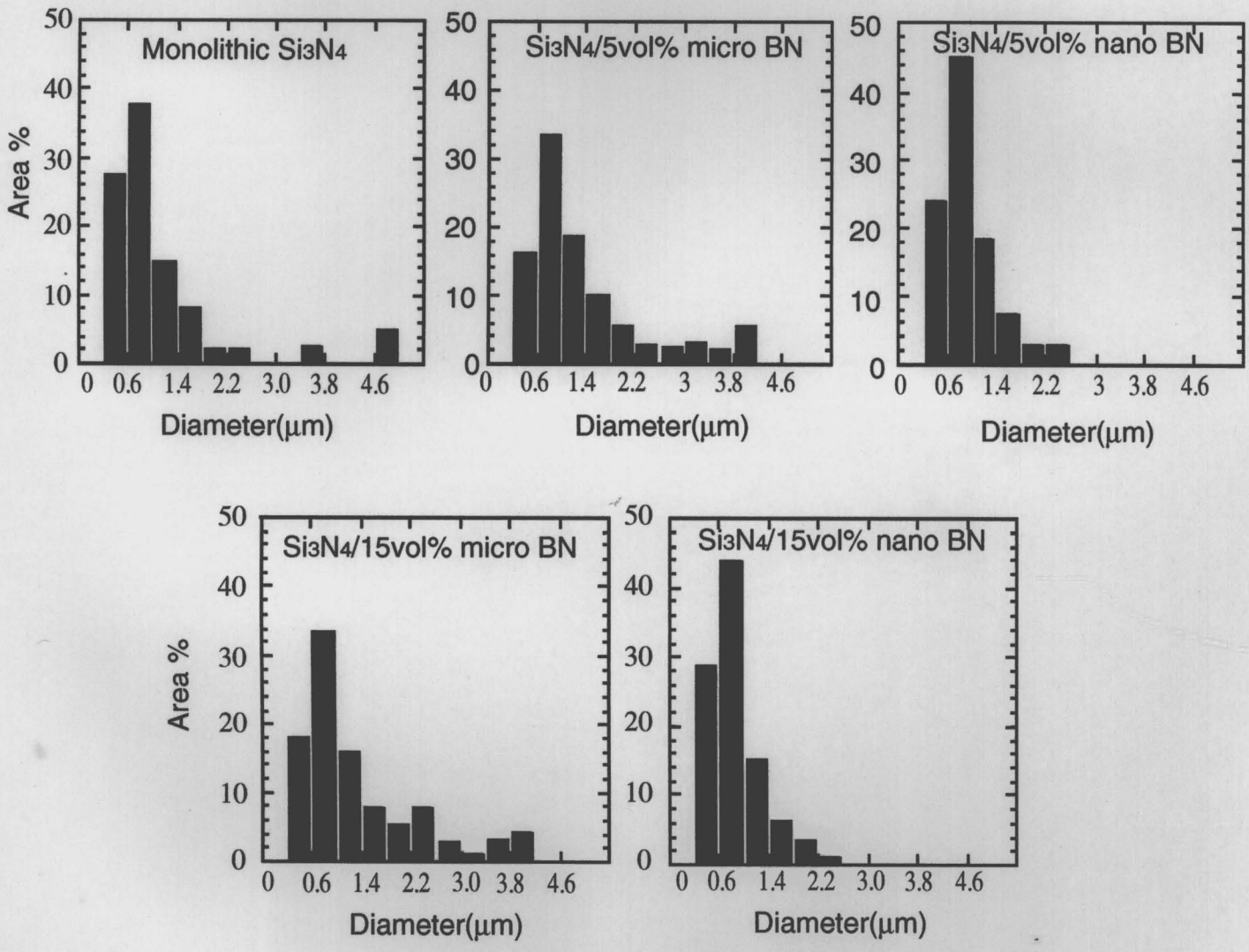

Fig. 3-10 Grain size distributions for monolithic Si_3N_4 and Si_3N_4/BN composites.

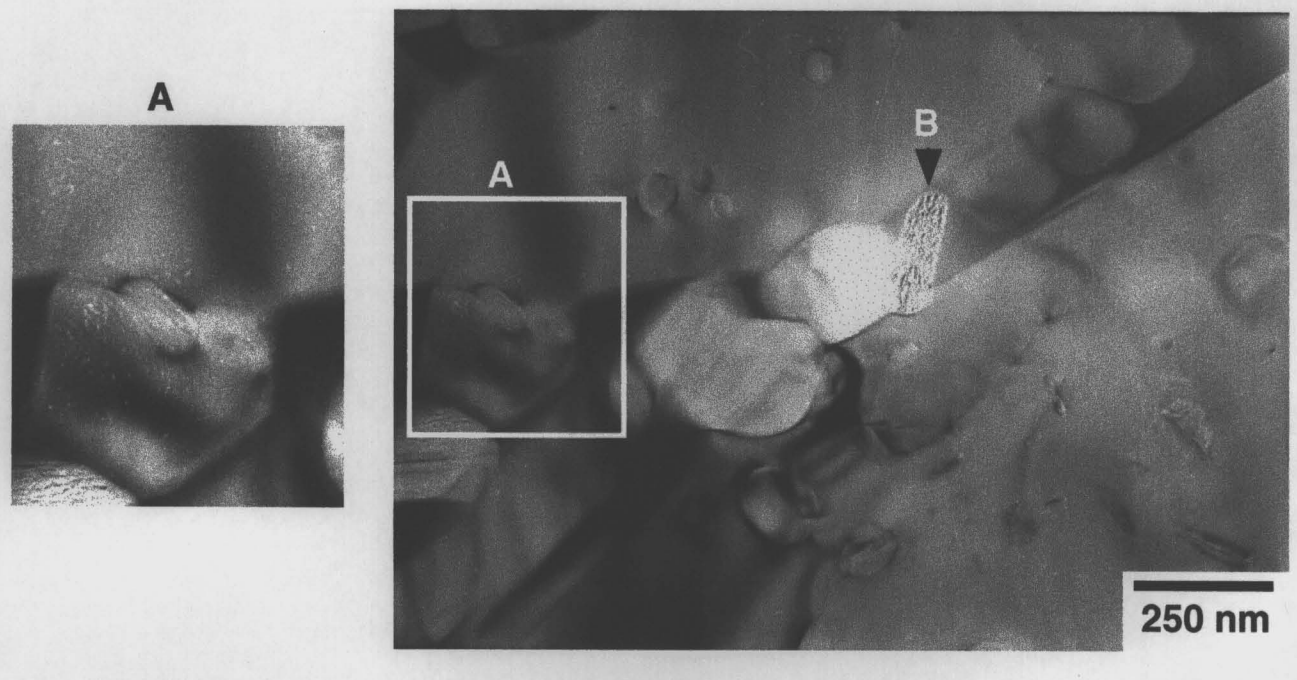

Fig. 3-11 TEM micrographs of the microstructure for Si_3N_4/BN nanocomposite. (A) pinning effect by h-BN particle, (B) h-BN particle at grain boundary

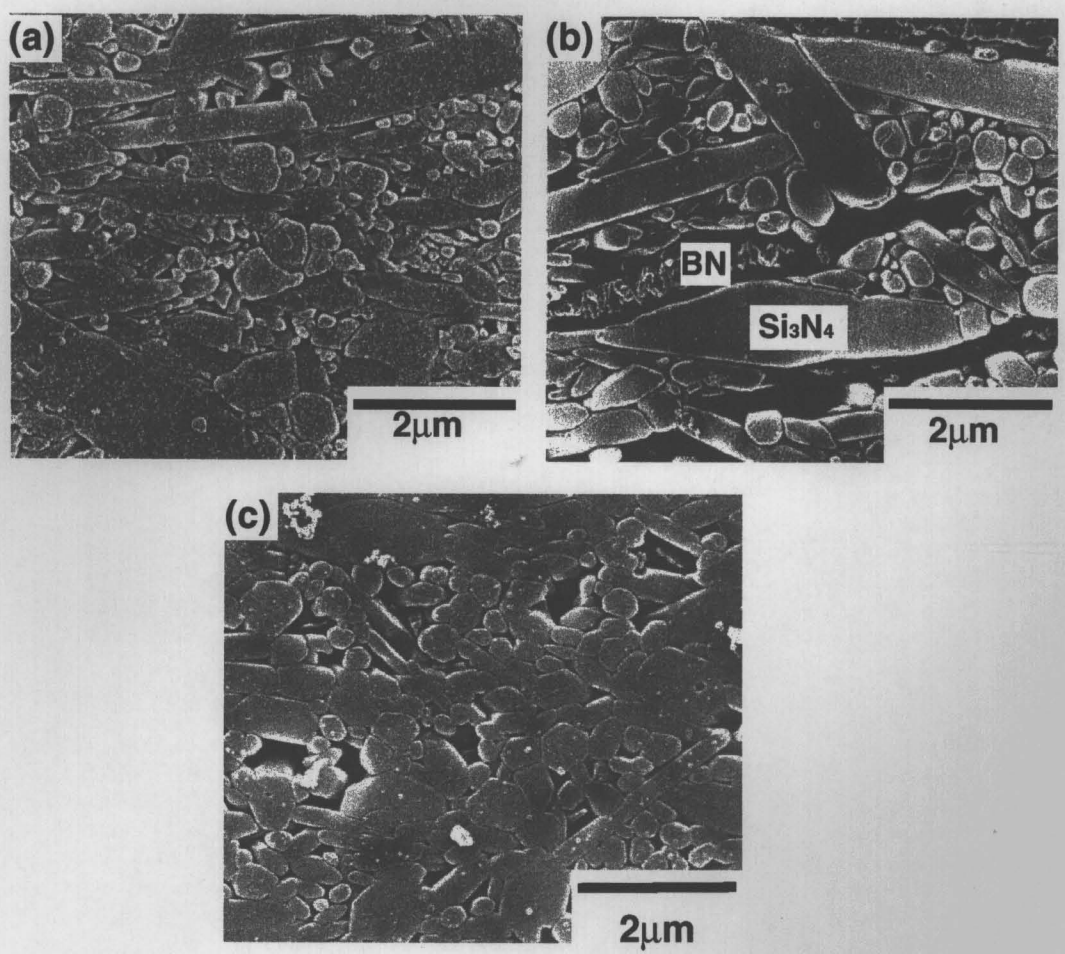

Fig. 3-12 SEM micrographs of polished and eched section parallel to the hot-pressing direction for (a) monolithic Si_3N_4 and (b) Si_3N_4/15vol%BN microcomposite and (c) Si_3N_4/15vol%BN nanocomposite.

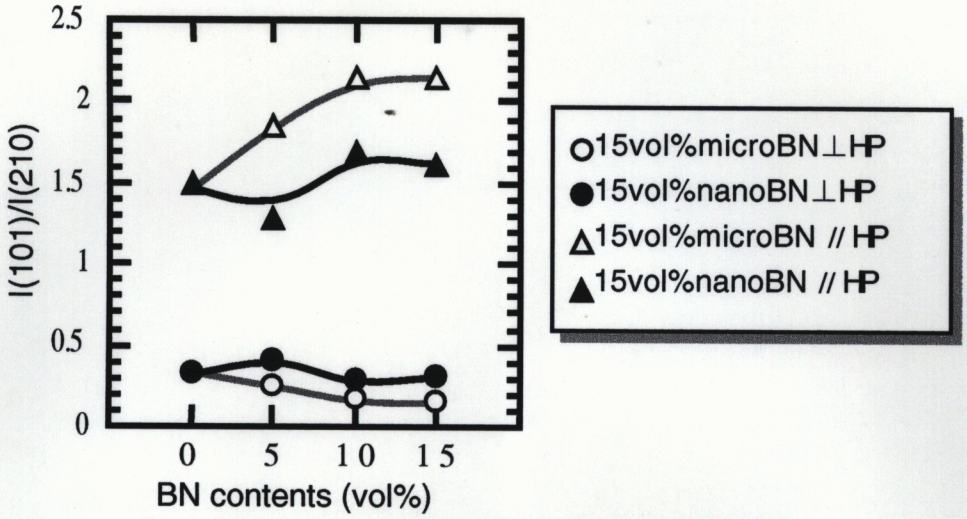

Fig. 3-13 X-ray intensity ratio I(101)/I(210) as a function of BN contents.

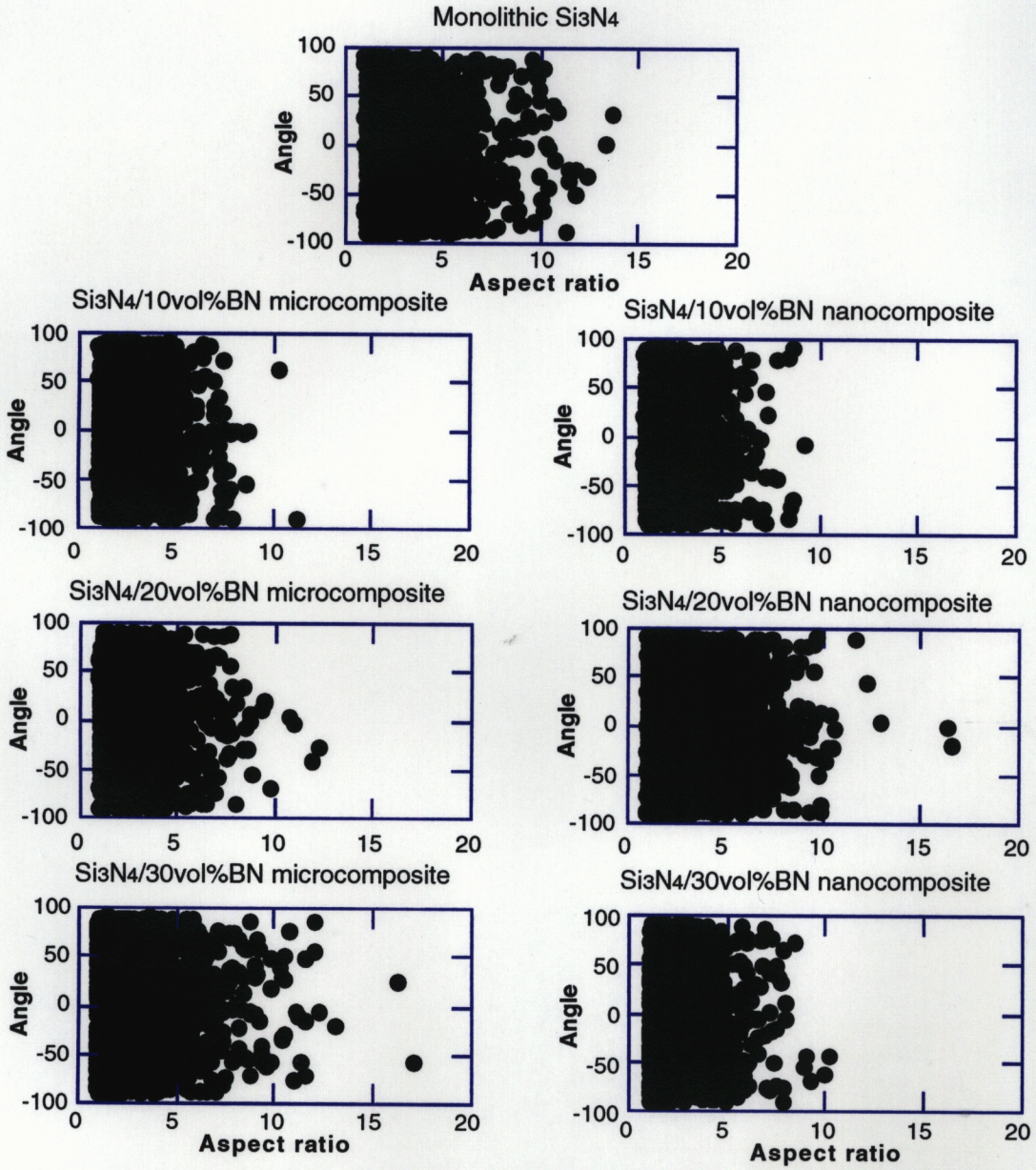

Fig. 3-14 Angle of elongated Si_3N_4 matrix grain from perpendicular to the hot-pressing direction as a function of aspect ratio in the surface perpendicular to the hot-pressing direction.

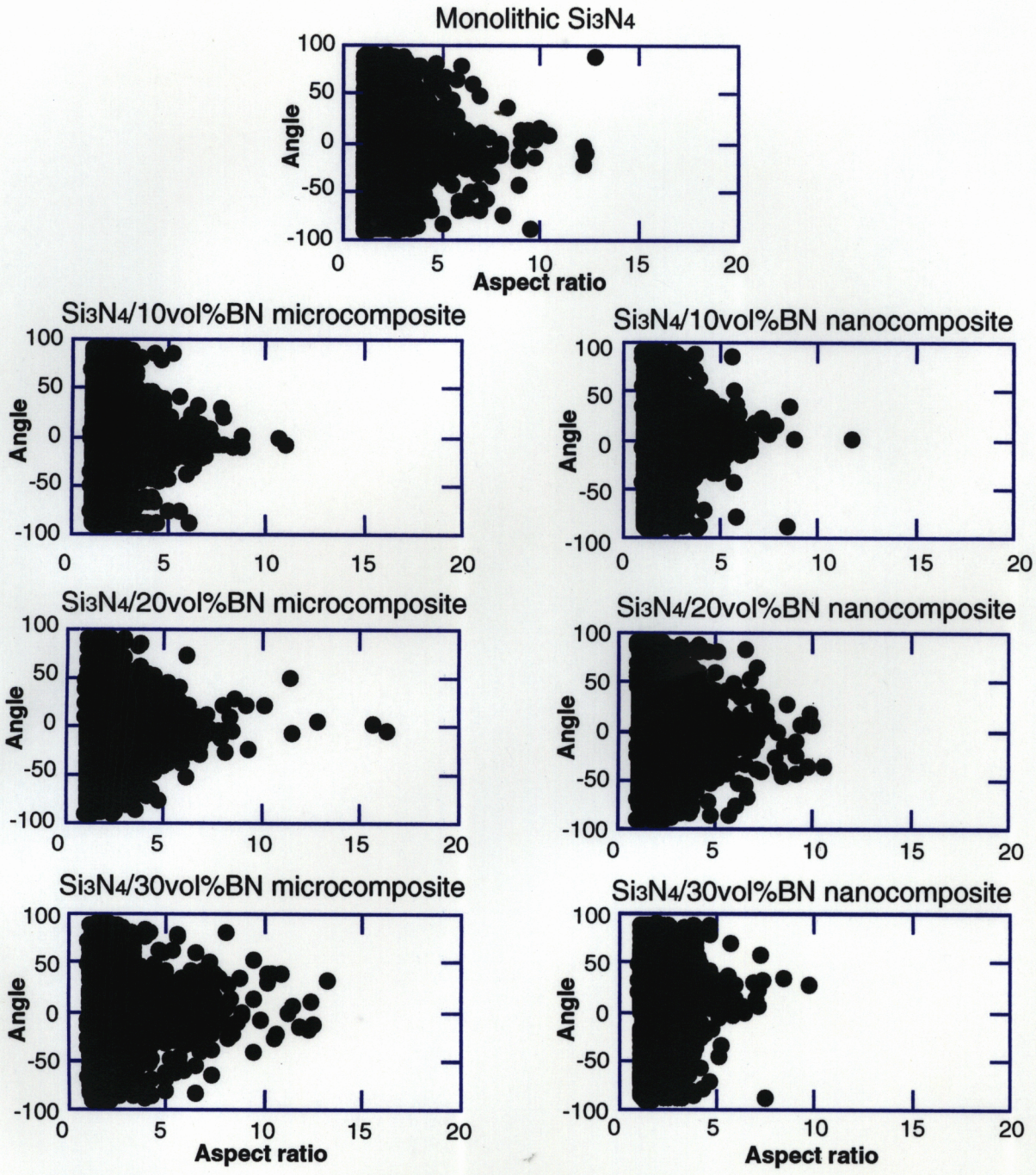

Fig. 3-15 Angle of elongated matrix grain from perpendicular to the hot-pressing direction as a function of aspect ratio in the surface parallel to the hot-pressing direction.

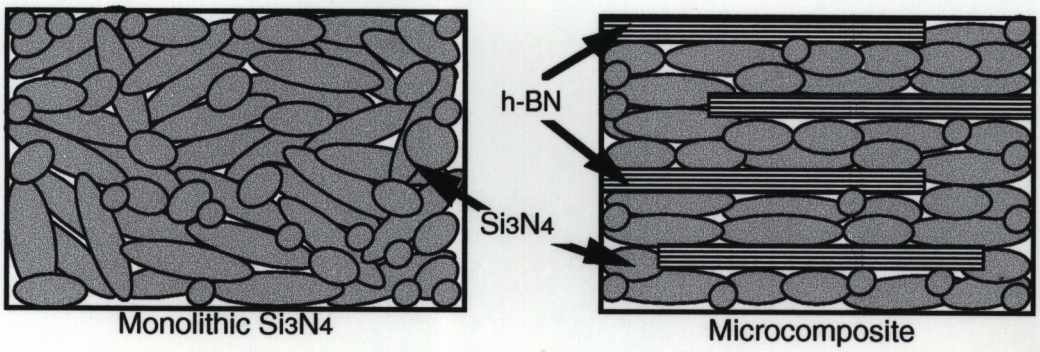

Fig. 3-16 Schematic image of section taken parallel to the hot-press direction.

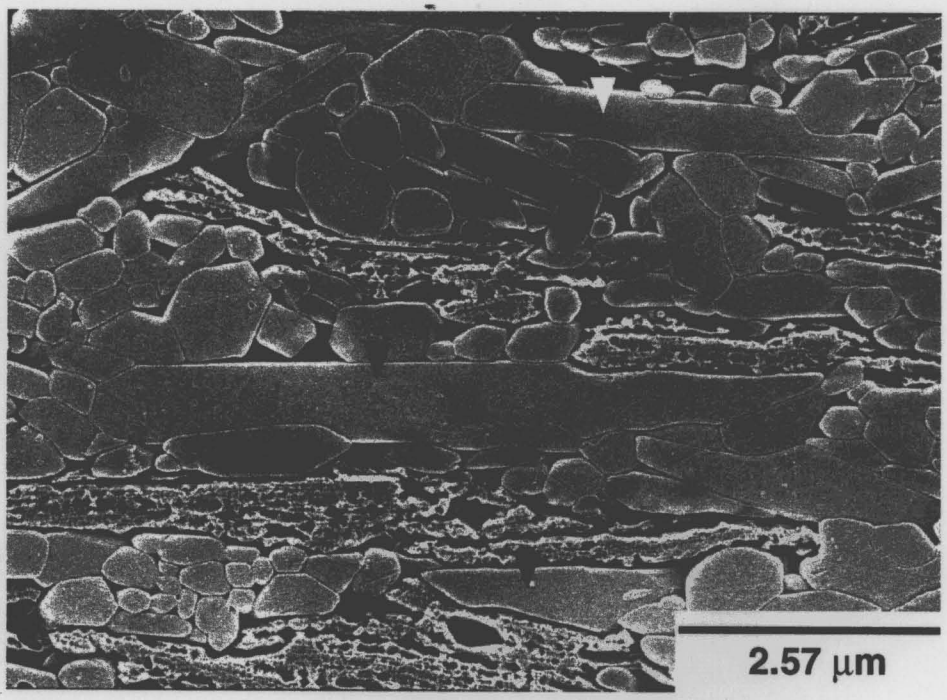

Fig. 3-17 Elongation of β-Si_3N_4 grains along h-BN plates (▼).

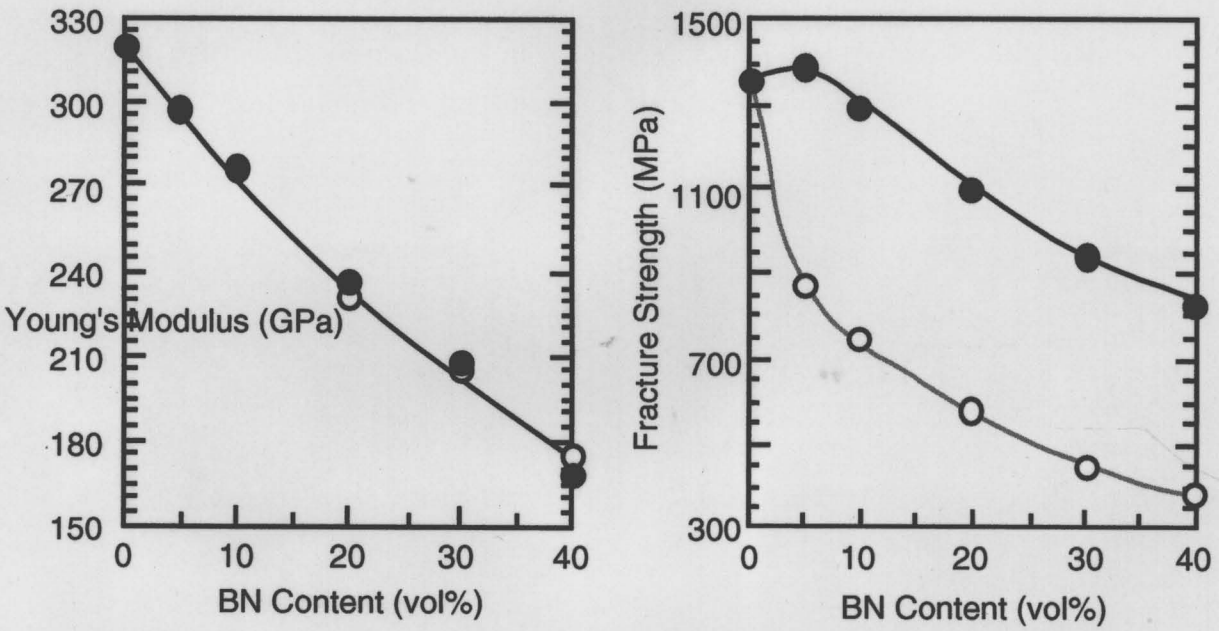

Fig. 3-18 Effects of h-BN content on Young's modulus (a) and fracture strength (b) of Si_3N_4/BN composites.
●: Si_3N_4/BN nanocomposites and ○: Si_3N_4/BN microcomposites.

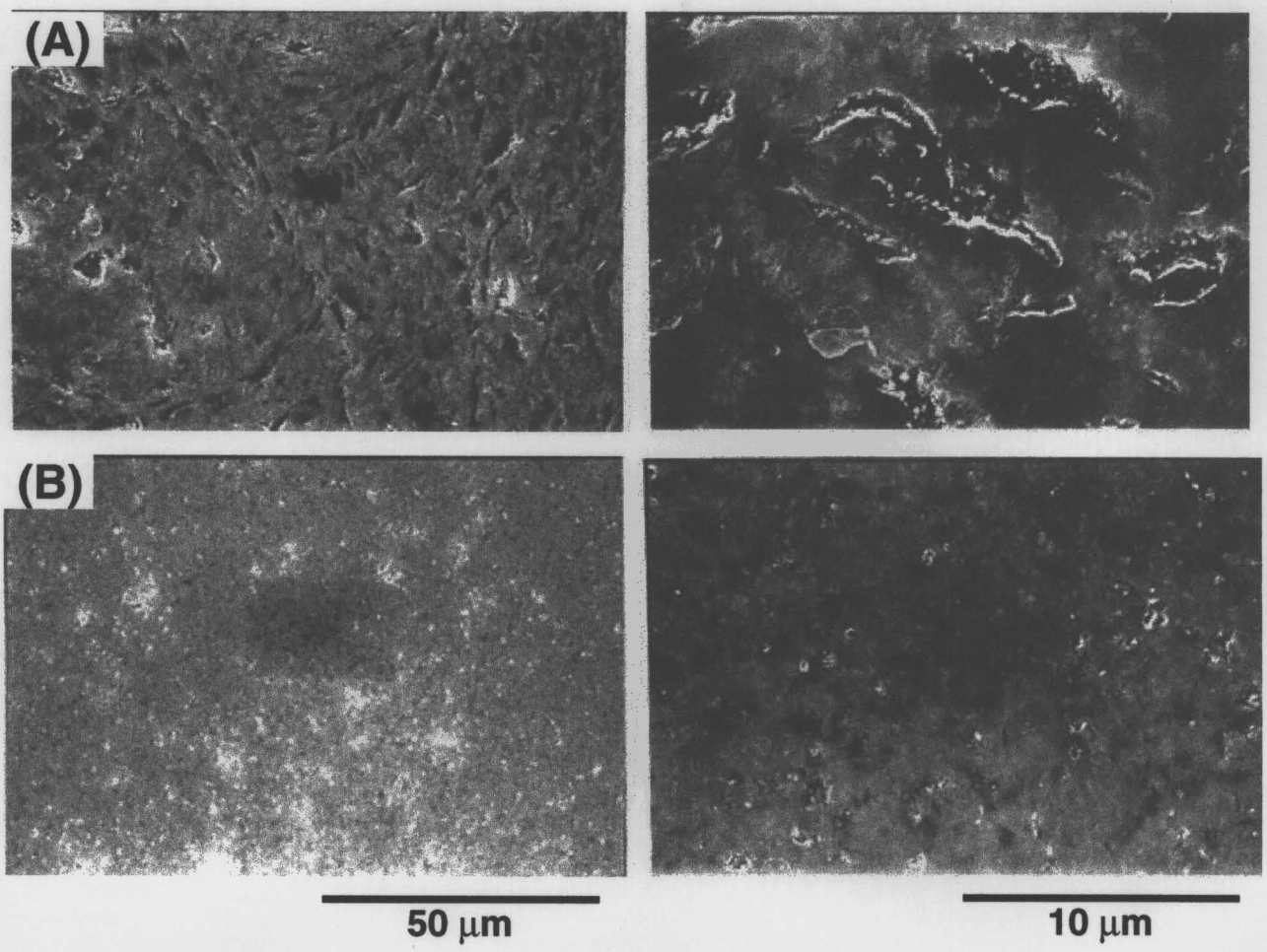

Fig. 3-19 SEM observations of polished surfaces for Si_3N_4/15vol%BN microcomposite(A) and nanocomposite (B).

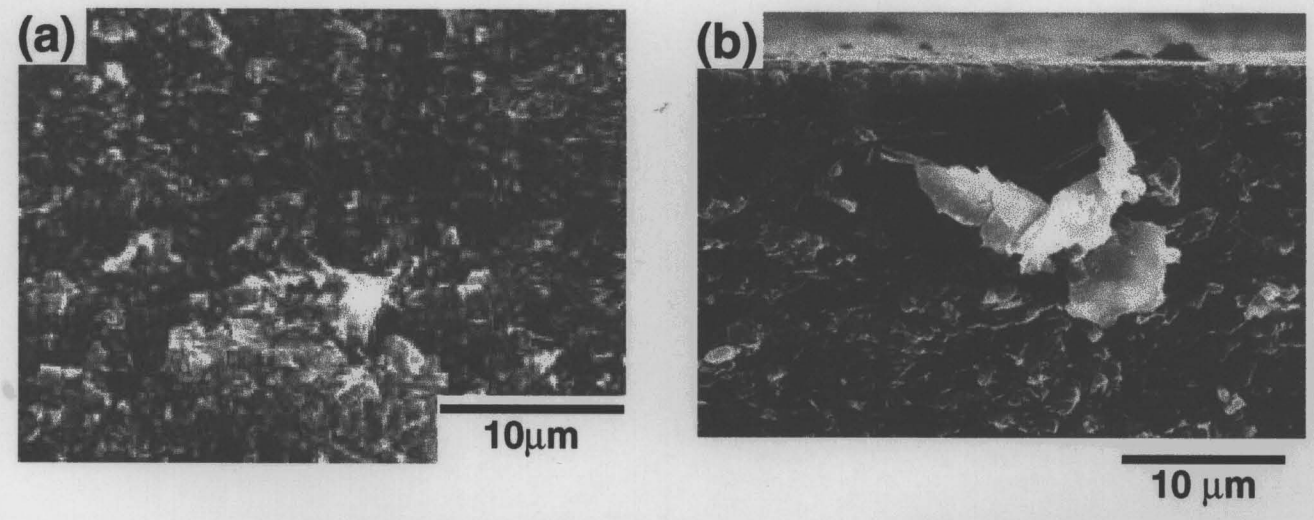

Fig. 3-20 Fracture origin of Si_3N_4/BN nanocomposite (a) and microcomposite (b).

Chapter 4

Thermal Shock Resistance of Si_3N_4/BN Composite

In order to extend the application of ceramics, in addition to their excellent properties, further improvement of thermal shock resistance is needed. In conventional Si_3N_4/BN microcomposite, the fracture strength decreased remarkably with increasing h-BN content, though thermal shock resistance was somewhat improved. In the chapter 3, we reported that new type of nanocomposite fabricated by the novel chemical method. The Si_3N_4/BN nanocomposites, fabricated by the chemical route in this work, exhibited a microstructure which contains nano-sized h-BN particles homogeneously dispersed within the Si_3N_4 grain as well as at the grain boundaries, indicating the significantly improved the fracture strength in comparison with the microcomposites. As a result, the thermal shock fracture resistance was drastically improved. This increase in the thermal shock fracture resistance is mainly attributed to the improved fracture strength, and also Young's modulus, coefficient of thermal expansion and low Poisson's ratio caused by the h-BN dispersions.

4. 1 Introduction

Si_3N_4 based ceramics have been widely used as high-temperature structural materials because of their superior mechanical and thermal properties. Specially, Si_3N_4/BN composite materials are of considerable interests for a range of wide applications such as components for automobiles and refractory nozzles, tubes, sliding gates and break rings for horizontal continuous casting of steel. The development of such advanced composites has taken place in the last decade, although it has been known for a number of decade that the addition of BN to TiB_2 composites greatly improves the thermal shock resistance for applications such as metal evaporator boats[1]. In addition, many researchers have established that the thermal shock resistance of many materials somewhat increases with the amount of BN added[2, 3, 4, 5]. However, it is reported that the fracture strength of these ceramics remarkably decreased with an increase in BN content. It is well-known that high thermal shock resistance can also be attained by the enhancement of fracture strength[6, 7, 8, 9]. Therefore, for further improvement in thermal shock resistance, it is necessary to retain high fracture strength.

In recent years, Niihara and his colleagues[10, 11, 12, 13, 14] have investigated

ceramic based nanocomposites, in which the nano-sized particles are dispersed within the matrix grains and/or at the grain boundaries. These nanocomposites showed the improved fracture strength and excellent creep resistance compared with the monolithic ceramics. In early nanocomposite, hard and strong materials as dispersoids were mainly incorporated into the matrix. But recently, soft and weak materials like metal were also used as dispersoids, and the remarkable enhancement of fracture strength was found even by the addition of soft and weak dispersoids[15,16,17]. However, it has not been reported the improvement of mechanical properties by nano-sized soft and weak ceramic dispersoid such as h-BN. If it is possible to accomplish the enhancement of the fracture strength by dispersing the nano-sized BN particles, the thermal shock resistance of Si_3N_4 ceramics will be remarkably improved.

The purpose of this study is to evaluate the thermal shock resistance for the Si_3N_4/BN nanocomposite fabricated by a newly developed chemical process. In addition, the coefficient of thermal expansion and Poisson's ratio, which influence thermal shock fracture resistance, were also evaluated to elucidate the mechanism.

4. 2 Experimental Procedures

4. 2. 1 Specimen Preparation

Monolithic Si_3N_4 and Si_3N_4/BN microcomposites were fabricated by the conventional metallurgical processing, and the Si_3N_4/BN nanocomposites were produced through the chemical process described in the previous chapter.

4. 2. 2 Evaluation

Thermal Shock Test by Water-Quench Method

Thermal shock fracture resistance was determined by measuring the bending strength of water-quenched samples. The cut and polished specimens, rectangular bars (3 x 4 x 37 mm), were soaked for 10 min at a selected temperature in a vertical tube furnace as shown in Fig. 4-1, and then dropped into a water bath which was maintained at 20°C. The depth of the water was 230 mm. After water-quenching, the residual fracture strength was evaluated by a three-point bending test. The tensile surfaces of specimens were perpendicular to the hot-pressing direction. The span length and crosshead speed were 30 mm and 0.5 mm/min, respectively.

Coefficient of Thermal Expansion

Measurements of coefficient of thermal expansion were performed in the temperature range of about 20 to 1000°C at a heating rate of 10 °C/min, using a dilatometer (TA-7000, Shinku Riko, Yokohama, Japan).

Poisson's Ratio

In order to evaluate Poisson's ratio, the sound velocities Vt (transverse wave) and Vl (longitudinal wave) were measured by a pulse-echo method using an ultrasonicpulsar / receiver 5052PRX (Panametrics Inc.) interfaced with a digital ocsilloscope 9400A (LeCroy Co.). The measurement was done for two directions, parallel and perpendicular to the hot-pressing direction.

4. 3 Results and Discussion

4. 3. 1 Thermal Shock Resistance

Fig. 4-2 shows the residual strength after water quenching for monolithic Si_3N_4, Si_3N_4/BN microcomposite and the nanocomposites. As shown in this figure, the thermal shock fracture resistance were significantly improved for the nanocomposite fabricated by the chemical processing. The residual strength of the monolithic Si_3N_4 and the Si_3N_4/15vol%BN microcomposite suddenly decreased at ΔT of 1200 and 1350 °C respectively, whereas the nanocomposite containing 15 vol% BN dispersion did not show the sudden decrease in residual strength even at ΔT of 1500 °C. The specimens, especially in the microcomposites, were often broken perpendicular to the hot-pressing direction, after water-quenching, as shown in Fig.4-3.

A general and simple approach to estimate the thermal shock fracture resistance of ceramic materials is given by following equation[1 8]:

$$\Delta Tc = \frac{\sigma(1-\nu)}{E\alpha} \qquad (4\text{-}1)$$

where ΔTc is the temperature difference above which the residual strength decreases suddenly, σ is the fracture strength, υ is Poisson's ratio, E is Young's modulus and α is the coefficient of thermal expansion.

Table 4-1 shows Young's modulus and fracture strength for the monolithic Si_3N_4 and Si_3N_4/BN composites.

Table 4-1. Mechanical properties of monolithic Si_3N_4 and Si_3N_4/15vol%BN composites.

Material	Monolithic Si_3N_4	Si_3N_4/9μmBN	Si_3N_4/nano BN
Young's Modulus (GPa)	**320**	**261**	**262**
Fracture strength (MPa)	**1350**	**644**	**1250**

As mentioned in Chapter 3, the fracture strength of the conventional microcomposites decreased with increasing the micro-sized BN dispersions up to 15vol%. On the other hand, the nanocomposites in this work were successful in retaining relatively high strength in spite of decreasing in Young's modulus due to the soft h-BN (Young's modulus of h-BN is about 65 GPa) addition. This increase in strength was attributed to the homogeneous distributions of nano-sized h-BN, which do not play as the fracture origins, and also to the decrease in the abnormal grain growth of Si_3N_4 matrix. Thus, the nanocomposites were found to exhibit strongly improved high strength and low Young's modulus caused by the dispersion of soft BN. As can be seen from equation 4-1, this unique properties can be thought to contribute to the excellent thermal shock fracture resistance. It is, however, necessary to discuss the possibility of other parameters, coefficient of thermal expansion and Poisson's ratio for the improvement.

4. 3. 2 Coefficient of Thermal Expansion

Table 4-2 shows the coefficient of thermal expansion for monolithic Si_3N_4 and Si_3N_4/ BN microcomposite and Si_3N_4/ BN nanocomposite including 15 vol% BN dispersion. In this table, the coefficient of thermal expansion calculated from equation 4-2[1 9] is also included.

From the theoretical calculation using equation 4-2, it is thought that the coefficient of thermal expansion of composites increases by adding h-BN because of its high coefficient of thermal expansion. But both micro- and nanocomposites indicated lower thermal expansivity than the monolith. This result may be attributed to the microstructure of the composites. As represented in Fig. 4-4, the h-BN particle in the composite has many pores caused by cleavage of basal plane of h-BN due to thermal expansion mismatch between β-Si_3N_4 and h-BN. It is expected that the expansion at elevated temperatures can be relaxed by these pores. The same effect has also been reported in porous materials[2 0]. For these

reasons, it is thought that the soft and porous-BN particle is playing an important role to relax the thermal expansion.

Table 4-2. Coefficient of thermal expansion for Si_3N_4 and Si_3N_4/15vol%BN composites.

	Si_3N_4	Si_3N_4/9mmBN	Si_3N_4/nano-sized BN	h-BN
α (10^{-6}°C^{-1})	3.5	3.4 (3.7)*	3.4 (3.7)*	11.6 c axis direction 40.5 a axis direction -2.9

*) $$\alpha = \frac{\alpha_1 K_1 V_1 + \alpha_2 K_2 V_2}{K_1 V_1 + K_2 V_2} \qquad (4\text{-}2)$$

α : Coefficient of thermal expansion
K : Bulk modulus
V : Volume

4. 3. 3 Poisson's Ratio

Fig. 4-5 shows the effect of BN content on Poisson's ratio for the Si_3N_4/BN microcomposites and nanocomposite perpendicular and parallel to the hot-pressing direction. The composite with anisotropic dispersoids induced the splitting of Poisson's ratio to the three independent level[2 1]. In this work, we noted two important directions for mechanical properties, parallel and perpendicular to the hot-pressing direction. The inverse trend between two directions in respect to BN content suggests that Poisson's ratio of composites is controlled by the orientation of plate-like h-BN and rod-like h-BN. In the nanocomposites with homogeneous microstructure, Poisson's ratios of the two directions were almost same, whereas the significant difference was observed between the two directions in the microcomposites with the oriented microstructure. Higher Poisson's ratio perpendicular to the hot-pressing direction in the microcomposites may be result from the weak Van der Waals bond among basal planes of h-BN. Moreover, as can be seen in Table 4-3, the fracture toughness perpendicular to the hot-pressing direction in the microcomposites was lower than another direction, because Van der Waals bond of h-BN lies perpendicular to the hot-pressing direction. For this low fracture toughness, the fracture strength in same direction can also be presumed to be low.

Thermal shock by water-quench is homogeneously applied to all surfaces of the

specimen. Therefore, the weakest part of a specimen initiates fracture. As shown in Fig.4-3 and 4-6, the fracture perpendicular to the hot-pressing direction by thermal shock is attributed to high Poisson's ratio and low fracture strength in this direction due to the orientation effect.

Table 4-3. Fracture resistance of Si_3N_4/15vol%BN micro- and nanocomposite.

Material	Si_3N_4/9μmBN		Si_3N_4/nano BN	
	⊥	//	⊥	//
($MPam^{1/2}$)	4	6	6	6.5

⊥ : perpendicular to the hot-pressing direction
// : parallel to the hot-pressing direction

4. 4 Conclusions

The Si_3N_4/BN nanocomposites fabricated by chemical process exhibited a fine and homogeneous microstructure in which the nano-sized h-BN particles were homogeneously dispersed within the Si_3N_4 grain and at the grain boundaries. As a result, in comparison with the conventional microcomposites to indicate the strength degradation by h-BN addition, the nanocomposites in this work were successful in retaining relatively high strength in spite of decreasing in Young's modulus due to the soft h-BN dispersion. Moreover, the coefficient of thermal expansion of the composites was lower than that of the monolith due to the relaxation of thermal expansion by h-BN particles, and also the nanocomposites indicated lower Poisson's ratio. Thus, remarkably improved thermal shock fracture resistance for the Si_3N_4/BN nanocomposites is mainly attributed to the high fracture strength, low Young's modulus, low coefficient of thermal expansion and low Poisson's ratio.

References

[1] R. Rice, Am. Ceram. Soc. Bull., 63(1984)256-62

[2] D. G. Launay. G. Brayet and F. Thevenot, J. Mater. Sci. Lett., 5(1986)940-42

[3] W. Sinclair and H. Simmons, J. Mater. Sci. Lett., 6(1987)627-29

[4] K. Isomura, T. Hukuda, K. Ogasawara, T. Hunahashi and R. Uchimura, pp.624-34 in UNITECR '89 Proceedings. Edited by L. J. Trostel, Jr. American Cerami Society, 1989

[5] D.Lewis and R. Rice, Ceram. Eng. Sci. Proc., 2(1981)712-18

[6] G.Ziegler, "Progress in Nitrogen Ceramics", p565-588 Edited by F. L. Riley.
[7] J. Heinrich, D. Munz and G. Ziegler, Powd. Met. Int., 14(1982)153
[8] G. Ziegler and J. Heinrich, Proceedings of the 4th International Meeting on Modern Ceramics Technologies, 768-779
[9] A. Shimpo, H. Ide and M. Ueki, J. Ceram. Soc. Jpn., 100 (1992) 504-508
[10] K. Niihara, J. Ceram. Soc. Jpn., 100 (1991) 974-982
[11] K. Niihara, K. Suganuma and K. Izaki, J. Mater. Sci., 9 (1990)112
[12] K. Niihara, T. Hirano, K. Izaki and F. Wakai, Ceram. Trans.,42(1994)207-219
[13] T. Ohji, Y. -K. Jeong, Y. -H. Choa and K. Niihara, J. Am. Soc.,77(1994)3259
[14] T. Hirano and K. Niihara, Mat. Lett.,22(1995)249-254
[15] T. Sekino, T. Nakajima, S. Ueda and K. Niihara, J. Am. Chem. Soc., 80(1997)1139-1148
[16] T. Sekino and K. Niihara, J. Mater. Sci., (1997) in print.
[17] T. Sekino and K. Niihara, Nanostructured Materials, 6(1995)663
[18] 15 D. P. H. hasselman, *Am. Ceram. Soc. Bull.*, 49(1970)1033-37
[19] Turner, J. Res. NBS, 37(1946)239
[20] C. Kawai and A. Yamakawa, J. Am. Soc.,80(1997)2705-708
[21] T. Mizutani, T. Kusunose, M. Sando and K. Niihara, pp. 876-881, in 6th International Symposium on Ceramic Materials and Components for Engines. Edited by K. Niihara, S. Kanzaki, K. Komeya, S. Hirano and K. Morinaga, 1997, Arita, Japan

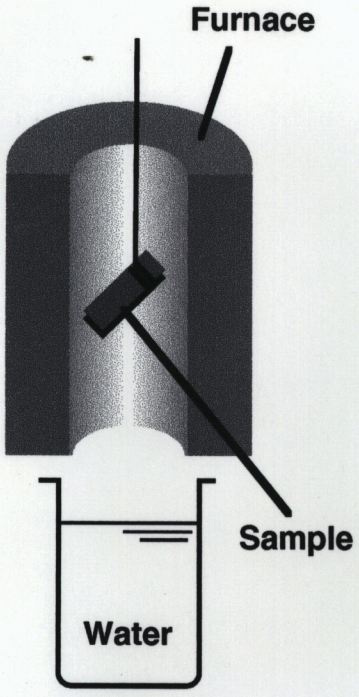

Fig. 4-1 Thermal shock test by water-quench method.

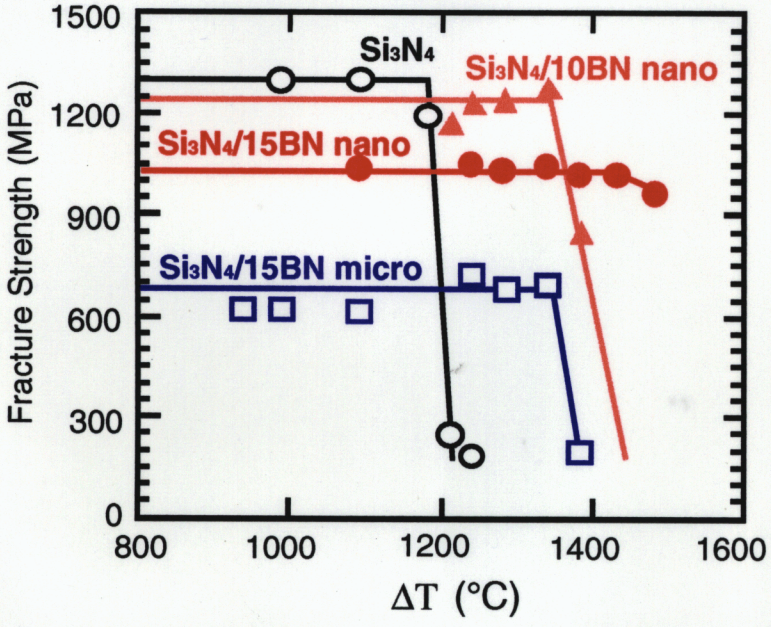

Fig.4-1 Residual strength of Si_3N_4/BN composites after thermal shock test.

○:monolithic Si_3N_4
□:Si_3N_4/15vol%BN microcomposite
●:Si_3N_4/15vol%BN nanocomposite
▲:Si_3N_4/10vol%BN nanocomposite

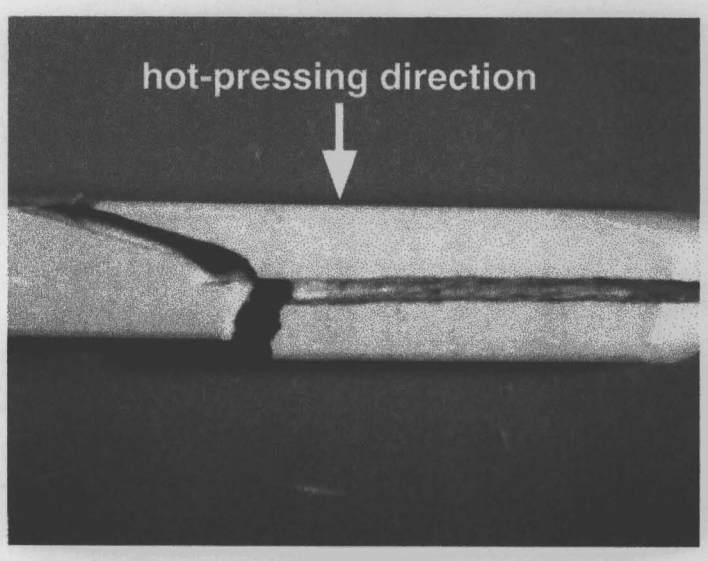

Fig. 4-3 The microcomposites showed fracture perpendicular to the hot-pressing direction by thermal shock.

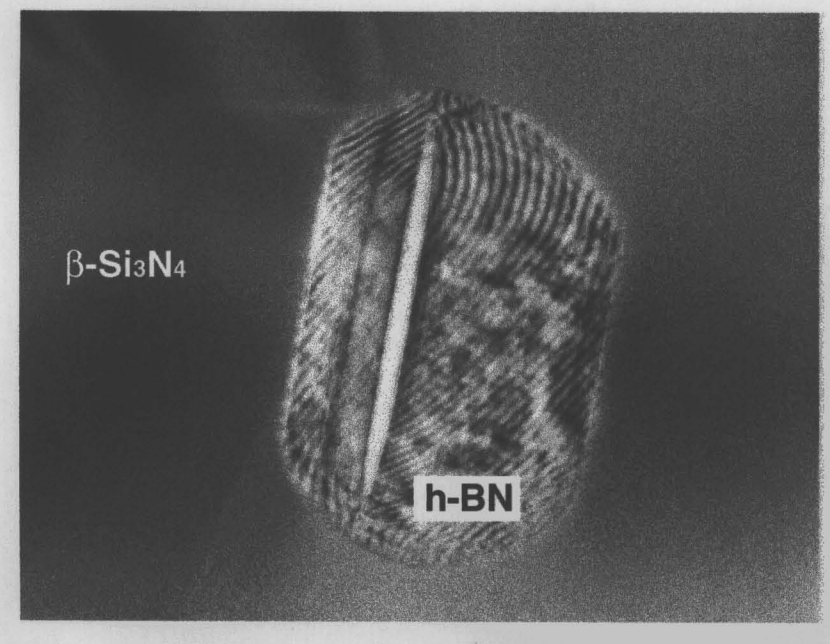

Fig. 4-4 Cleavage of basal plane of h-BN in Si_3N_4/BN composites.

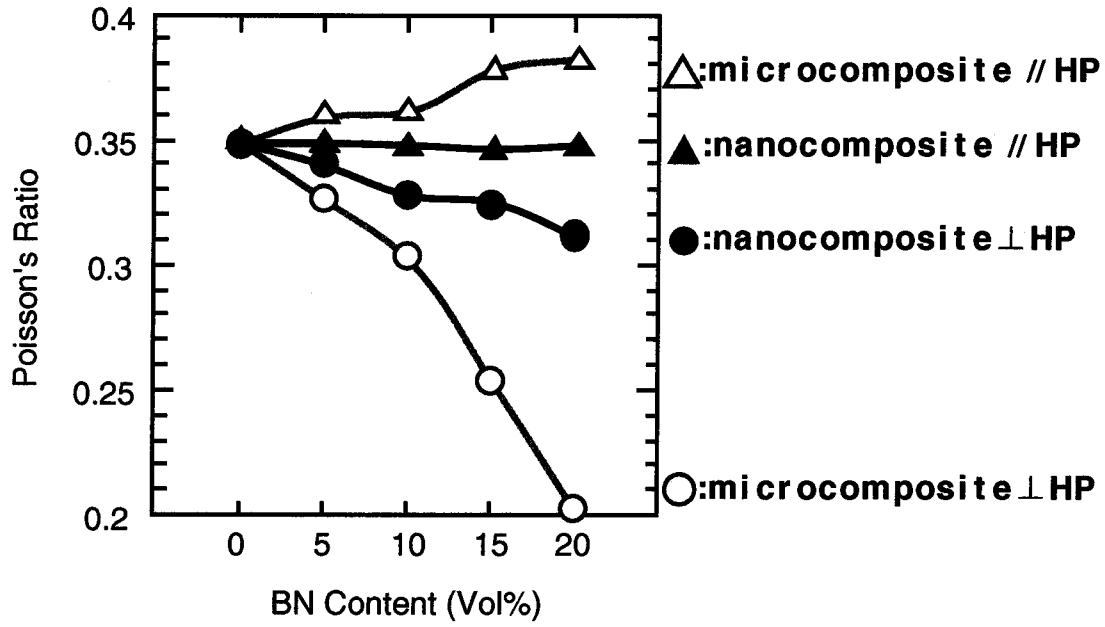

Fig. 4-5 Poisson's ratio as a function of BN content.
// HP : parallel to the hot-pressing direction.
⊥HP : perpendicular to the hot-pressing direction.

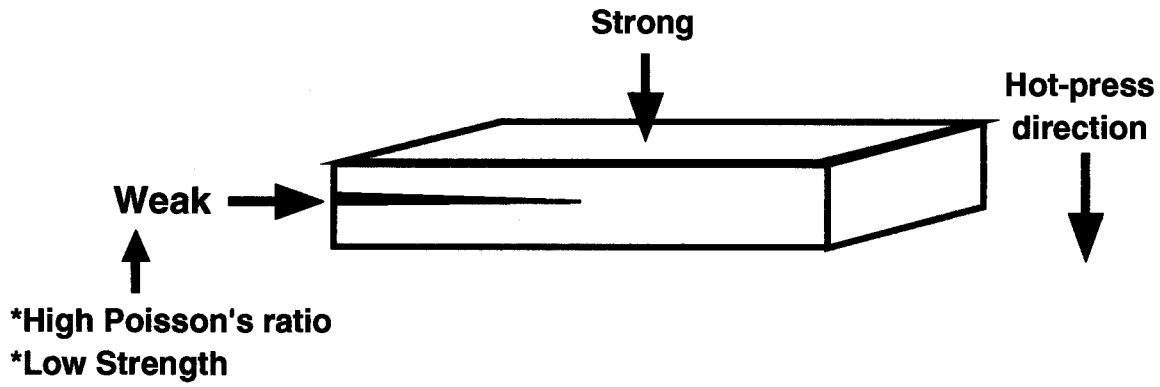

Fig. 4-6 Schematic illustration for the fracture of the microcomposites by thermal shock.

Chapter 5

High-Temperature Properties of Si_3N_4/BN Nanocomposites

It is well-known that Si_3N_4 ceramics has the excellent mechanical properties at elevated temperatures. Furthermore, the crystal structure of h-BN is similar to that of graphite, and then the h-BN can be expected to show high temperature properties like graphite, of which fracture strength and Young's modulus increase with a rise in temperature. It is, therefore, interesting to investigate the effect of h-BN dispersoids with unique high temperature mechanical properties on the high temperature mechanical properties of ceramics matrix composites.

In this chapter, thus, high temperature mechanical properties of Si_3N_4/BN nanocomposites were evaluated to make clear the role of fine h-BN at elevated temperatures. As a result, it was found that the improvements of high temperature strength and hardness for the nanocomposite were attributed to the inhibition of the softening of grain boundary phases by intergranular nano-sized h-BN particles and the increase in Young's modulus of h-BN at elevated temperatures like graphite.

5. 1 Introduction

Si_3N_4 ceramics are one of the most promising engineering materials because of the excellent thermomechanical properties such as high elevated temperature strength, low coefficient of thermal expansion and relatively high resistance to thermal shock and chemical attack. In particular, its applications have been expected in the field of high-temperature structural ceramics, such as in gas turbine engines, rocket and laser nozzles, radomes and antenna windows. Si_3N_4 ceramics, however, somewhat decrease in fracture strength at high temperatures due to the softening of grain boundary glassy phases and consequent grain boundary sliding and cavity formation, although it has good fracture strength and fracture toughness at room temperature. Therefore, the incorporation of second phases such as SiC and h-BN with superior mechanical properties at high temperatures is thought to be effective to enhance the properties of grain boundary phases[1,2,3,4], and then to obtain Si_3N_4 ceramics with excellent high-temperature mechanical properties. Among these materials,

especially h-BN has the same crystal structure as graphite which indicates the increasing fracture strength and Young's modulus at high temperatures.

Many researchers investigated the effect of SiC particle addition on the mechanical properties of Si_3N_4, in order to take advantage of both materials[5,6,7,8,9,10]. On the other hand, the studies of Si_3N_4/BN composites in respect to high temperature properties have hardly been reported because of the undesirable properties of h-BN such as considerably low Young's modulus and low fracture strength, in spite of its excellent high temperature properties and chemical stability. In these works, moreover, most of the added h-BN[11,12,13,14] were micrometer sized particulates, platelets or fibers. Addition of micrometer-sized second phases often increased the fracture energy[15,16]. In almost cases, however, the fracture strength was remarkably decreased because the large dispersoids or its agglomerations increased the flaw size.

In the last 10 years, Niihara and his colleagues[17,18,19,20,21] have investigated ceramic based nanocomposites, in which the nano-sized particles are dispersed within the matrix grains and/or at the grain boundaries. These nanocomposites showed the improved fracture strength and excellent creep resistance compared with the monolithic ceramics and its microcomposites. In early nanocomposites, the hard and strong dispersoids such as SiC, TiC and TiN were incorporated into the matrix to mainly improve fracture strength and high temperature properties. But, recently, it was found that even soft and weak materials like a metal or h-BN showed the same enhancement of fracture strength, as mentioned in chapter 3. In these nanocomposites, the improvement of mechanical properties can be also expected at elevated temperatures. However, there are no reports on the improvement of mechanical properties at high temperatures by nano-sized soft and weak ceramic dispersoids.

The purposes in this chapter were to evaluate fracture strength, hardness and Young's modulus up to elevated temperatures, and to clarify the effect of fine h-BN dispersions on them.

5. 2 Experimental Procedures

5. 2. 1 Specimen Preparation

Monolithic Si_3N_4 and Si_3N_4/BN nanocomposites were fabricated through the conventional metallurgical processing and the chemical process newly developed in the present work, in order to evaluate various high-temperature mechanical properties as

mentioned below.

5. 2. 2 Evaluation

High Temperature X-ray Diffraction Analysis

The variation of lattice spacing at elevated temperatures was observed by *in-situ* XRD technique in an X-ray diffractometer (X1 system, Scintag Inc., CA., U.S.A). A Pt direct heating stage (10 mm x 50 mm x 0.15 mm) was used, welded to a $Pt_{90}Rh_{10}$/Pt thermocouple. The XRD patterns were acquired using CuKα radiation operated at 45kV and 40mA in the range between room temperature and 1000 °C. Specimens with dimension 3 mm x 4 mm x 0.2 mm were cut and machined for XRD measurement

High Temperature Fracture Strength

Flexural strength was measured at elevated-temperatures up to 1400°C. Three-point bending test was conducted with outer span of 30 mm. The rectangular specimens with dimension of 3 mm x 4 mm x 37 mm were cut and machined from the hot-pressed disks. The edges were chamfered to eliminate machining flaws. The high temperature bending tests were conducted in nitrogen atmosphere with a crosshead speed of 0.5 mm/min. For high-temperature bending tests, a box furnace was placed between frames of a testing instrument (AG-10TC, Shimadzu Co. Ltd., Kyoto, Japan). The heating rate was 10 °C/min and after reaching the test temperature, the temperature was maintained for an additional 10 min prior to testing for thermal stability.

High Temperature Hardness

Hardness at high temperatures was measured using Vickers indenter by a high temperature hardness tester (QM, NICON Co. Ltd., Tokyo, Japan) on polished surfaces of specimens. Vickers diamond indentations were carried out under a condition of 9.8 N load with loading duration of 15 s in vacuum up to 1300°C. Vickers hardness, H_V, was calculated with the standard equation:

$$Hv = \frac{1854.4P}{(2a)^2} \qquad (5\text{-}1)$$

where P is the applied load (N) and 2a is the indentation diagonal (μm).

High Temperature Young's Modulus

Young's modulus (E) was measured with a resonance technique in air at elevated-

temperatures up to 1400°C. The shape of the specimen was a rectangular bar 2 mm x 15 mm x 55 mm. E was calculated from equation (2-1)[22].

5. 3 Results and Discussion

5. 3. 1 X-ray Diffraction Pattern

Fig. 5-1 shows high temperature XRD patterns for the Si_3N_4/BN nanocomposite including 30 vol% BN dispersion up to 1400°C. No big change was observed for the all peaks of β- Si_3N_4, but the peak of (002) reflection of h-BN was considerably shifted to lower angle from 26.8° at 20°C to 25.58° at 1400°C. As considered from the shifts of peaks for β-Si_3N_4 and h-BN, it is found that c-axis of h-BN extend preferentially with a rise of temperature, compared to β- Si_3N_4. This result implies that residual tensile stress caused by thermal expansion mismatch between h-BN and β-Si_3N_4 are relaxed by restructuring in BN particulates at elevated temperatures.

5. 3. 2 Fracture Strength

Fig. 5-2 shows the variations of fracture strength with temperature for monolithic Si_3N_4 and Si_3N_4/30vol%BN nanocomposite. In Fig. 5-3, the same data is also expressed as the temperature dependence of the σ_h/σ_r ratio, which indicate a rate of strength degradation and can be obtained by dividing the strength (σ_h) at high temperatures by that (σ_r) at room temperature.

The σ_h/σ_r ratio of the monolithic Si_3N_4 remarkably decreased with a rise of temperature compared to the nanocomposite containing 30vol%BN dispersion. Especially at 1300°C, the monolith showed the suddenly decrease in fracture strength. On the other hand, the nanocomposite did not show such a degradation, and also the strength slightly decreased up to 1600°C. It is well-known that the strength degradation of Si_3N_4 at elevated temperatures is caused by the softening of the grain boundary glassy phase and consequent grain boundary sliding and cavitation[23,24]. The sudden decrease at 1300°C observed in the monolithic Si_3N_4 is attributed to the softening of the grain boundary glassy phase. The improvement of high temperatures strength for the nanocomposite, therefore, can be explained by the inhibition of the softening of grain boundary phases by the intergranular nano-sized h-BN particles with excellent high temperature mechanical properties.

5. 3. 3 Hardness and Young's Modulus

The variation of Vickers hardness with temperature for monolithic Si_3N_4 and Si_3N_4/30vol%BN nanocomposite is represented in Fig. 5-4. Additionally, in Fig. 5-5 the same data is also expressed as the temperature dependence of the H_h/H_r ratio, where H_h and H_r are hardness at high temperatures and room temperature, respectively.

The nanocomposite showed rather mild decrease in the H_h/H_r ratio with increasing test temperature, compared to the monolithic Si_3N_4. The hardness of the monolithic Si_3N_4 rapidly decrease, especially at 1300°C, whereas that of the nanocomposite did not show such strong degradation. The sudden decrease in hardness for the monolith at 1300°C is consistent with the degradation of the fracture strength observed at 1300°C. As described previously, it has been reported that the mechanical properties of Si_3N_4 at elevated temperatures is predominantly determined by the properties of the grain boundary glassy phase. Thus, the retention of hardness for the nanocomposite at elevated temperatures also results from the suppression of softening of the grain boundary glassy phase.

Furthermore, the composites containing h-BN can be anticipated that the Young's modulus increases with a rise in temperature, because h-BN has the same crystal structure and properties as graphite[25,26,27,28], of which Young's modulus increases at elevated temperatures. Fig. 5-6 shows the temperature dependence of Young's modulus for monolithic Si_3N_4 and h-BN, and Si_3N_4/30vol%BN nanocomposite. In monolithic Si_3N_4, the linear degradation of the Young's modulus was observed up to about 1300°C, and steep degradation occurred above that temperature, as reported by other researchers[29]. This steep degradation corresponded to the degradation of the strength of this material. In the nanocomposite, however, such a degradation of Young's modulus was not observed, and moreover its Young's modulus increased at high temperatures up to 1400°C. The Young's modulus of the monolithic h-BN could not be estimated due to severe oxidation above at 1100°C, but the same trend as the nanocomposite was confirmed. It is well-known that Young's modulus is closely correlated with hardness, and the hardness increases with increasing Young's modulus. Considering these results, it is though that the excellent hardness observed in the nanocomposite is influenced not only by the inhibition of softening of grain boundary phases but also by the increase in Young's modulus at high temperatures.

5. 4 Conclusions

The Si_3N_4/30vol%BN nanocomposite exhibited superior mechanical properties at high

temperatures compared to the monolithic Si_3N_4.The improvements of high temperature strength and hardness for the nanocomposite were attributed to the inhibition of the softening of grain boundary phases by intergranular nano-sized h-BN particles with excellent high temperature mechanical properties and the increase in Young's modulus at elevated temperatures.

References

[1] A. Tsuge, K. Nishida and M. Komatsu, J. Am. Ceram. Soc., 58(1975)323-26

[2] F. F. Lange, Am. Ceram. Soc, Bull., 62(1983)1369-74

[3] D. R. Clarke, F. F. Lange and G. D. Schnittgrund, J. Am. Ceram. Soc., 65(1982)c-51-53

[4] W. A. Sanders and D. M. Mieskowski, J. Am. Ceram. Soc., 64(1985)304-309

[5] F. F. Lange, J. Am. Ceram. Soc., 56(1973)445

[6] K. Ueno and S. Sodeoka, Yogyo-Kyokai-Shi, 94(1986)981

[7] P. D. Shalek, J. J. Petrovic, G. F. Hurley and F. D. Gac, Am. Ceram. Soc. Bull., 66(1987)347

[8] H. Kodama, T. Suzuki, H. Sakamoto and T. Miyoshi, J. Am. Ceram. Soc., 73(1990)445

[9] Y. Akimura, N. Hirosaki and T. Ogasawara, J. Mater. Sci.,27(1992)6017

[10] G. Ssaki, H. Nakase, K. Suganuma, T. Fujita and K. Niihara, J. Ceram. Soc. Jpn., 100(1992)536

[11] W. Sinclair and H. Simmons, J. Mater. Sci. Lett., 6(1987)627-29

[12] K. Isomura, T. Hukuda, K. Ogasawara, T. Hunahashi and R. Uchimura, pp.624-34 in UNITECR '89 Proceedings. Edited by L. J. Trostel, Jr. American Cerami Society, 1989

[13] K. S. Mazdiasni and R. Ruh, J. Am. Ceram. Soc., 64(1981)415

[14] D. G. Launay. G. Brayet and F. Thevenot, J. Mater. Sci. Lett., 5(1986)940-42

[15] E. H. Lutz and M. V. Swain, J. Am. Ceram. Soc., 75(1992)67-70

[16] S. Hayama, M. Ozawa and S. Suzuki, J. Ceram. Soc. Jpn., 103(1995)833-837

[17] K. Niihara, J. Ceram. Soc. Japan., 100 (1991) 974-982

[18] K. Niihara, K. Suganuma and K. Izaki, J. Mater. Sci., 9 (1990)112

[19] T. Ohji, Y. -K. Jeong, Y. -H. Choa and K. Niihara, J. Am. Soc., 77(1994)3259

[20] T. Hirano and K. Niihara, Mat. Lett., 22(1995)249-254

[21] T. Sekino, T. Nakajima, S. Ueda and K. Niihara, J. Am. Chem. Soc., 80(1997)1139-1148

[22] S. Sakaguchi, F. Wakai and Y.Matsuno, J. Ceram. Soc. Japan. 95(1987)476

[23] A. G. Evans and A. Rana, Acta Metall., 28(1980)129

[24] C. Chu, J. P. Singh and J. L. Roubort, J. Am. Chem. Soc., 86(1993)1349
[25] V. Brozek and M. Hubacek, J. Solid State Chem., 100(1992)120-129
[26] A. Lipp, K. A. Schwetz and K. Hunold, J. Euro. Ceram. Soc., 5(1989)3-9
[27] R. T. Paine and C. K. Nalula, Chem. Rev., 90(1990)73-91
[28] S. Alkoy, C. Toy, T. Gonul and A. Tekin, J. Euro. Ceram. Soc., 17(1997)1415-1422
[29] S. Sakaguchi, N. Murayama, Y. Kodama and F. Wakai, J. Mater. Sci. Lett., 10(1991)282-284

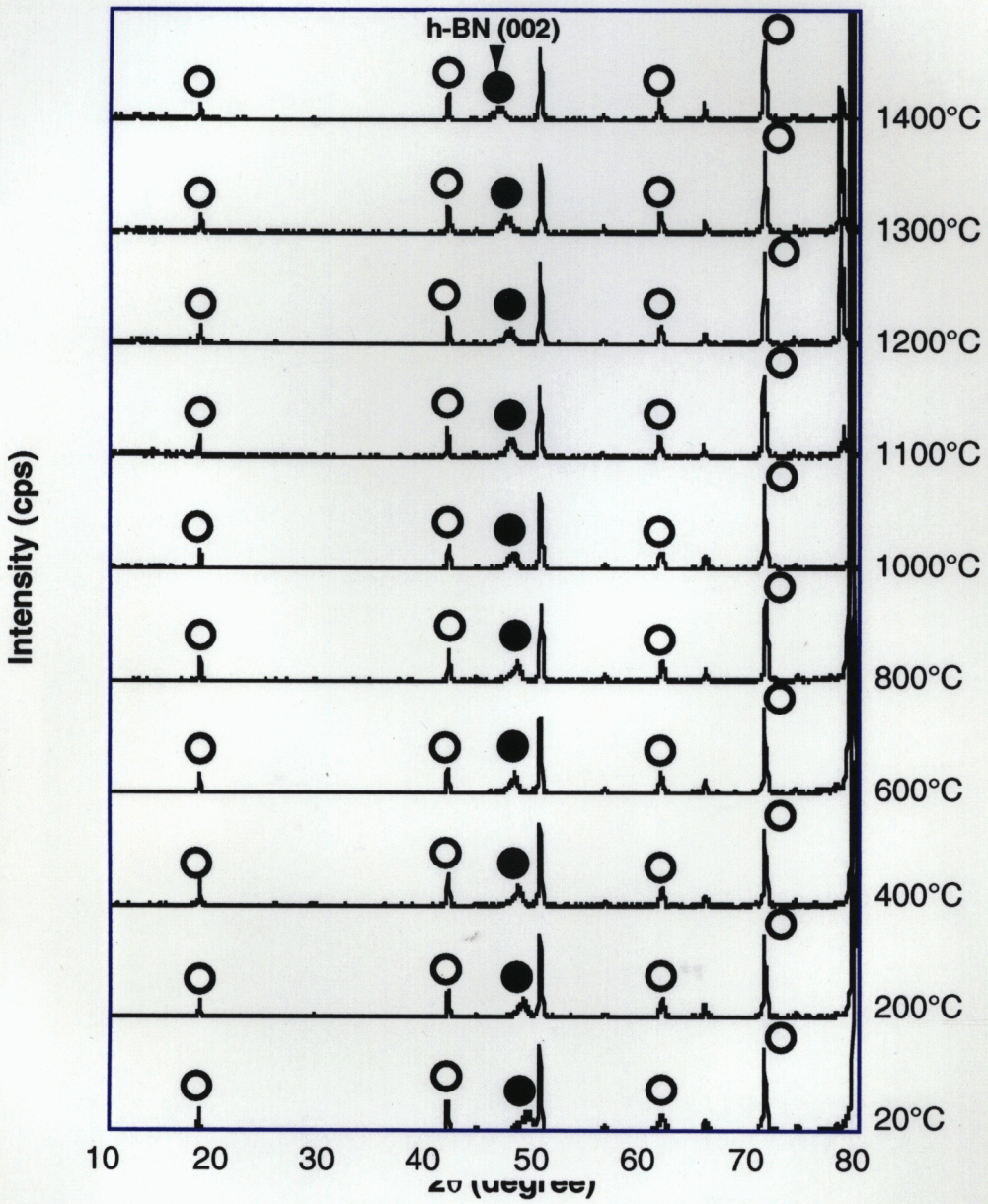

Fig. 5-1 Temperature dependence of XRD patterns of Si_3N_4/30vol%BN nanocomposite.
○: β-Si_3N_4, ●: h-BN

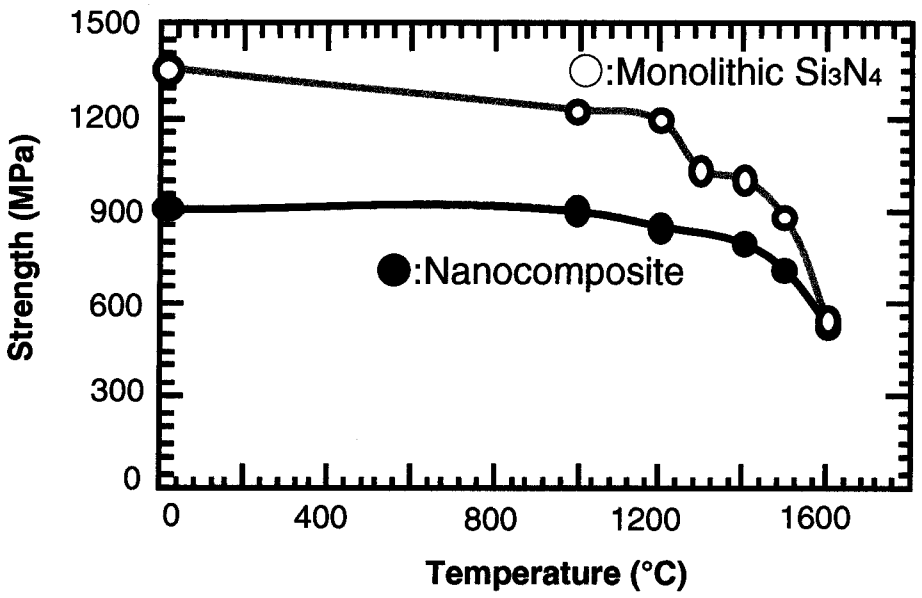

Fig. 5-2 Temperature dependence of bending strength for monolithic Si_3N_4 and Si_3N_4/30vol%BN nanocomposite.

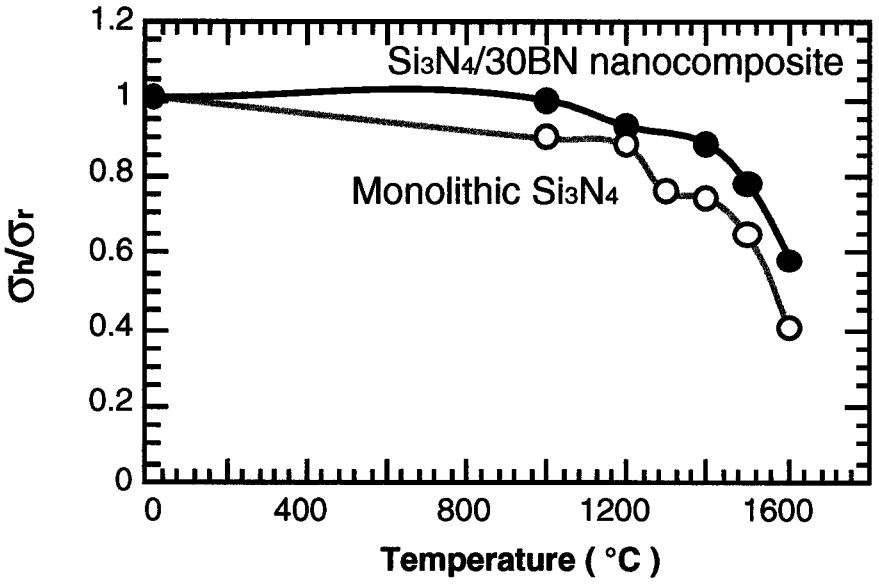

Fig. 5-3 Temperature dependent of σ_h/σ_r for monolithic Si_3N_4 and Si_3N_4/30vol%BN nanocomposite.

σ_r : Room temperature strength
σ_h : High temperature strength

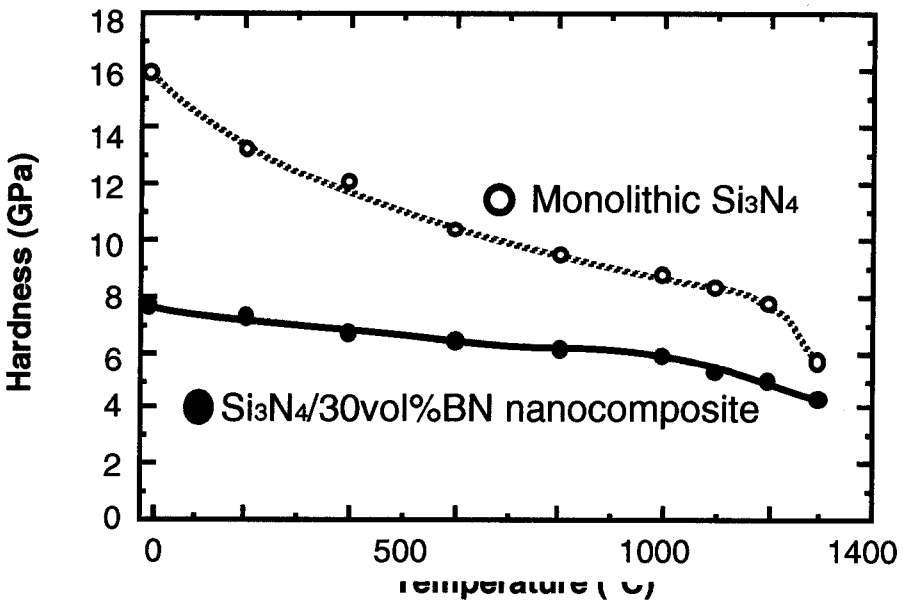

Fig. 5-4 Temperature dependence of Vickers hardness for monolithic Si_3N_4 and Si_3N_4/30vol%BN nanocomposite.

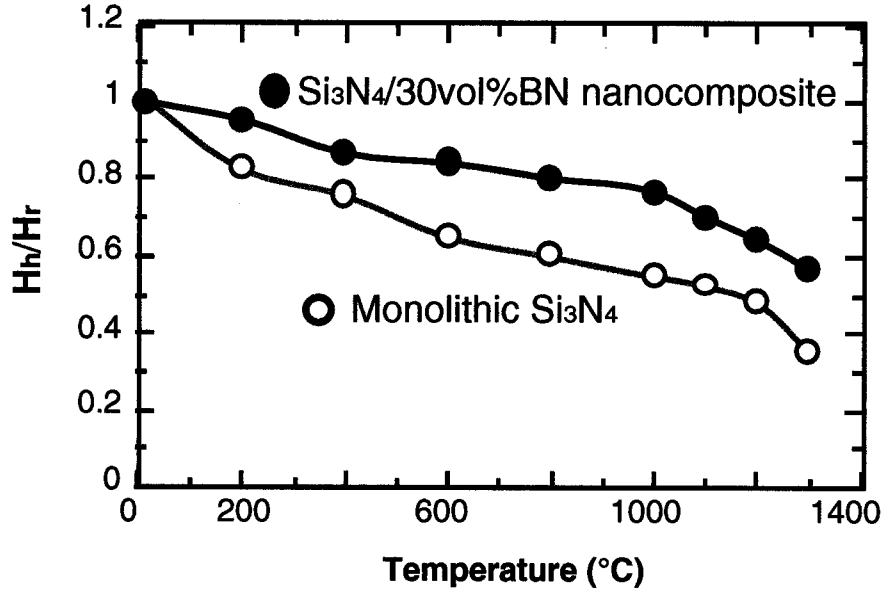

Fig. 5-5 Temperature dependent of **Hh/Hr** for monolithic Si_3N_4 and Si_3N_4/30vol%BN nanocomposite.

Hr : Room temperature hardness

Hh : High temperature hardness

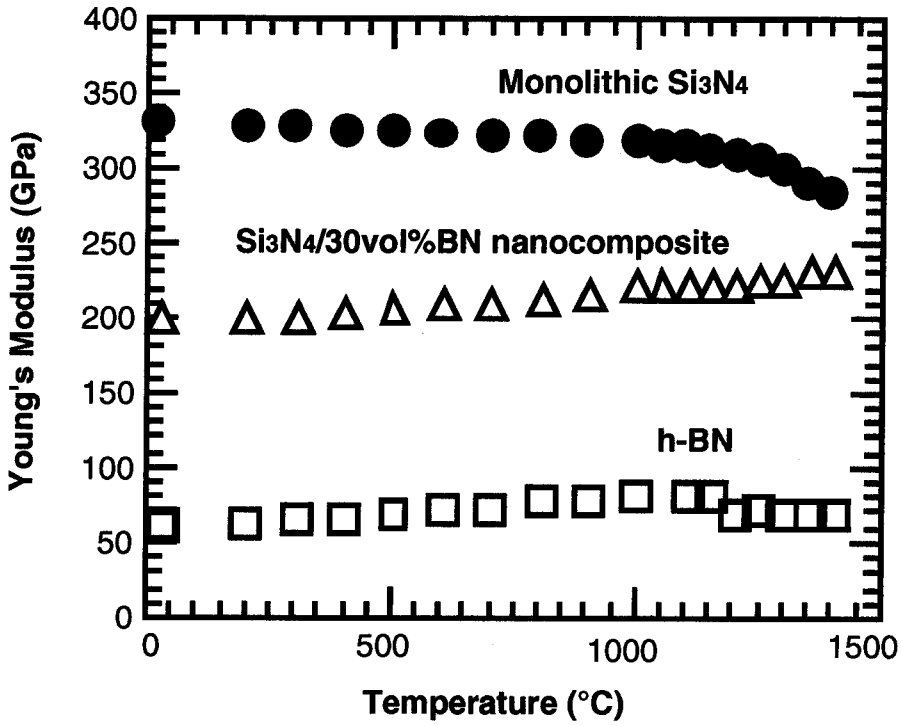

Fig. 5-6 Temperature dependence of Young's modulus for monolithic Si_3N_4 (●), h-BN (□) and Si_3N_4/30vol%BN nanocomposite (△).

Chapter 6

Machinability of Si_3N_4/BN Composites

Generally, ceramic materials have been considered as materials with hard machinability compared to metals. This significant disadvantage of ceramics leads to high machining cost. For their practical uses, the development of machinable ceramics without losing their excellent properties is very important. In this chapter, it is reported that for conventional Si_3N_4/BN microcomposite, the fracture strength remarkably decreased with increasing h-BN content, although machinability was somewhat improved. However, the nanocomposites fabricated by the new chemical method were successful in attaining simultaneously high fracture strength and good machinability. Hertzian contact test was performed to clarify the deformation behavior by machining. As a result of this test, the damage of the monolithic Si_3N_4 and Si_3N_4/BN microcomposites indicated a classical Hertzian cone fracture and many large cracks, whereas the damage observed in the nanocomposites appeared to be quasi-plastic deformation, which is expected to absorb and to disperse the damage force. The excellent machinability for the nanocomposites could be explained by the quasi-plastic deformation, which was originated from the weak interface between the Si_3N_4 matrix and the h-BN dispersion.

6.1 Introduction

Ceramics are increasingly used in such engineering components as rotors, nozzles, valves and sliding gates because of their high strength, high hardness and good chemical inertness. Among ceramics materials, Si_3N_4 is recognized to be one of the most promising engineering ceramics due to its high fracture toughness and strength, excellent wear resistance and oxidation resistance. However, such properties as corrosion resistance to molten metals, thermal shock fracture resistance and machinability are insufficient for their practical uses as various machine parts. Especially, the machinability is thought to be important, because most of engineering components have complex shapes and hence require machining by highly expensive diamond tools. Their difficulty in machining after sintering leads to high machining cost. To decrease it, various ceramics having machinability, called machinable ceramics[1,2,3], have been developed. Typical machinable ceramics are mica-based

glass-ceramics, which are made of glass matrix and plate-like mica with layered structure[4,5,6,7,8,9]. In such glass ceramics, the machinability appears due to the layer-structured dispersoids. However, these machinable glass ceramics are poor in fracture strength and high temperature properties. Therefore, the h-BN with the layered structure like a mica and the excellent high temperature properties[10,11,12,13] has recently been studied as a second phase dispersion into the Si_3N_4 matrix[14,15]. In the conventional Si_3N_4/BN composites, machinability was guaranteed due to the laminar structure of h-BN dispersoids, although the significant decrease in fracture strength was observed with an increase in BN content[16]. This decrease in fracture strength of these Si_3N_4/BN microcomposites could be attributed to the aggregation of h-BN grains caused during mixing of commercial powders. Therefore, the homogeneous dispersions of h-BN particles into the matrix is probably effective to enhance the fracture strength of machinable Si_3N_4/BN composites.

Niihara and his colleagues[17,18,19,20,21,22] have investigated ceramic based nanocomposites in which the nano-sized particles are dispersed within the matrix grains and/or at the grain boundaries, and revealed that the dispersion of nano-sized particles remarkably improve the mechanical properties of oxide and non-oxide ceramic materials. In early nanocomposites, hard and strong dispersoids were mainly incorporated into the matrix to improve the mechanical properties. But in later years soft and weak materials like metals were also used as dispersoids, and the enhancement of the fracture strength was also found by addition of even soft and weak dispersoids[23,24,25]. This approach implies that the nano-sized h-BN dispersion could be expected to improve the mechanical properties of Si_3N_4 ceramics with good machinability, if the homogeneous dispersion of nano-sized BN is realized in the composites. However, it has not been reported that the mechanical and machinable properties of Si_3N_4 ceramics are improved simultaneously by the nano-sized soft and weak ceramic dispersoid such as h-BN.

Furthermore, it is important to investigate the deformation mechanisms of these materials with extremely soft and weak h-BN dispersion. Hertzian contact test was reported as a method to clarify the deformation mechanisms by mechanical shock [26,27,28,29,30]. Hertzian indentation of homogeneous brittle materials, such as glasses and single crystals, has received extensive attentions in the literature. Above a critical load, a ring crack initiates in the weakly tensile region just outside the circle of contact with the indenting sphere, propagates downward as a surface-truncated cone, and is finally arrested at a depth approximately equal to the contact radius. This is the so-called Hertzian cone crack, which is common for brittle ceramics.

Few Hertzian indentation studies have been made for the new generation of tougher polycrystalline and ceramics matrix composites, where microstructure plays a critical role in the fracture behavior. Some cone fracture observations have been reported on low-toughness fine-grain monolithic ceramics, for example Al_2O_3 with fine grain size[31, 32]. However, examination of Hertzian indentation in Al_2O_3 ceramics with large grain size or relatively high porosity has revealed a fundamental transition from classical Hertzian cone fracture to quasi-plastic deformation with the accumulated damage[33]. It is established that this deformation mechanism has a potential to disperse and absorb mechanical shock and to enhance the machinability and residual strength after machining[34]. Additionally, thermal shock resistance is also thought to be improved by this mechanism.

The purposes of this chapter is to evaluate the machinability of Si_3N_4/BN micro- and nanocomposites. Special emphasis was placed on understanding the effect of micro- and nanostructure on the machinability using the Hertzian contact test.

6. 2 Experimental Procedures

6. 2. 1 Specimen Preparation

Monolithic Si_3N_4 and Si_3N_4/BN microcomposites including 15 and 30vol% BN dispersions were fabricated by the conventional metallurgical processing, and the Si_3N_4/BN nanocomposites were produced through the chemical process developed in the present work. The detailed processes are included in chapters 2 and 3.

6. 2. 2 Evaluation of Machinability

Machinability of each composites was tested using tungsten carbide (WC/Co) cermet drill of 1 mm in diameter as shown schematically in Fig. 6-1. The drilling test were done using a standard drill press operating at 660 rpm. The composite specimens were mounted on a load cell and tested by manually applying a constant normal force to the drill at a load of 50 N.SEM observation of the drilled surface for each composites was performed to investigate the magnitude of the damage caused by drilling.

6. 2. 3 Hertzian Contact Test

Ball indentation measurement

The sintered materials were cut and machined to rectangular specimens of 3 mm X 4

mm X 20 mm. The surfaces for the indentation stress-strain testing were polished with the diamond past of 0.5 μm finish, and then coated with gold. Indentations were made using WC/Co spheres of radii r = 0.5, 1, 1.5 and 2 mm, with a load range from P = 0 to 2940 N using an universal testing machine (Autograph, AG-10TC, Shimadzu Co. Ltd., Japan), as shown in Fig. 6-2. Contact radius (a) at each applied load was determined by residual traces in the gold layer after ball indentation [3 5], and thence contact pressure (p_0) as a function of indentation strain (a/r) was plotted (see Sec *6.3.3 Indentation Stress-Strain Curve*).

Damage Observations

Examination of sub-surface contact damage by ball-indentation was made using a bonded-interface technique[3 6, 3 7, 3 8, 3 9, 4 0, 4 1], consisting of two polished half blocks joined together by adhesive. Indentations were made symmetrically across the traces of the interface at loads of 980 and 1960N with a tungsten carbide (WC) sphere of radius 1 mm. After testing, the bonded materials were separated and the surfaces and sections cleaned with acetone. The polished specimens were viewed in an optical microscope using Nomarski interface contrast to reveal the macroscopic damage patterns[4 2, 4 3], as also represented in Fig. 6-2.

Strength Degradation

Bars 3 x 4 x 37 mm were machined for measurement of strength degradation from Hertzian contact damage. The prospective test faces and sides of these bars were polished to 3 μm finish. The strength tests were conducted in three-point bending. An indentation was made at the center of each polished surface at a specified contact load, using a sphere of radius 1 mm. Some specimens were left unindented to measure "natural" strength. The tests were conducted with a crosshead speed of 0.5 mm/min. Broken specimens were examined to ensure that the fracture originated from the indentation sites.

6. 3 Results and Discussion

6. 3. 1 Machinability

At 15vol% BN dispersion, these composite materials were somewhat difficult to machine by a WC/Co drill. However, both Si_3N_4/BN micro- and nanocomposites containing more than 20 vol% BN exhibited good machinability like metals as shown in Fig. 6-3. Especially the nanocomposites represented excellent machinability with retaining high

strength. The difference of machinability between 15 and 20vol%BN contents is attributed to the BN particles dispersed at grain boundaries. The intergranular BN particles, rather than the intragranular BN particles, are effective for machinability. It has been reported that machinability is caused by the weak interface between matrix grains and second phases at grain boundaries. Actually, even considerably hard material, SiC, exhibited machinability due to easy grain detachment caused by incorporating heterogenities, specially weak interface, long grains and high thermal expansion mismatch stresses, into the microstructure. The machinability observed in the nanocomposites with high strength were probably achieved by grain detachment promoted by weak interface formed between Si_3N_4 matrix grains and intergranular h-BN particles.

6. 3. 2 Drilling Damage

Fig. 6-4 shows the drilled surfaces of the micro and nanocomposite containing 30vol% BN dispersion. In the drilled surface of all samples, the intergranular fracture is visible. From these SEM micrographs, the significant different micromechanism of material removal was recognized between micro- and nano composites. In the microcomposite, the damage caused by drilling was very severe because of lager crack path along micro-sized BN grain. By contrast, the damage in the nanocomposites, characterized by finer h-BN dispersion, was relatively minor. The superior damage property of nanocomposites presumably results from the homogeneous dispersion of finer h- BN particles, which is expected to absorb and to disperse the damage force during the machining operations by many finer cracks formed at the grain boundary. In the next 3 sections (6. 3. 3, 6. 3. 4 and 6. 3. 5), Hertzian contact test were performed, in order to demonstrate these damage mechanisms.

6. 3. 3 Indentation Stress-Strain Curve

Fig. 6-5 showed indentation stress-strain curve for the monolithic Si_3N_4 and Si_3N_4/BN nanocomposites including 20 and 30 vol% BN dispersions. The responses were obtained by monitoring mean contact pressure (p_0)

$$p_0 = \frac{P}{\pi \cdot a^2} \qquad (6\text{-}1)$$

as a function of the geometrical ratio a/r, where P, a and r are the indentation load, the radius of contact and the sphere radius, respectively. For reference, the dashed line at the right axis

represents Vickers hardness value for the test material.

The monolithic Si_3N_4 behaved in an ideal brittle manner, with near-linear response up to p_0 = 8.5 GPa, but above that stress, the curve slightly deviated because of deformation of the WC/Co spherical indenter. By contrast, the curves of the Si_3N_4/BN nanocomposites including 20 and 30 vol% BN dispersions showed dramatically deviated from the linear response at p_0=5.5 and 4.5 GPa. Considering these responses of the monolith and the nanocomposites, it was found that some deformation occurred at lower indentation stresses with increasing in BN content. These results imply that the deformation can be promoted by h-BN dispersion.

6. 3. 4 Microscopic Observations of Subsurface Damage

Fig. 6-6 presented the half-surface (upper) and side section (lower) views of Hertzian contact damage for Si_3N_4 monolith and Si_3N_4/BN micro- and nanocomposite containing 30vol%BN dispersion, respectively. The damage in the monolithic Si_3N_4 showed a typical Hertzian cone fracture with no sign of residual surface depression and near-circular surface ring cracks, penetrating downward into classical subsurface Hertzian cones. And the detectable deformation could not be observed beneath the contact in the monolith. These observations demonstrate that the monolithic Si_3N_4 in this work behaves as ideally brittle solid, as also recognized in the stress-strain curves. On the other hand, the Si_3N_4/30vol%BN microcomposite represented many large cracks in the subsurface deformation zone beneath the contact. These large cracks were evidently different from the classical Hertzian cone crack observed in the monolith, and may be attributed not only to the dispersion of larger h-BN particles but also to the microstructure with the orientation of rod-like β-Si_3N_4 and plate-like h-BN perpendicular to the hot-pressing direction. By further observation of the deformation area, it was found that these cracks lie perpendicular to the hot pressing direction. As mentioned in chapter 3 and 4, h-BN and β-Si_3N_4 easily oriented perpendicular to the hot-pressing direction during hot-press sintering. Because of this orientation effect, the strength perpendicular to the hot-pressing direction of bulk specimen will be very weak, and hence cracks propagate easily in this direction. As a result, it is presumed that such large cracks were observed in the microcomposite.

In contrast to previous two materials, in the nanocomposite, the damage observed in subsurface deformation zone appears to be quasi-plastic deformation, reminiscent of the plastic deformation zone in ductile metals. And also, this deformation accompanied the residual surface depression the disappearance of surface ring crack, and this fact represents the transition from brittle to ductile by finer h-BN dispersion. The nanocomposite has the

microstructure in which fine h-BN particles were homogeneously dispersed within Si_3N_4 grain as well as at the grain boundary. Therefore, it is thought to be possible to disperse and absorb the stresses from the ball-indentation by fine cracks originated from finer h-BN particle dispersed at the grain boundary.

Fig. 6-7 showed SEM micrographs of unindented surface and quasi-plastic deformation zone observed in the nanocomposite. The significant interface crackings of grain boundaries were observed in the damaged zone. From this observation, it is assumed that the bonding strength of grain boundary was decreased by nano-sized intergranular BN particles. It has been reported that the quasi-plasticity is driven by a strong shear component. In the case of the nanocomposites, one of the reasons for good machinability should be quasi-plasticity caused by the weak interfaces between the Si_3N_4 matrix grain and the h-BN dispersion at the grain boundary.

6. 3. 5 Strength Degradation

Results from the Hertzian-indentation/inert-strength tests were plotted in Fig. 6-8 for the Si_3N_4/15vol%BN microcomposite and the nanocomposite. For the microcomposite, the strength maintained its high strength for natural surface up to the critical indentation load for large clacks as shown in Fig. 6-9, but at the critical load it drops precipitously. Whereas, the strength of the nanocomposite indicated a steady decline without a precipitously degradation. The small decrease in the strength was observed at a load of 490 N, and this decrease may be attributed to a low damage caused by the quasi -plastic deformation as shown in Fig. 6-10. These results strongly imply that the quasi-plastic deformation is unable to absorb and disperse a mechanical shock.

Thus, the quasi-plastic deformation will be important to maintain high strength after machining as well as to shape hard sintered materials into complex shape. Furthermore, one of the reasons of the excellent thermal shock fracture resistance for the nanocomposites (described in chapter 4) will be also explained by this deformation which can be expected to absorb and disperse a thermal shock.

6. 4 Conclusions

The Si_3N_4/BN nanocomposite fabricated by the new chemical method successfully attained high fracture strength and excellent machinability simultaneously. The observed excellent machinability was attributed to the quasi-plasticity, which can be expected to absorb

and to disperse the damage force during the machining operation. Furthermore, SEM observation showed that this deformation was originated at the weak interfaces between the Si_3N_4 matrix and the h-BN dispersion. Now it is concluded that this uncommon deformation behavior realize excellent machining of strong ceramics, as shown in Fig. 6-11. For these superior properties, practical uses of the Si_3N_4/BN nanocomposite ceramics might be expected in the wide engineering fields.

References

[1] N. P. Padture, C. J. Evans, H. K. Xu and B. R. Lawn, J. Amer. Ceram. Soc., 78(1995)215-17

[2] J. B. Davis, D. B. Marshall, R. M. Housley and P.E. D. Morgan, J. Amer. Ceram. Soc., 81(1998)2169-75

[3] C. Kawai and A. Yamakawa, J. Amer. Ceram. Soc.,80(1997)2705-708

[4] Y. Ikeda, M. Sitoh and T. Murakami, Kogyou Ziryo, 35(1987)100-104

[5] T. Hamazaki, Kikaigizyutu, 39(1991)65-70

[6] V. Saraswati and S. Raoot, J. Mater. Sci., 27(1992)429-32

[7] T. Uno, T. Kasuga and S. Nakayama, J. Ceram. Soc. Jpn., 100(1992)315-19

[8] T. Uno and T. Kasugaboundary, 9(1993)11-17

[9] T. Uno, T. Kasuga and K. Niihara, J. Amer. Ceram. Soc., 74(1991)3139-41

[10] V. Brozek and M. Hubacek, J. Solid State Chem., 100(1992)120-129

[11] A. Lipp, K. A. Schwetz and K. Hunold, J. Euro. Ceram. Soc., 5(1989)3-9

[12] R. T. Paine and C. K. Nalula, Chem. Rev., 90(1990)73-91

[13] S. Alkoy, C. Toy, T. Gonul and A. Tekin, J. Euro. Ceram. Soc., 17(1997)1415-1422

[14] T. Funabashi, K. Isomura, A. Harita, and R. Uchimura, p. 968-976 (1986), Ceramic materials and Components for Engines. Edited by V. J. Tenney, Amer. Ceram. Soc.,Las Vegas, NV, 1986

[15] K. S. Mazdiyasni and Robert Ruh, J. Am. Ceram. Soc., 64 [7] 415-418 (1981)

[16] D. Goeuriot-Launay, G. Brayet, F. Thevenot, J. Mater. Sci. Lett.., 5 (1986) 940-942

[17] K. Niihara, J. Ceram. Soc. Japan., 99(1991)974-982

[18] T. Ohji, Y. -K. Jeong, Y. -H. Choa and K. Niihara, J. Am. Soc.,77(1994)3259

[19] F. Wakai, Y. kodama, S. Sakaguchi, N. Murayama, K. Izaki & K. Niihara, Nature, 344(1990)421-423

[20] K. Niihara, J. Jpan. Powd. and Powd Metal., 37(1990) 348-351

[21] K. Niihara, K. Izaki and A. Nakahira, J. Jpn. Powd. and Powd. Metal., 37(1990) 352-356
[22] K. Niihara and T. Hirai, 21(1986)598-604
[23] T. Sekino and K. Niihara, Nanostructured Materials, 6(1995)663
[24] T.Sekino and K. Niihara, J. Mater. Sci., (1997) in print.
[25] T.Sekino, T. Nakajima, S. Ueda and K. Niihara, J. Am. Chem. Soc., 80(1997)1139-1148
[26] V. R. Howes and S. Tolansky, Proc. R. Soc. London, A230(1955)287-293
[27] V. R. Howes and S. Tolansky, Proc. R. Soc. London, A230(1955)294-301
[28] F. C. Frank and B. R. Lawn, Proc. R. Soc. London, A299(1967)291-306
[29] B. R. Lawn,j. Appl. Phys. 39(1968)4828-36
[30] M. V. Swain and J. T. Hagan, J. Phys. D: Appl. Phys. 9(1976)2201-14
[31] F. Guiberteau, N. P. Padture and B. R. Lawn, J. Amer. Ceram. Soc., 77(1994)1825-1831
[32] M. Belmonte and S.-K. Lee, J. Mater. Sci. Lett., 16(1997)379-81
[33] B. A. Latella, B. H. O'Connor, N. P. Padture and B. R. Lawn, J. Amer. Ceram. Soc., 80(1997)1027-31
[34] N. P. Padture and B. R. Lawn, J. Amer. Ceram. Soc., 78(1995)1431-38
[35] F. Guiberteau, N. P. Padture, H. Cai and B. R. Lawn, Philos. Mag., A68(1993)1003-16
[36] B. R. Lawn, J. Amer. Ceram. Soc., 81(1998)1977-94
[37] B.R. Lawn, N. P. Padture,H. Cai and F. Guiberteau, Science, 263(1994)1114-1116
[38] A.C. Fischer-Cripps and B.R. Lawn, J. Amer. Ceram. Soc., 79(19968)2609-18
[39] N. P. Padture and B. R. Lawn, J. Amer. Ceram. Soc., 77(1994)2518-22
[40] F. Guiberteau, N. P. Padture, H. Cai and B. R. Lawn, Phil. Mag., A68(1993)1003-1016
[41] A.C. Fischer-Cripps and B.R. Lawn, Acta mater., 44(1996)519-527
[42] H. Cai, M. A. Stevens Kalceff, and B. R. Lawn, J. Mater. Res., 9(1994)762-770
[43] T. O. Mulhearn, J. Mech. Phys. Solids, 7(1959)85-96

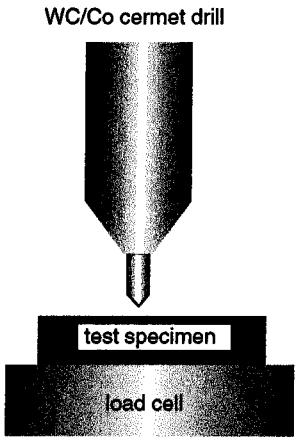

Fig. 6-1 Schematic diagram illustrating the test set-up for drilling measurements.

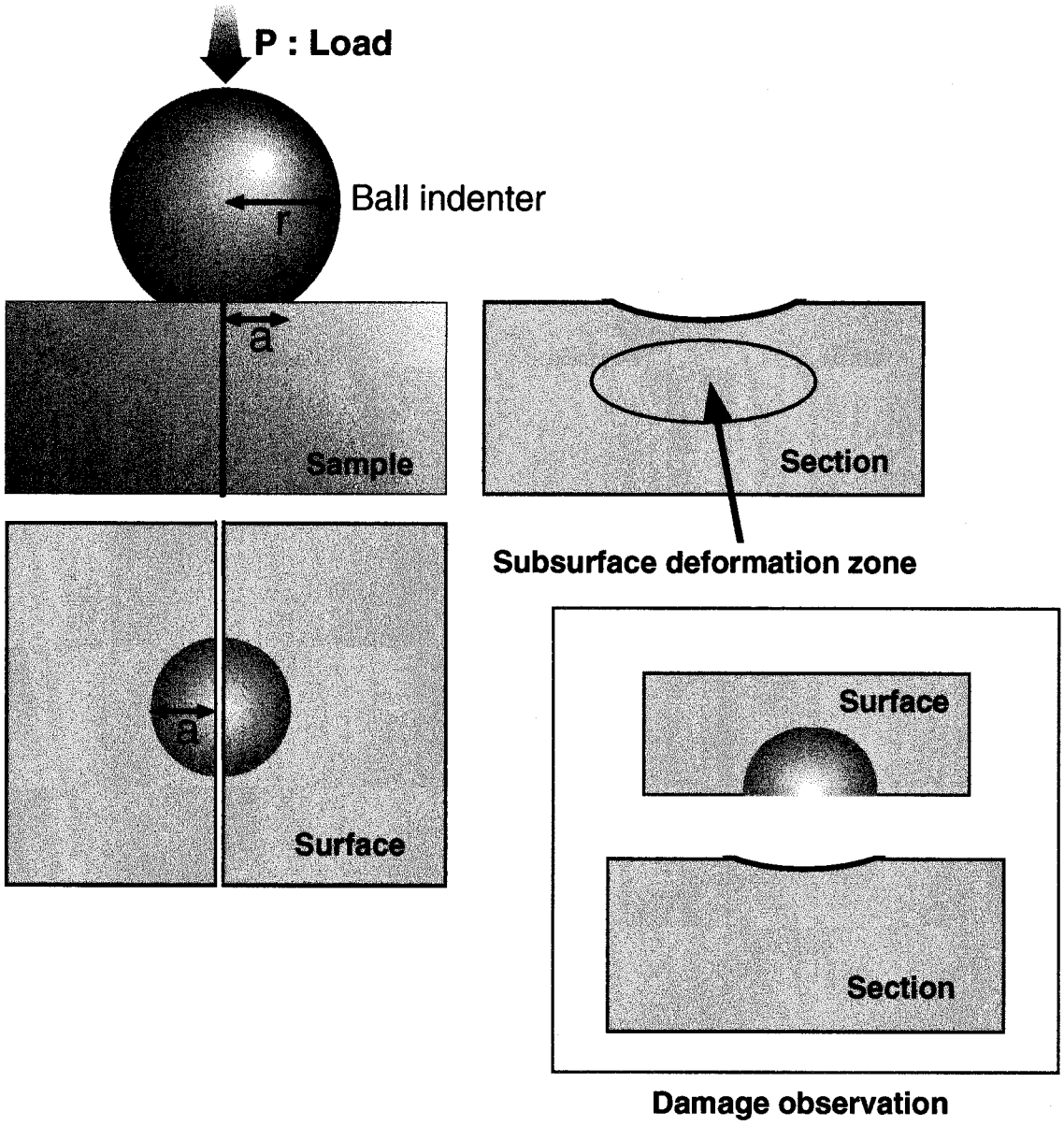

Fig. 6-2 Schematic diagram illustrating the test set-up for ball-indentation measurements including indentation stress-strain test and damage observation using a bonded interface specimen.

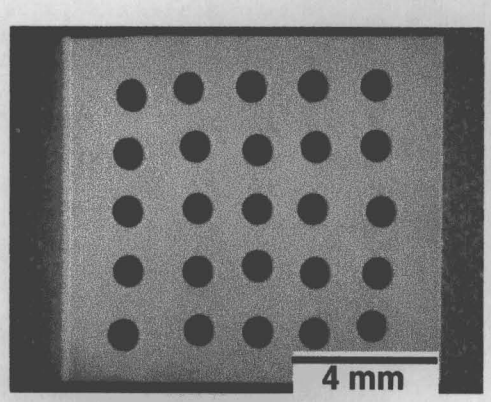

Fig. 6-3 Si_3N_4/20vol%BN nanocomposite machined by WC/Co drill.

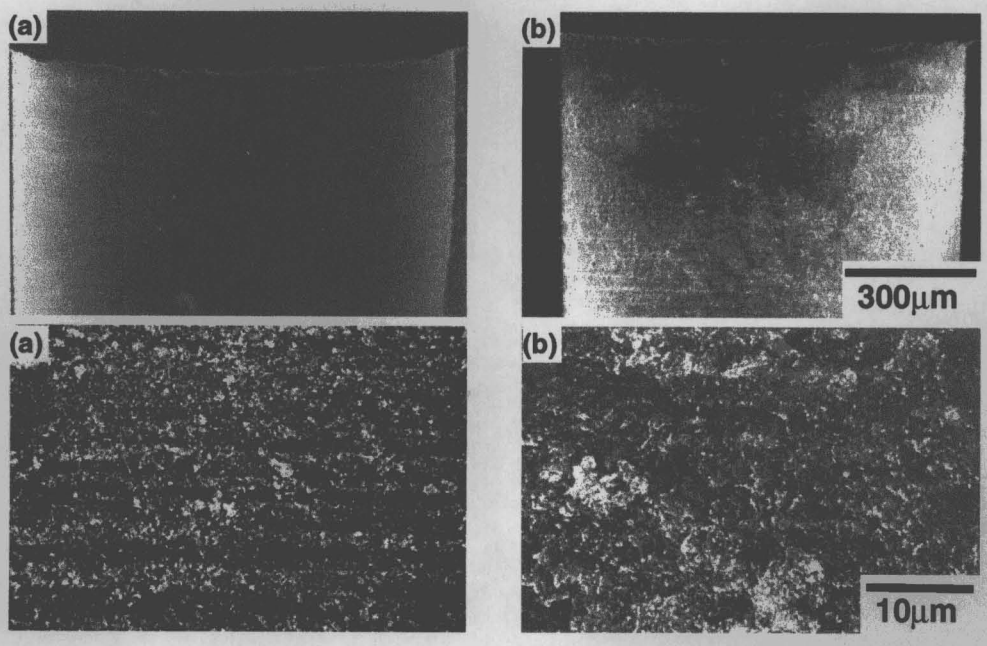

Fig. 6-4 SEM micrographs of drilled surfaces for Si_3N_4/30vol%BN nanocomposite (a) and Si_3N_4/30vol%BN microcomposite (b).

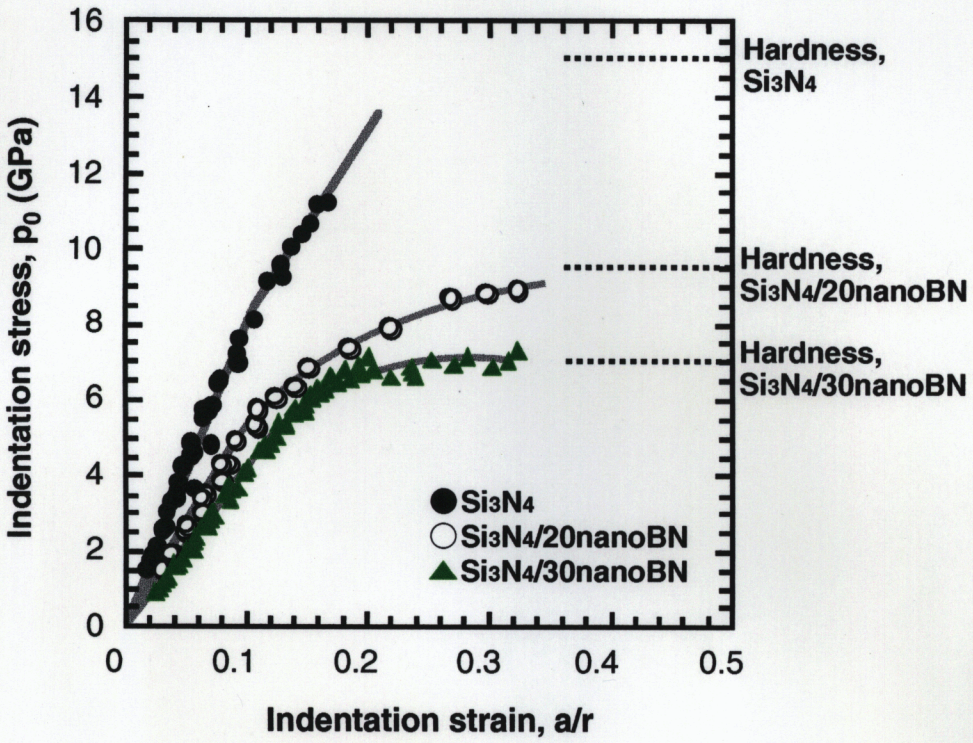

Fig. 6-5 Indentation stress-strain curve of monolithic Si_3N_4 and nanocomposite including 20 and 30vol% BN.

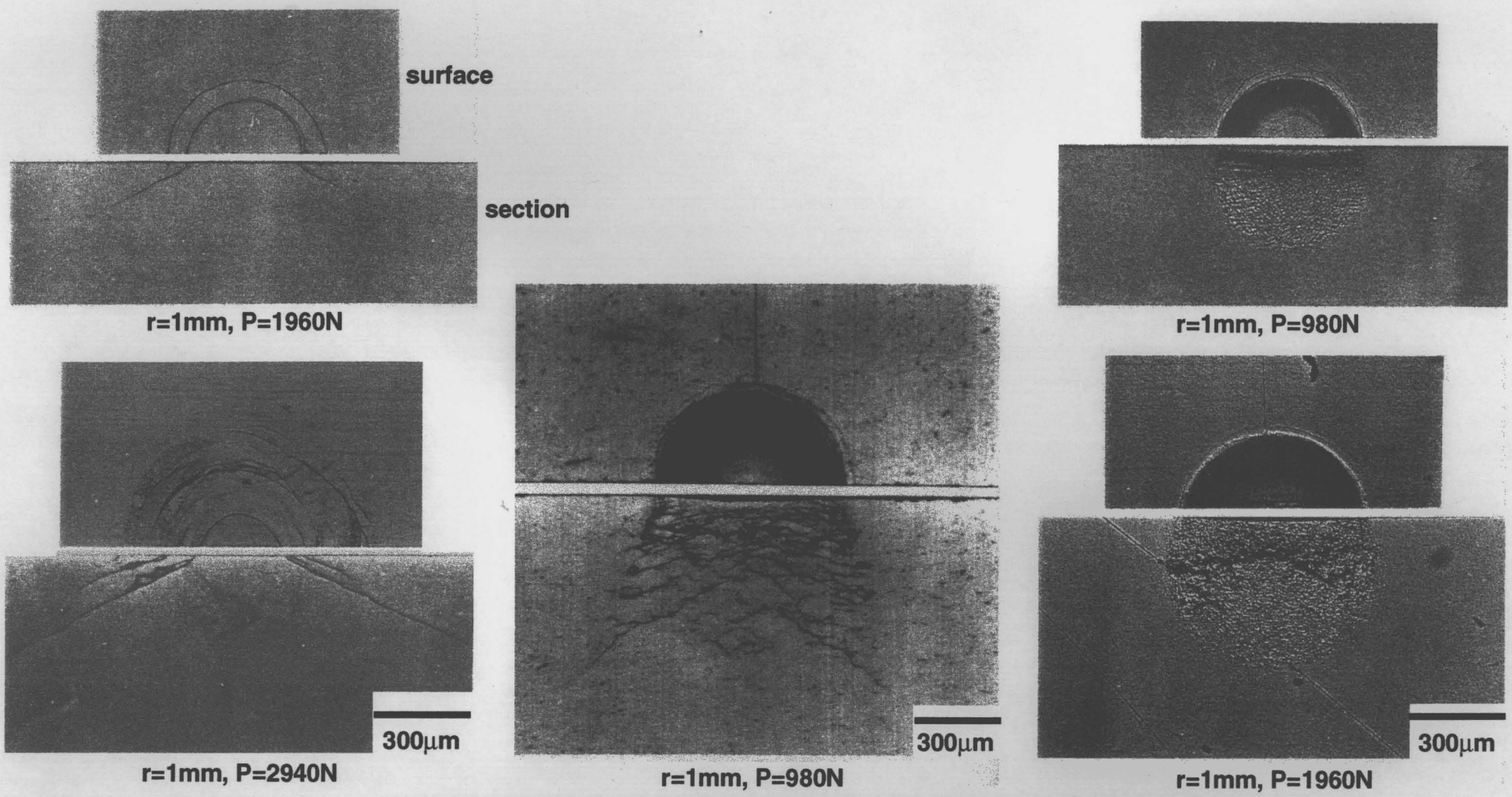

Fig. 6-6 Hertzian contact damage of monolithic Si_3N_4 (A), Si_3N_4/30vol% BN micro- (B) and nanocomposites (C).

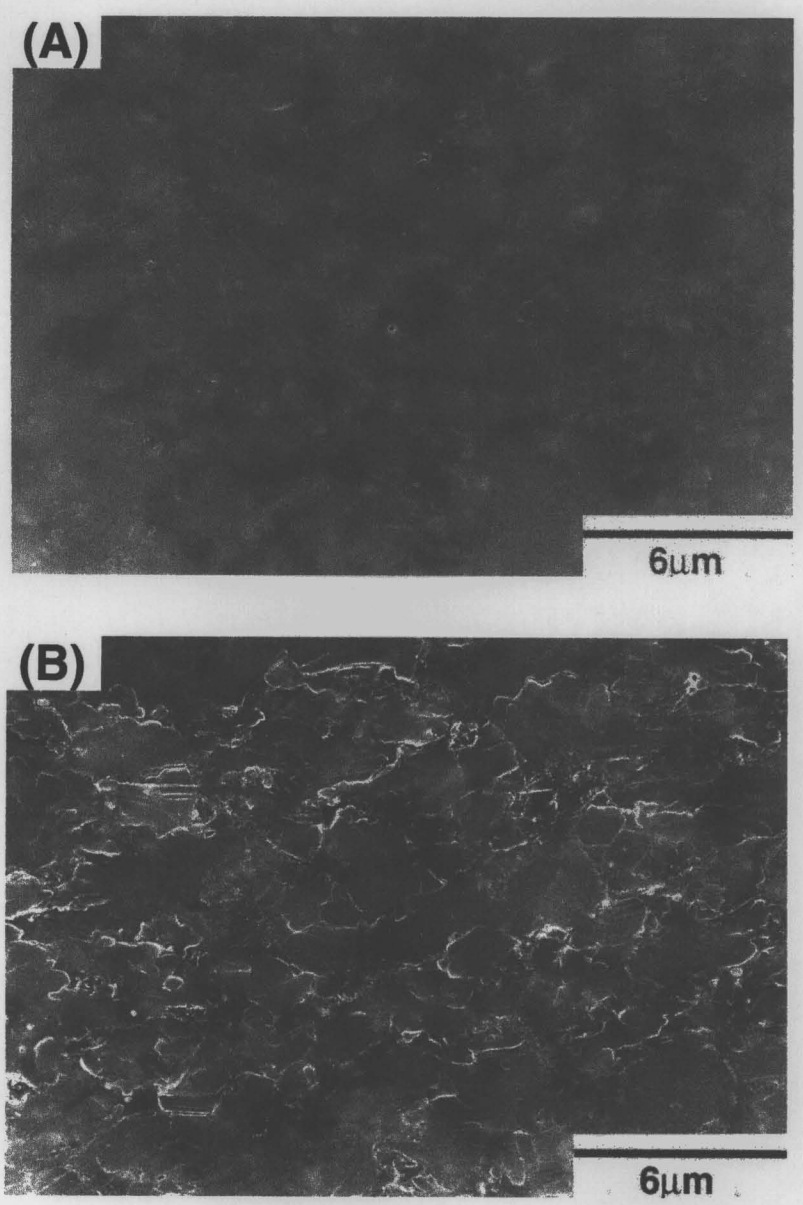

Fig. 6-7 SEM micrographs of subsurface deformation zone of Si_3N_4/30vol%BN nanocomposite. (a) polished surface and (b) quasi-plastic deformation zone.

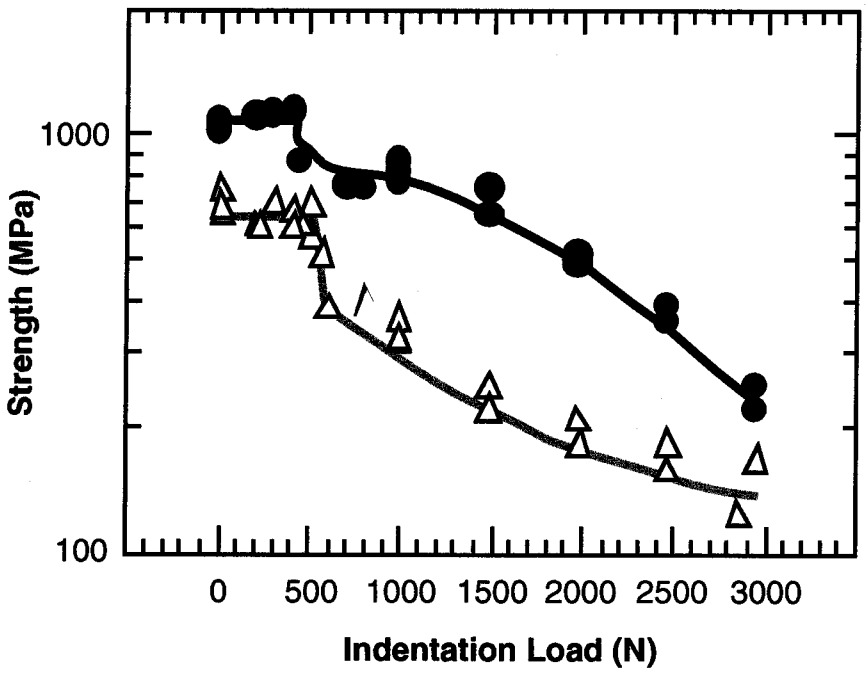

Fig. 3-8 Inert strength of Si_3N_4/15vol%BN nanocomposite (●) and microcomposite (△) after ball indentations .

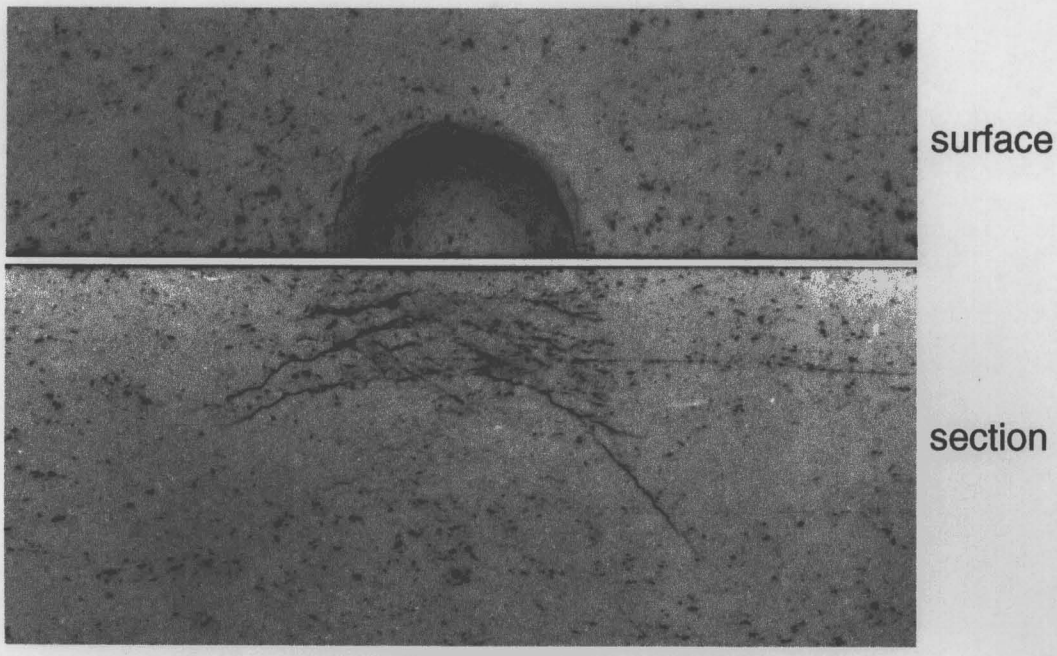

r=1mm, P=980N

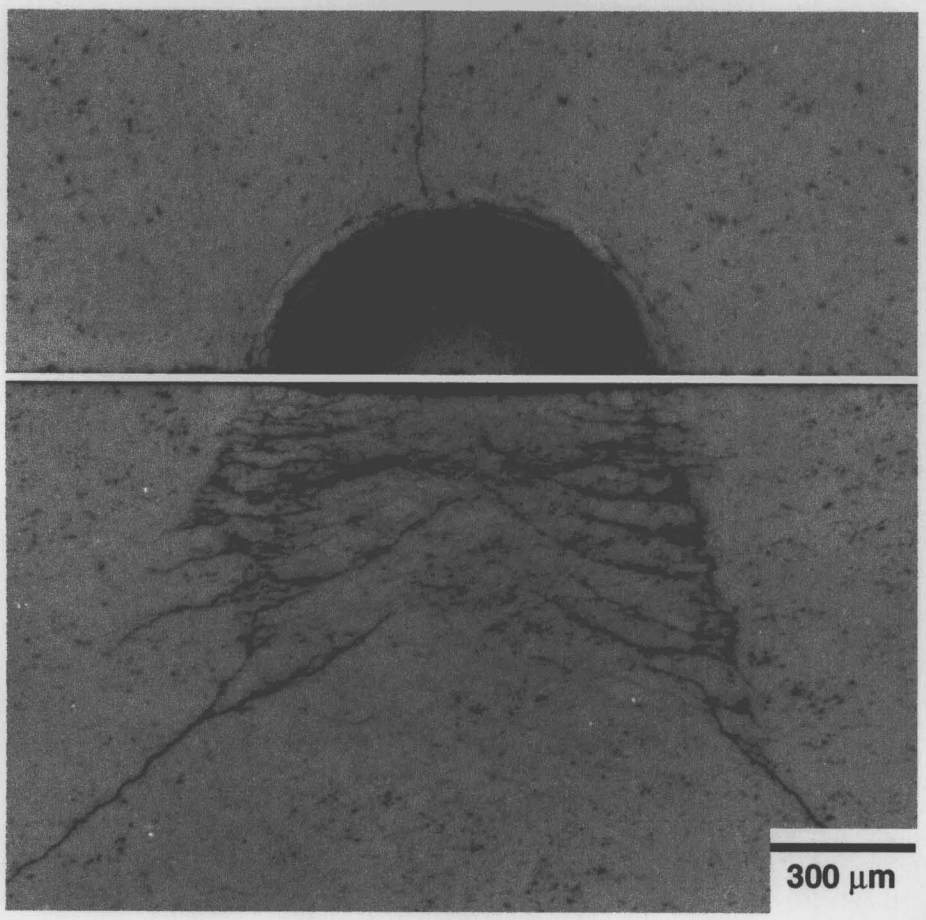

r=1mm, P=2940N

Fig. 6-9 Hertzian contact damage for Si_3N_4/15vol%BN microcomposite.

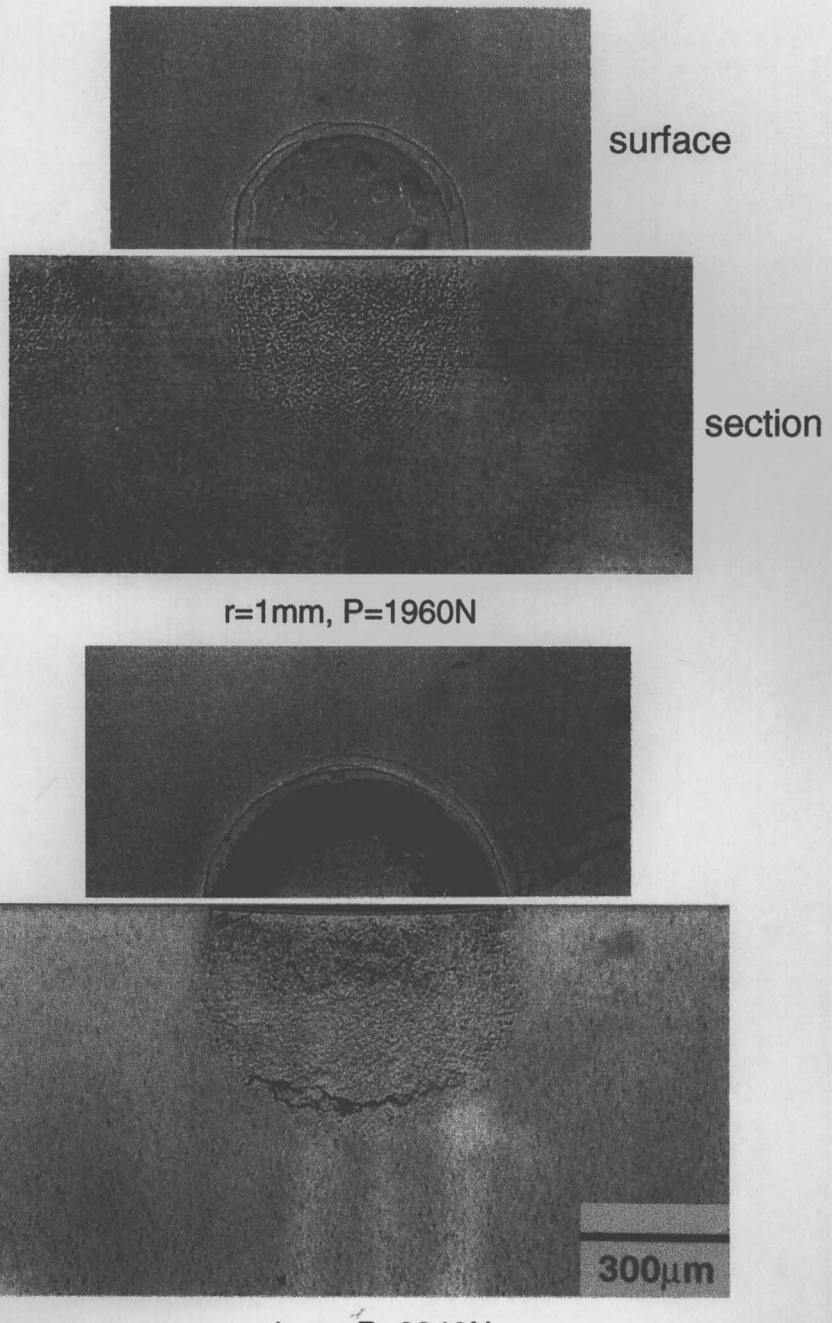

Fig. 6-10 Hertzian contact damage for Si_3N_4/15vol%BN nanocomposite.

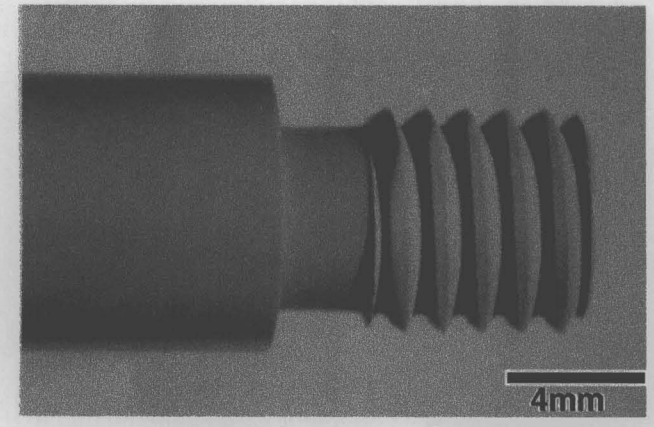

Fig. 6-11 Machinable Si_3N_4/40Vol%BN nanocomposite with high strength.

Chapter 7

Summary and Conclusions

In this thesis, the development of Si_3N_4/BN composites with multiple functionality was attempted without appearing the disadvantageous properties of each material by using the nanocomposite technology, and the novel fabrication method including chemical processes was devised to achieve this purpose. This thesis also considers the influence of nano-sized hexagonal BN (h-BN) dispersion on the improved mechanical properties such as fracture strength, thermal shock fracture resistance, high temperature mechanical properties (fracture strength, hardness and Young's modulus), and machinability. The main results and conclusions obtained in this study are summarized as follows:

In chapter 2, in order to devise the microstructure and the new fabrication method for Si_3N_4/BN composites with excellent properties, the microstructure and the mechanical properties were investigated for Si_3N_4/BN composites fabricated by the conventional metallurgical process with hot-pressing.

The Si_3N_4/BN composite fabricated by the conventional process indicated a typical microcomposite in which micro-sized h-BN grains dispersed at the grain boundaries. The bending strength of the composites suddenly decreased with BN contents. The sudden decrease was due to the increase in the size of h-BN particle or its agglomeration as a processing defect. These observations implies that the nanocomposite structure will be effective to eliminate the processing defects and to improve the mechanical properties.

In chapter 3, the novel chemical process for fabrication of Si_3N_4/BN nanocomposite was devised to improve the mechanical properties. The Si_3N_4/BN nanocomposites containing 0 - 40 vol% h-BN were successfully fabricated by hot-pressing α-Si_3N_4 powders, on which turbostratic BN (t-BN) with the disordered layer structure was partly coated. The t-BN coating on α-Si_3N_4 particles was prepared by heating α-Si_3N_4 particles covered with a mixture of boric acid and urea at 1100°C 8h in hydrogen gas. TEM observations of this nanocomposite revealed that nano-sized hexagonal BN (h-BN) particles were homogeneously dispersed within Si_3N_4 grains as well as at grain boundaries. And also, SEM observation showed that the nanocomposites had finer and more homogeneous microstructure due to inhibition of

abnormal grain growth by nano-sized BN dispersions and its low preferred orientation, compared to the monolith and the microcomposites.

Young's modulus of both microcomposites and nanocomposites decreased with increasing h-BN content according to the rule of mixtures, but the strength of the nanocomposites was significantly improved, compared with the conventional microcomposites. The enhancement of the fracture strength was attributed to the inhibition of grain growth by nano-sized h-BN dispersions and also due to a decrease in flaw size.

In the chapter 4, the thermal shock resistance of the monolithic Si_3N_4 and Si_3N_4/BN composites was studied. In addition, the coefficient of thermal expansion and Poisson's ratio, which influence the thermal shock fracture resistance, were evaluated to elucidate the mechanism. The thermal shock resistance of the Si_3N_4/15vol%BN nanocomposite were remarkably improved compared to the monolith and the microcomposites, and the sudden decrease in residual strength was not observed even at ΔT of 1500°C.

The Si_3N_4/BN nanocomposites in this work were successful in retaining relatively high strength, notwithstanding decreasing in Young's modulus due to the soft h-BN, as described in the chapter 3. Moreover, the coefficient of thermal expansion of the composites was lower than that of the monolith due to the relaxation of thermal expansion by h-BN particles, and also the nanocomposites indicated lower Poisson's ratio. The remarkably improved thermal shock fracture resistance of the Si_3N_4/BN nanocomposites could be explained mainly by the high fracture strength, low Young's modulus, low coefficient of thermal expansion and low Poisson's ratio.

In the chapter 5, high temperature mechanical properties of monolithic Si_3N_4 and Si_3N_4/BN nanocomposite were investigated to make clear the role of fine h-BN at elevated temperatures.

The Si_3N_4/30vol%BN nanocomposite exhibited superior strength and hardness at high temperatures compared to the monolithic Si_3N_4. Furthermore, Young's modulus of Si_3N_4/BN nanocomposites and monolith h-BN exhibited unique tendency that its Young's modulus increased with a rise of temperature. The improvements of high temperature strength and hardness for the nanocomposite were achieved by inhibition of the softening of grain boundary phases by intergranular nano-sized h-BN particles with excellent high temperature mechanical properties and the increase in Young's modulus at elevated temperatures like graphite.

In the chapter 6, the machinability of Si_3N_4/BN micro- and nanocomposite was

examined. The special emphasis was placed on understanding the effect of micro- and nanostructure on the machinability using the Hertzian contact test.

The Si_3N_4/30vol%BN nanocomposite fabricated by new chemical method successfully attained simultaneously high fracture strength and excellent machinability. The observed excellent machinability was attributable not only to the dispersion of h-BN characterized by cleavage properties but also to the quasi-plastic deformation, which can be expected absorb and to disperse the damage force during the machining operation. From the SEM observations, it was found that this deformation was originated at the weak interfaces between the Si_3N_4 matrix and the h-BN dispersion. Thus, it was concluded that this uncommon deformation behavior realized excellent machining of strong ceramics.

In order to realize multi-functional ceramics, the novel fabrication method including chemical processes was devised to fabricate the Si_3N_4/BN nanocomposite. The Si_3N_4/BN nanocomposite fabricated by this method successfully archived the significant enhancement of fracture strength, thermal shock fracture resistance, high temperature mechanical properties such as strength, hardness and Young's modulus, and machinability. In consideration of these results, that the nanocomposites created in this work must be newly developed silicon nitride based ceramics with multiple functionality. Finally, these excellent multi-functionality will widen the application fields of Si_3N_4 ceramics in the near future.

List of Publications

1) T. Kusunose, Y. H. Choa, T. Sekino and K. Niihara
Mechanical Properties of Si_3N_4/BN Composite by Chemical Processing
Key Engineering Materials, Vol.**161-163**(1999)475-480

2) T. Ohji, T. Kusunose and K. Niihara
Threshold Stress in Creep of Alumina/Silicon Carbide nanocomposites
J. Am. Ceram. Soc., Vol. **81**(1998)2713-2716.

3) T. Kusunose, Y. H. Choa, T. Sekino and K. Niihara
STRONG MACHINABLE NANO-COMPOSITE CERAMICS
Ceramic Transactions, (In Press).

4) K. Niihara, T. Kusunose, Y. H. CHOA and T. SEKINO
Multi-Functional Ceramic Composites through Nanocomposite Technology
Key Engineering Materials, Vol.**161-163**, (1999), 527-534

Proceeding

1) T. Mizutani, T. Kusunose, M. Sando and K. Niihara
MICROSTRUCTURE AND PROPERTIES OF NANO-SIZED BN-PARTICULATE-DISPERSED SIALON CERAMICS
6th International Symposium on Ceramic Materials and Components for Engines, (1997)876-881(October 19-23, 1997, Arita Japan)

2) T. Mizutani, T. Kusunose, M. Sando and K. Niihara
FABRICATION AND PROPERTIES OF NANO-SIZED BN-PARTICULATE-DISPERSED SiALON CERAMICS
Ceramic Engineering & Science Proceedings, Vol.**18**(1997)669-677(21st Annual Conference on Composites, Advanced Cramics, Materials, and Structures-B)

List of Supplementary Publications

1) 新原晧一, 楠瀬尚史
多機能調和型の高強度マシナブル Si_3N_4/BN ナノコンポジット
(解説) 化学と工業, Vol. **51**(1998)1221-1223

2) 新原晧一, 楠瀬尚史
高次に機能が調和したマシナブル窒化ケイ素系セラミックスの設計・開発
(解説) Materials Integration, Vol. **12**(1999)9-16

3) K. Yanagisawa, T. Kusunose, K. Ioku, N. Yasaki, P. B. Malla and S. Komarnen
Hydrothermal crystallization mechanism of sodium beidellite from amorphous gel
J. Mater. Sci. Lett., Vol.**14**(1995)1770-1772.

4) K. Yanagisawa, T. Kusunose, K. Ioku, N. Yasaki, P. B. Malla and S. Komarnen
Hydrothermal synthesis of Na beidellite from coprecipitated gel
J. Mater. Sci. Lett., Vol.**15**(1996)861-863.

Acknowledgment

The author would like to express his greatest appreciation and gratitude Professor Koichi Niihara at The Institute of Scientific and Industrial Research, Osaka University for his kind guidance, invaluable suggestions and encouragement in coordinating this investigation. The author would also like to thank Professor Gin-ya Adachi and Mitsuo Komatsu for reviewing this thesis. Grateful thanks are given to Dr. Satoru Ueda, Dr. Tohru Sekino, Dr. Atsuo Koreeda, Dr. Doh-Hyung Riu, Dr. Manuar Hussain and special thanks to Dr. Yong-Ho Choa at Niihara Laboratory.

The author wishes to make grateful acknowledge to Dr. Takeshi Hirano at the Japan Defense Agency, Dr. Atsushi Nakahira at Kyoto Institute of Technology, Mr. Norikazu Tachibana at Murata Co. Ltd. and Mr. Takeshi Kawase in Niihara Laboratory for their helpful discussions and encouragement during this study.

The author is grateful to Professor Nakamichi Yamasaki and Dr. Kazumichi Yanagisawa at The Hydrothermal Laboratory in Kochi University for giving the opportunity to come to Osaka University and his hearty encouragement.

Grateful acknowledgments are given to Dr. Ken-ichi Ohta and Mr. Takanori Tanaka at Osaka University for important measurements and helpful advices.

Grateful acknowledgments are made to Mrs. Emiko Kitaura and Mrs. Rie Suehiro for their hearty encouragement and helpful assistance. The author thanks to the author's colleagues Mr. Jian-Feng Yang and Mr. Hiroyuki Hayashi and all other members of Niihara Laboratory for their kind discussion and encouragement.

Finally, the author wishes to express the deep appreciation to the author's parents, grand parents and sister, Akihiko Kusunose, Hiroko Kusunose, Kamehide Kusunose, Hanae Kusunose and Atsuko Kusunose for their hearty encouragement and understandings.

楠瀬尚史

Takafumi Kusunose

January, 1999

Osaka, Japan